

**MEMBRANE PROTEIN COMPLEXES INVOLVED IN THROMBOSPONDIN-1
REGULATION OF NITRIC OXIDE SIGNALING**

by

Toni Green

A **Dissertation** Submitted to the Faculty of the

DEPARTMENT OF CHEMISTRY AND BIOCHEMISTRY

In Partial Fulfillment of the Requirements

For the Degree of

**DOCTOR OF PHILOSOPHY
WITH A MAJOR IN BIOCHEMISTRY**

In the Graduate College

THE UNIVERSITY OF ARIZONA

2013

THE UNIVERSITY OF ARIZONA
GRADUATE COLLEGE

As members of the **Dissertation** Committee, we certify that we have read the **dissertation** prepared by **Toni Green**, titled **Membrane Protein Complexes Involved in Thrombospondin-1 Regulation of Nitric Oxide Signaling** and recommend that it be accepted as fulfilling the **dissertation** requirement for the Degree of Doctor of **Philosophy**.

_____ Date:
Dr. William R. Montfort

_____ Date:
Dr. Tsu-Shuen Tsao

_____ Date:
Dr. Matthew Cordes

_____ Date:
Dr. Megan McEvoy

_____ Date:
Dr. S. Scott Saavedra

Final approval and acceptance of this **dissertation** is contingent upon the candidate's submission of the final copies of the **dissertation** to the Graduate College.

I hereby certify that I have read this **dissertation** prepared under my direction and recommend that it be accepted as fulfilling the **dissertation** requirement.

_____ Date:
Dissertation Director: **Dr. William R. Montfort**

STATEMENT BY AUTHOR

This **dissertation** has been submitted in partial fulfillment of requirements for an advanced degree at the University of Arizona and is deposited in the University Library to be made available to borrowers under rules of the Library.

Brief quotations from this **dissertation** are allowable without special permission, provided that accurate acknowledgment of source is made. Requests for permission for extended quotation from or reproduction of this manuscript in whole or part may be granted by the author.

SIGNED: Toni Green

ACKNOWLEDGEMENTS

Dr. Bill Montfort: Thank you for all of your support, understanding, and advice during my graduate career. You taught me to look critically at my data, and I am a better scientist because of it. You are a wonderful advisor and I am thankful for being a part of your lab.

Committee Members: Dr. Tsao, Dr. McEvoy, Dr. Saavedra, and Dr. Cordes, thank you for your advice, in the classroom and out. You were always available when I had a question about an experiment or anything else, and I appreciate your willingness to help in any way possible.

Dr. Matt Kaplan: You are such an amazing person, I learned more from you in the last couple months of my graduate career than I ever expected. Thank you so much for your flow cytometry and life advice, I will never forget it.

Dr. Brooke Beam: Thank you for always being willing to teach, you helped me fall in love with microscopy. You helped me whenever I needed it, and you inspire me by your dedication to what you do.

Dr. Lisa Rezende: I don't know what I would have done without you! You were there for me through everything, even the birth of my daughter. You are a kind and loving person, and are truly like a second mother to me. Thank you for all of the advice, dinners, and babysitting. You mean the world to me.

Montfort Lab: Thank you for all of your help through the years, for countless amounts of advice on how to do an experiment, and for how to do research. **Jacquie**, you are the best lab manager that ever existed and became a great friend. Thank you for all of our breakfasts and great conversation.

My family: My parents, **Tom and Rhonda**, thank you for pushing me to be the best person I could be, for always believing in me and telling me I could do it. Your support means everything to me. My wonderful husband **Sean**, you supported me through everything, even when the Air Force sent you to Las Vegas for the past two years. Words cannot express how grateful I am to you helping me achieve my dream. You are the love of my life, and I couldn't have done this without you. My amazing daughter **Grace**, I know this has been hard on you, and thank you for putting up with the long days of daycare and the weekends of coming to the lab. You are the reason I work so hard and made all of hours of research worth it. You always put a smile on my face, even on the worst of days. I love you so much my darling.

DEDICATION

To Sean, Grace, and my unborn child: Family is everything. No matter what I accomplish in life, it is nothing without you by my side.

TABLE OF CONTENTS

LIST OF TABLES	13
LIST OF FIGURES	14
ABSTRACT.....	18
CHAPTER 1. THROMBOSPONDIN-1 REGULATION OF NITRIC OXIDE	
SIGNALING.....	20
1.1 Nitric oxide signaling.....	20
1.1.1 Nitric oxide as a second messenger	20
1.1.2 Isoforms of nitric oxide synthases	21
1.1.3 The nitric oxide receptor soluble guanylate cyclase	22
1.1.4 Mechanism of sGC activation.....	22
1.2 Ligands of CD47.....	23
1.2.1 Thrombospondins	23
1.2.2 TSP-1 structure and domains	23
1.2.3 TSP-1 as an inhibitor of angiogenesis	24
1.2.4 Signal Regulatory Protein α (SIRP α).....	28
1.3 CD47 as a receptor for TSP-1	29
1.3.1 Discovery of CD47	29
1.3.2 CD47 structure	30
1.3.3 E3CaG1.....	30
1.4 CD47 associates with other membrane proteins.....	32
1.4.1 Integrins	32

TABLE OF CONTENTS - *Continued*

1.4.2 VEGFR2	32
1.5 TSP-1 as a nitric oxide regulator	33
1.5.1 TSP-1 binding to CD47 downregulates sGC through a rise in intracellular Calcium.....	33
1.5.2 TSP-1, VEGFR2, and calcium.....	34
1.6 Research Topic.....	35
CHAPTER 2. DEVELOPMENT OF PLASMON-WAVEGUIDE RESONANCE (PWR) SPECTROSCOPY FOR MEASUREMENT OF THROMBOSPONDIN-1 BINDING TO NATIVE JURKAT MEMBRANES	
2.1 Introduction to PWR.....	38
2.2 Materials and Methods.....	40
2.2.1 Materials	40
2.2.2 Cell Culture.....	41
2.2.3 Preparation of plasma membrane fragments.....	41
2.2.4 Purification of E3CaG1.....	43
2.2.5 Preparation of prisms for PWR spectroscopy.....	43
2.2.6 Deposition of membrane fragments onto PWR prism.....	44
2.2.7 Addition of E3CaG1 to sample cell.....	44
2.2.8 Addition of CD47/isotype antibodies to sample cell	45
2.2.9 PWR instrument	45
2.2.10 Data Analysis	46

TABLE OF CONTENTS - *Continued*

2.3 Results.....	47
2.3.1 CD47 is required for E3CaG1 binding	47
2.3.1.1 Addition of anti-CD47 antibody inhibits E3CaG1 binding.....	49
2.3.1.2 Addition of an isotype antibody and Angiotensin II do not inhibit E3CaG1 binding.....	57
2.3.2 E3CaG1 binds to CD47 on purified Jurkat plasma membranes with picomolar and nanomolar dissociation constants.....	60
2.3.3 Determining the measurement of equilibrium dissociation constants	66
2.3.4 E3CaG1 binds to CD47 on purified MCF-7 plasma membranes	68
2.3.5 CD47 is not sufficient for E3CaG1 binding	68
2.3.6 SIRP α binds to CD47 on Jurkat plasma membranes	72
2.4 Discussion.....	75
CHAPTER 3. IDENTIFICATION OF MEMBRANE PROTEINS IN COMPLEX WITH CD47 INVOLVED IN THROMBOSPONDIN-1 BINDING.....	77
3.1 Introduction.....	77
3.2 Materials and Methods.....	78
3.2.1 Materials	78
3.2.2 Cell culture.....	78
3.2.3 Cloning of CD47-eGFP	79
3.2.4 Generation of lentivirus	79
3.2.5 Stable transduction of cells	80

TABLE OF CONTENTS - *Continued*

3.2.6 Confocal Microscopy.....	81
3.3 Results.....	81
3.3.1 E3CaG1 binds to CD47 in complex with VEGFR2 with a picomolar K_d ...	83
3.3.2 E3CaG1 binds to CD47 in complex with integrin $\alpha_v\beta_3$ with a nanomolar K_d	83
3.3.3 The loss of E3CaG1 binding correlates to a decrease in VEGFR2 expression	83
3.3.3.1 Determination of transduction by confocal microscopy	92
3.3.4 Expression of CD47-eGFP in CD47-null (JinB8) cells using a lentiviral transduction system.....	92
3.3.4.1 Determination of transduction by PWR spectroscopy and confocal microscopy.....	97
3.3.5 A CD47-null Jurkat cell line in which CD47 is re-introduced behaves similarly to native Jurkat T cells.....	97
3.3.5.1 E3CaG1 binds to CD47 in complex with VEGFR2 with a picomolar K_d on JinB8 cells stably transduced with CD47-eGFP and another complex involving VEGFR2 with a nM K_d	101
3.3.6 E3CaG1 binds to VEGFR2 in complex with integrin $\alpha_v\beta_3$ with a nM K_d ...	106
3.4 Discussion.....	111
CHAPTER 4. APPLICATION OF A FLUORESCENCE-BASED CALCIUM ASSAY AS A FUNCTIONAL READOUT FOR THROMBOSPONDIN-1 BINDING TO	

TABLE OF CONTENTS - *Continued*

CD47	115
4.1 Introduction.....	115
4.2 Materials and Methods.....	115
4.2.1 Materials	116
4.2.2 Cell culture.....	116
4.2.3 Flow Cytometry Calcium Assay.....	116
4.3 Results.....	117
4.3.1 Measurement of TSP-1 induced $[Ca^{2+}]_i$ increase by flow cytometry	117
4.3.2 Anti-VEGFR2 antibody inhibits E3CaG1-induced $[Ca^{2+}]_i$ in Jurkat cells ..	117
4.3.3 E3CaG1 binds to CD47 in complex with VEGFR2 to cause an increase in $[Ca^{2+}]_i$ in JinB8 cells stably transduced with CD47-eGFP	118
4.3.4 E3CaG1 binds to VEGFR2 in complex with $\alpha_v\beta_3$ to cause a decrease in $[Ca^{2+}]_i$ in CD47-null cells	118
4.4 Discussion	124
CHAPTER 5. IDENTIFICATION OF MEMBRANE PROTEINS REQUIRED FOR THROMBOSPONDIN-1 INDUCED CALCIUM SIGNALING.....	128
5.1 Introduction.....	128
5.2 Materials and Methods.....	128
5.2.1 Materials	128
5.2.2 Cell culture.....	129

TABLE OF CONTENTS - *Continued*

5.2.3	Flow cytometry binding studies.....	129
5.2.4	Confocal microscopy	130
5.2.5	Generation of lentivirus	130
5.2.6	Stable transduction of cells	130
5.2.7	Transfection of HEK 293T cells	131
5.2.8	Flow cytometry calcium assay.....	131
5.3	Results.....	132
5.3.1	Determination of relative CD47 and VEGFR2 levels in native HEK 293T cells by flow cytometry.....	132
5.3.2	Determination of CD47 and VEGFR2 levels in CD47- and VEGFR2-null HEK 293T cells by flow cytometry	132
5.3.3	Determination of re-introduction of CD47-eGFP and VEGFR2-mCherry to CD47- and VEGFR2-null HEK 293T cells by confocal microscopy.....	135
5.3.4	VEGFR2 is required for E3CaG1-induced intracellular calcium increase in endothelial cells	135
5.4	Discussion	141
CHAPTER 6. CONCLUSIONS AND FUTURE DIRECTIONS		146
6.1	Conclusions.....	146
6.2	Future Directions	150
6.2.1	Purification of CD47-eGFP	150
6.2.1.1	Structural studies of CD47-eGFP by X-ray crystallography	150

TABLE OF CONTENTS - *Continued*

6.2.2. Insertion of purified CD47-eGFP into synthetic lipid bilayer and determination of E3CaG1 binding by PWR spectroscopy	151
6.2.2.1 Identification of residues in CD47 critical for TSP-1 binding by mutagenesis.....	151
REFERENCES	153

LIST OF TABLES

TABLE 2.1	List of dissociation constants determined by PWR spectroscopy.....	50
TABLE 2.2	List of <i>p</i> - and <i>s</i> -polarization resonance position shifts from addition of membrane and E3CaG1 to the PWR prism surface.....	69

LIST OF FIGURES

Figure 1.1 Mechanism of NO production and physiologic effects of sGC activation.....	25
Figure 1.2 sGC domain structure.....	26
Figure 1.3 TSP-1 monomer and E3CaG1 structure and domains.....	27
Figure 1.4 Diagram of CD47 structure	31
Figure 1.5 Diagram of research goal.....	37
Figure 2.1 PWR instrument setup.....	42
Figure 2.2 Typical PWR spectra observed for <i>p</i> - and <i>s</i> -polarized light.....	48
Figure 2.3 CD47 is present on low-passage Jurkat plasma membranes	52
Figure 2.4 CD47 is present on high-passage Jurkat plasma membranes.....	53
Figure 2.5 E3CaG1 does not bind to the prism surface	54
Figure 2.6 E3CaG1 binds to CD47	55
Figure 2.7 Negative resonance position shifts do not inhibit subsequent antibody binding	58
Figure 2.8 Addition of an isotype Ab does not inhibit E3CaG1 binding	61
Figure 2.9 Angiotensin II binds to low-passage Jurkat membranes with a nM K_d	63
Figure 2.10 E3CaG1 binds to low-passage Jurkat plasma membranes with a pM K_d ..	64
Figure 2.11 E3CaG1 binds to low-passage Jurkat plasma membranes with a nM K_d ..	65
Figure 2.12 Example of PWR spectra upon pM E3CaG1 addition to low-passage Jurkat plasma membranes.....	67
Figure 2.13 E3CaG1 binds to purified MCF-7 plasma membranes with a pM K_d	70

LIST OF FIGURES - *Continued*

Figure 2.14 E3CaG1 does not appear to bind to high-passage Jurkat cells.....	71
Figure 2.15 SIRP α -Fc binds to CD47 on low-passage Jurkat membranes.....	73
Figure 2.16 SIRP α -Fc binds to CD47 on high-passage Jurkat membranes.....	74
Figure 3.1 VEGFR2 is present on low-passage Jurkat plasma membranes	84
Figure 3.2 E3CaG1 binds to CD47/VEGFR2 with a pM K_d and CD47/ $\alpha_v\beta_3$ with a nM K_d on low passage Jurkat plasma membranes.....	85
Figure 3.3 Dot plots showing fluorescence from anti-His-FITC secondary Ab bound to E3CaG1, with and without prior incubation of anti-VEGFR2 (260.4) and anti-CD47 (B6H12) antibodies	87
Figure 3.4 E3CaG1 binds to CD47 in complex with VEGFR2 by flow cytometry	89
Figure 3.5 Integrin α_v is present on low-passage Jurkat plasma membranes	91
Figure 3.6 Dot plots showing fluorescence upon anti-VEGFR2 (260.4) Ab addition to low and high-passage Jurkat cells.....	93
Figure 3.7 VEGFR2 levels decrease on Jurkat cells over time.....	94
Figure 3.8 There is a significant decrease in anti-VEGFR2 Ab binding in high-passage Jurkat membranes compared to anti-CD47 Ab binding	95
Figure 3.9 CD47 is present on CD47-JinB8 cells by PWR spectroscopy	98
Figure 3.10 CD47 is expressed on CD47-JinB8 cells by confocal microscopy	100
Figure 3.11 E3CaG1 binds to CD47-JinB8 plasma membranes with a pM K_d	102
Figure 3.12 E3CaG1 binds to CD47-JinB8 plasma membranes with a nM K_d	103

LIST OF FIGURES - *Continued*

Figure 3.13 E3CaG1 binds to CD47/VEGFR2 with a pM affinity and another VEGFR2 complex with a nM affinity on CD47-JinB8 plasma membranes.....	104
Figure 3.14 E3CaG1 binds to VEGFR2/ $\alpha_v\beta_3$ on CD47-JinB8 (expression off) membranes	107
Figure 3.15 E3CaG1 inhibits anti- α_v and anti-VEGFR2 Ab binding to JinB8 plasma membranes	109
Figure 3.16 E3CaG1 binding curve to CD47-JinB8 (expression off) plasma membranes	112
Figure 4.1 Dot plots showing calcium fluorescence upon addition of E3CaG1 in low-passage Jurkat cells	119
Figure 4.2 CD47 associates with VEGFR2 to produce an E3CaG1-induced rise in $[Ca^{2+}]_i$ in Jurkat cells.....	120
Figure 4.3 Dot plots showing E3CaG1-induced calcium increase in CD47-JinB8 cells	122
Figure 4.4 CD47 associates with VEGFR2 to produce an E3CaG1-induced rise in $[Ca^{2+}]_i$ in CD47-JinB8 cells	123
Figure 4.5 Dot plots showing changes in intracellular calcium fluorescence upon E3CaG1 binding in JinB8 cells.....	125
Figure 4.6 E3CaG1 binds to VEGFR2/ $\alpha_v\beta_3$ to decrease $[Ca^{2+}]_i$	126
Figure 5.1 Dot plots showing fluorescence upon addition of anti-VEGFR2 (260.4) and anti-CD47 (B6H12) antibodies on native HEK 293T cells	133

LIST OF FIGURES - *Continued*

Figure 5.2 CD47 and VEGFR2 are present on HEK 293T cells	134
Figure 5.3 Dot plots showing fluorescence of HEK 293T (CD47- and VEGFR2-null) cells upon addition of anti-VEGFR2 (260.4) and anti-CD47 (B6H12) antibodies	136
Figure 5.4 CD47 and VEGFR2 are not present on HEK 293T (CD47- and VEGFR2-null) cells.....	137
Figure 5.5 Confocal microscopy images of HEK 293T (CD47- and VEGFR2-null) cells transfected with CD47-eGFP, VEGFR2-mCherry, or both.....	138
Figure 5.6 Dot plots showing $[Ca^{2+}]_i$ increases upon E3CaG1 addition in HEK 293T (CD47 and VEGFR2-null) cells transfected with CD47-eGFP, VEGFR2-mCherry, or both.....	142
Figure 5.7 CD47 and VEGFR2 are required for E3CaG1-induced $[Ca^{2+}]_i$ increase	144
Figure 6.1 Research summary.....	148

ABSTRACT

Thrombospondin-1 (TSP-1) binding to its membrane receptor CD47 results in an inhibition of the nitric oxide (NO) receptor soluble guanylate cyclase (sGC) and a decrease in intracellular cGMP levels. This causes physiologic effects such as vasoconstriction and a rise in blood pressure. The mechanism by which TSP-1 binds to CD47 at the membrane to decrease sGC activity is largely unknown. CD47 can physically associate with a number of binding partners, including $\alpha_v\beta_3$ and vascular endothelial growth factor receptor 2 (VEGFR2). Binding of a C-terminal fragment of TSP-1 called E3CaG1 to CD47 leads to a rise in intracellular calcium ($[Ca^{2+}]_i$), which decreases sGC activity via a phosphorylation event. Binding of E3CaG1 is also known to disrupt the interaction between CD47 and VEGFR2, leading to a decrease in endothelial nitric-oxide synthase (eNOS) activity and cGMP levels through an Akt signaling pathway. However, it is not known whether other membrane proteins associated with CD47 are required for E3CaG1 binding and a subsequent $[Ca^{2+}]_i$ increase. Plasmon-waveguide resonance (PWR) spectroscopy was employed to elucidate the mechanism of TSP-1 inhibition of sGC activity through membrane complexes involving CD47. Using PWR, I found E3CaG1 can bind specifically to CD47 within native Jurkat membranes with picomolar and nanomolar dissociation constants (K_d), suggesting multiple CD47 complexes are present. Among these complexes, CD47/VEGFR2 was found to bind E3CaG1 with a picomolar K_d and CD47/ $\alpha_v\beta_3$ was found to bind E3CaG1 with a nanomolar K_d . In addition, the presence of an anti-VEGFR2 antibody inhibited the E3CaG1-induced calcium response, which suggested CD47 in complex with VEGFR2

was responsible for TSP-1 reduction of sGC activity. I show that when both CD47 and VEGFR2 are returned to a HEK 293T cell line that does not contain these receptors, an increase in $[Ca^{2+}]_i$ upon E3CaG1 binding is restored. Interestingly, E3CaG1 was also found to bind to VEGFR2 in complex with the integrin $\alpha_v\beta_3$ on CD47-null cell lines and their derivations, causing a decrease in $[Ca^{2+}]_i$ levels. Therefore, the third type 2 repeat and C-terminal domains of TSP-1 can cause both increases and decreases in calcium based upon the availability of protein complexes to which it binds.

CHAPTER 1

THROMBOSPONDIN-1 REGULATION OF NITRIC OXIDE SIGNALING

1.1 Nitric oxide signaling

Nitric oxide plays a fundamental role in the body and is involved in the regulation of blood pressure, neurotransmission, cardiovascular function, and platelet aggregation via its receptor soluble guanylate cyclase (sGC) (1-4). Nitric oxide is a small, uncharged molecule containing an unpaired electron, making it a reactive free radical. Being uncharged, nitric oxide can readily traverse cell membranes, where it binds to target proteins containing iron, including heme groups and iron-sulfur complexes (5).

Endothelium-derived relaxing factor (EDRF), which was originally identified as a substance that relaxed sections of aorta (6), was identified to be nitric oxide several years later (7).

1.1.1 Nitric oxide as a second messenger

Nitric oxide is generated by a class of enzymes called nitric oxide synthases (NOS). These enzymes use arginine and oxygen as substrates, producing citrulline and nitric oxide as products. Nitric oxide is required for basal blood flow, as demonstrated, for example, by the endothelium-derived nitric oxide synthase inhibitor N-monomethyl-L-arginine (L-NMMA), which caused a 50% decrease in blood flow in live human subjects (8). Nitric oxide is continuously produced in endothelial cells and diffuses into target cells, including vascular smooth muscle cells, where it binds to its targets and regulates blood pressure and cardiovascular health. Nitric oxide acting as a second messenger can not only bind to iron in heme-containing proteins such as hemoglobin,

sGC, and oxidoreductase, but it can also undergo oxidation to produce dinitrogen trioxide. This molecule can then nitrosate base pairs, which in turn causes deamination and damage of DNA (9). Nitric oxide also acts as a neurotransmitter, and inhibition of neuronal nitric oxide synthase was shown to decrease nonadrenergic noncholinergic relaxation of muscle (2, 3). Macrophages can produce large amounts of nitric oxide in order to inhibit bacterial growth (10), thus this signaling molecule plays a role in the immune system as well. In addition to its role in the cardiovascular and immune systems, nitric oxide is also involved in the reduction of platelet aggregation. S-nitroso-N-acetylpenicillamine, which releases nitric oxide, was shown to produce similar effects as prostacyclin, a known inhibitor of platelet aggregation (11).

1.1.2 Isoforms of nitric oxide synthases

Nitric oxide synthases are expressed in various tissues to generate nitric oxide through the conversion of arginine to citrulline in a reaction that requires oxygen, NADPH, and FAD (12). There are three main isoforms of nitric oxide synthases: neuronal NOS (nNOS), endothelial NOS (eNOS), and inducible NOS (iNOS). eNOS and nNOS are constitutively expressed in endothelial cells and neurons, respectively, and require calcium-dependent calmodulin for their activation (13-15). iNOS, which is found in cells such as macrophages, fibroblasts, and smooth muscle cells, has delayed NO production and, while also binding calmodulin, is not as dependent upon calcium for its activation compared to the other two isoforms (16-18). iNOS is transcriptionally induced by the presence of cytokines or bacteria and releases large amounts of NO to kill invading pathogens (5, 16).

1.1.3 The nitric oxide receptor soluble guanylate cyclase

There are two forms of guanylate cyclase, NO-sensitive (generally soluble) and NO-insensitive (membrane-bound). However, NO-sensitive soluble guanylate cyclases can be localized to synaptic membranes (19, 20). Once NO is generated by NOS, it binds to a heme moiety on its major receptor in target cells, soluble guanylate cyclase (sGC) (21, 22) (Figure 1.1). NO does not activate NO-insensitive membrane-bound GC, which is instead activated by peptide hormones (19, 21). sGC is ~150 kDa and consists of two α and β subunits. Two isoforms of each exist: α_1 , α_2 , β_1 , and β_2 (23-25). The structure of sGC consists of an N-terminal Heme-Nitric oxide/Oxygen (H-NOX) domain, a PAS domain, a coiled-coil domain, and a C-terminal catalytic domain (26) (Figure 1.2). NO binds to the ferrous heme within the β subunit of the H-NOX domain to cause a conformational change in the protein, allowing its substrate GTP to be converted to cGMP in a process requiring magnesium (Mg^{2+}) as a cofactor (22, 27, 28).

1.1.4 Mechanism of sGC activation

sGC activation involves a proximal histidine residue within the H-NOX domain that is coordinated to the heme iron of the β subunit. When the iron atom is in its ferrous state, NO binds and subsequently causes a break of the His-Fe(II) bond (29). Using a purified sGC fragment from *Manduca sexta* not containing the cyclase domain, two phases of NO binding were observed. The first involved the rapid formation of a 6-coordinate intermediate upon initial NO binding, and the second, slower step involved the release of His to re-form a 5-coordinate structure (30). This 2-step process has also been found to occur in full-length sGC (31). However, the cleavage of the His-Fe(II) bond was

shown to be dependent on NO concentration using full-length sGC, whereas this step was not dependent on NO concentration using the truncated form that did not contain the cyclase domain. Therefore, it has been suggested that a second, non-heme NO binding site within the catalytic domain influences the loss of His within the NO-bound heme pocket (30), but this theory remains to be confirmed.

1.2 Ligands of CD47

1.2.1 Thrombospondins

There are 5 types of thrombospondins that are known to exist: Thrombospondin-1 (TSP-1) and Thrombospondin-2 (TSP-2), which exist as trimers, and Thrombospondin-3, -4, and -5 (TSP-3, -4, and -5), which are pentameric (32). The overall structure of TSP-1 and TSP-2 consists of an N-terminal domain followed by an oligomerization domain, a procollagen homology domain, three properdin-like/Type 1 repeats, three epidermal growth factor (EGF)-like/Type 2 repeats, a calcium-binding domain, and a globular C-terminal domain (32). TSP-3, -4 and -5 do not contain procollagen homology domains or Type 1 repeats, and have an additional Type 2 repeat (33).

1.2.2 TSP-1 structure and domains

TSP-1 is a homotrimeric ~450 kDa matricellular protein that is known for its role in wound healing and angiogenesis (34, 35). TSP-1 consists of three identical monomeric chains that are connected by disulfide bonds (32). Starting from the N-terminus, TSP-1 contains a domain that binds heparin, a procollagen homology domain, three Type 1 repeats that contain binding sites for the transmembrane protein CD36, three EGF-like type 2 repeats, 7 Type 3 repeats that bind calcium, and a C-terminal CD47-

binding domain (Figure 1.3) (32, 34). In addition to binding heparin, the N-terminal domain of TSP-1 can bind fibrinogen, and β_1 integrins such as $\alpha_3\beta_1$ and $\alpha_6\beta_1$ (34). After the N-terminal and oligomerization domains, there is a procollagen homology domain that is known to contain multiple cysteines and inhibit neovascularization and endothelial cell migration (32, 36). Type I repeats (TSR1) are not only known to bind to CD36 to regulate angiogenesis, but the AAWSHW sequence within TSR1 also binds to and activates TGF- β (37, 38). The last Type 2 repeat (TSR2) contains an RGD binding site that is known to bind to integrin $\alpha_v\beta_3$ on endothelial cells, smooth muscle cells, and platelets (39-41). Each type 3 repeat (TSR3) binds approximately 2 calcium ions (32). In the absence of calcium, the structure of TSR3 elongates to expose a thrombin cleavage site, which is not available in the presence of calcium (42). Therefore, calcium contributes to the overall structure and stability of the protein (34). The major receptor for the C-terminal domain of TSP-1 is CD47, which is involved in the inhibition of NO-stimulated endothelial and smooth muscle cell adhesion, proliferation, and migration (43). Therefore, TSP-1 is a multifunctional protein with multiple domains and binding receptors, and is involved in physiological processes ranging from blood clotting to cell migration.

1.2.3 TSP-1 as an inhibitor of angiogenesis

CD36 is an anti-angiogenic membrane receptor that binds to the type I repeats (TSR) of TSP-1 (44, 45). Ligation of CD36 by TSP-1 inhibited NO-induced proliferation and cGMP production in vascular smooth muscle cells (VSMCs) and CD36 is also known to translocate the endothelial nitric oxide synthase (eNOS) activator

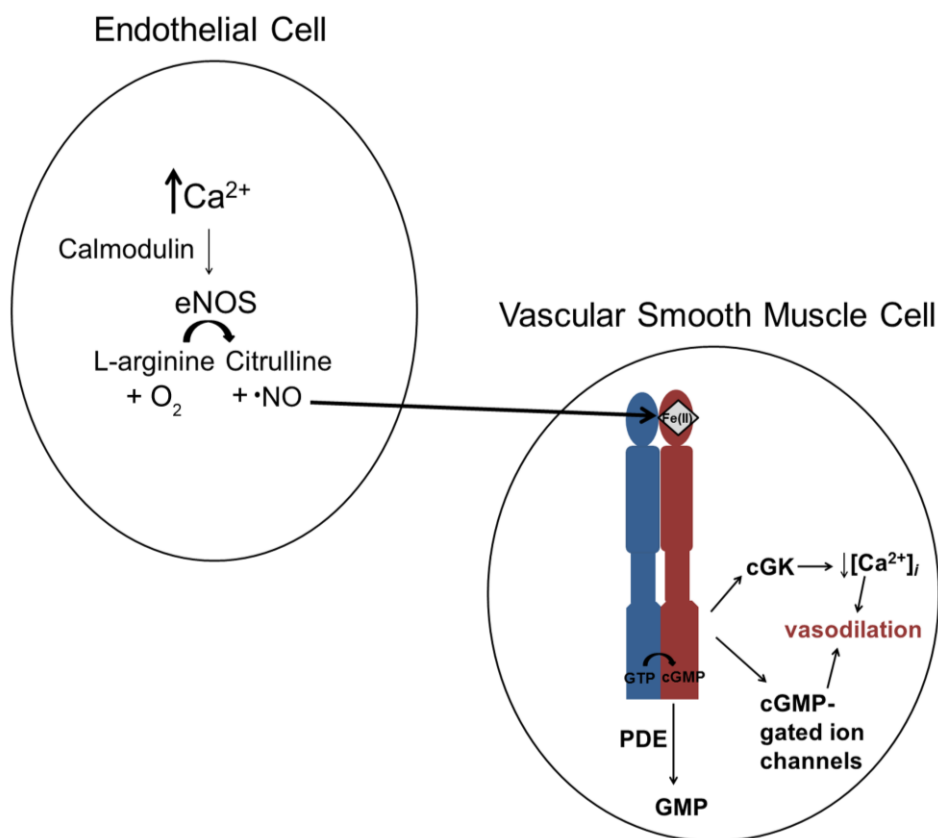


Figure 1.1. Mechanism of NO production and physiologic effects of sGC activation. In endothelial cells, increases in $[Ca^{2+}]_i$ lead to calcium binding to calmodulin, which in turn activates eNOS. eNOS converts L-arginine to citrulline, producing NO. As a small uncharged molecule, NO can traverse cell membranes, where it diffuses into vascular smooth muscle cells to bind to and activate sGC. cGMP is produced, which can bind to cGMP-dependent kinase (cGK) to decreased calcium ion levels. cGMP can also bind to cGMP-gated ion channels to increase influx of Na^+ in exchange for Ca^{2+} , also decreasing calcium levels within the cell. This causes vasodilation and a decrease in blood pressure. cGMP is degraded by phosphodiesterases (PDE) to yield GMP, attenuating the NO signal in a negative feedback manner.

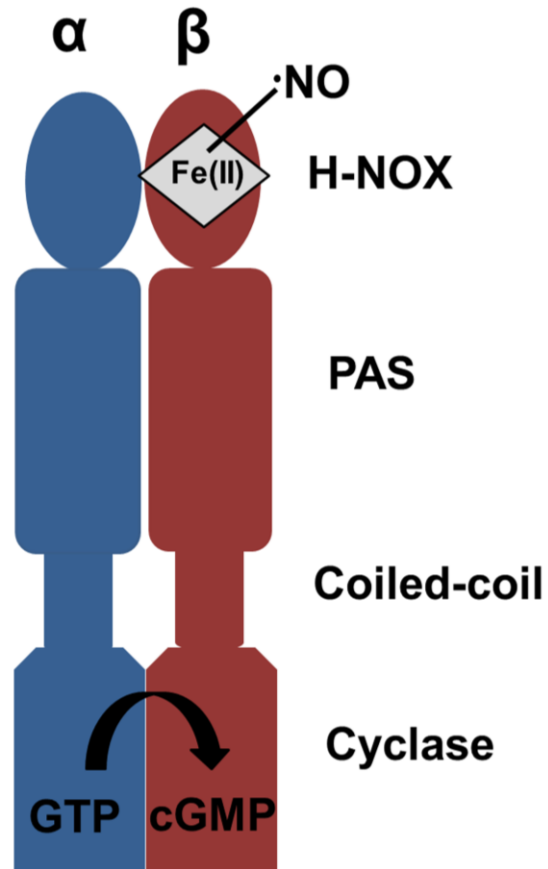


Figure 1.2. sGC domain structure. sGC is a heterodimer and consists of α and β subunits. Each has an N-terminal H-NOX domain, followed by PAS, coiled-coil, and cyclase domains. NO binds to the heme subunit within the B H-NOX domain, causing a conformational change that allows GTP to be converted to cGMP within the catalytic cyclase domain.

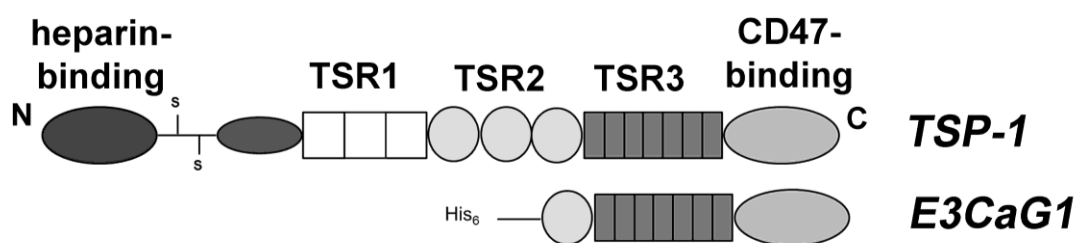


Figure 1.3. TSP-1 monomer and E3CaG1 structure and domains. TSP-1 consists of an N-terminal heparin-binding domain, an oligomerization domain, a procollagen homology domain, three TSR1 domains, three TSR2 domains, 7 calcium-binding TSR3 domains, and a CD47-binding C-terminal domain. E3CaG1 is a C-terminal fragment of TSP-1, consisting of the third TSR2, all of the TSR3 domains, and the C-terminal CD47-binding domain. E3CaG1 was purified using an N-terminal poly-(His)₆ tag.

myristic acid (46, 47). It was then shown that the inhibition of nitric oxide signaling was connected to inhibition of myristic acid uptake by CD36 and subsequent decrease in eNOS activity (48). Peptides to the CD36 binding region of TSP-1 also display anti-angiogenic activity by inhibiting VEGF-driven capillary formation (49). Although CD36 has been shown to have TSP-1 induced anti-angiogenic effects, TSP-1 binding to the membrane receptor CD47 plays a significant role in reduction of angiogenic cellular effects such as migration and proliferation (43). TSP-1 binding to CD47 decreases the amount of time it takes for platelets to aggregate in the presence of nitric oxide (50). TSP-1 was also able to inhibit NO-induced cell migration in CD36-null, but not CD47-null, muscle explants, indicating CD47 was the primary receptor for anti-angiogenic TSP-1 effects (43).

1.2.4 Signal Regulatory Protein α (SIRP α)

Signal regulatory protein α (SIRP α), also known as SHPS-1, is the other known ligand of CD47 (51, 52). It is a single transmembrane spanning protein tyrosine phosphatase that has three extracellular Ig-like domains (53). CD47 acts as a “marker of self” when bound to SIRP α on circulating macrophages, limiting phagocytosis of red blood cells (54, 55). Therefore, the SIRP α /CD47 interaction plays a key role in the immune system. Binding of CD47 to SIRP α also regulates cell adhesion, with ligation of SIRP α causing a decrease in melanoma cell migration (56). It is important to note that SIRP α can bind to CD47 alone, without another membrane protein binding partner. This is evidenced by the fact CD47 can bind SIRP α on erythrocytes, which have no known integrins on its membrane (57). There has also been recombinant expression of the

extracellular domain of SIRP α , which was shown to bind to a recombinant extracellular domain of CD47 *in vitro* with a 1.2 μm K_d (58). The crystal structure of the extracellular domain of SIRP α bound to the extracellular domain of CD47 showed a high surface complementarity between the two, involving the N-terminal loops of SIRP α (58). The interaction between CD47 and SIRP α involve numerous salt bridges and hydrogen bonds, and an aspartate residue within SIRP α has been shown to be critical to CD47 binding.

1.3 CD47 as a receptor for TSP-1

CD47 is a ~50 kDa transmembrane protein expressed on nearly all cell types and is the receptor for the C-terminal domain of the extracellular matrix protein TSP-1 (59, 60). The binding of TSP-1 to CD47 results in a variety of physiological effects, including platelet aggregation, vasoconstriction, and endothelial cell adhesion and proliferation (43, 50, 61). This has implications in wound healing, cardiovascular disease, and angiogenesis.

1.3.1 Discovery of CD47

CD47 was first identified in 1990 when attempting to discover the antigen that bound to an antibody called B6H12, which was shown to inhibit integrin-dependent phagocytosis (59). It was originally hypothesized that B6H12 was an antibody to an integrin with an RGD-binding site. However, it was shown that B6H12 was an antibody to an integrin-associated protein that physically associated with β_3 integrins on platelets and also affected their function (59). Integrin-associated protein (IAP) was proven to be the same protein as CD47 by use of anti-CD47 as well as anti-IAP antibodies in flow cytometry experiments (62). Later, it was determined that the C-terminal domain of

TSP-1 bound to integrin-associated protein through affinity labeling of a C-terminal peptide of TSP-1 and immunoprecipitation with anti-CD47 antibodies (60).

1.3.2 CD47 structure

CD47 is a widely distributed membrane protein, and has been found on multiple cell types, including monocytes, lymphocytes, platelets, and erythrocytes (59). CD47 is composed of an immunoglobulin-like extracellular domain, followed by five transmembrane helices and intracellular alternatively spliced cytoplasmic domain (63, 64) (Figure 1.4). Based on IgV homology, CD47 is also predicted to contain a disulfide bond between two cysteine residues in the extracellular domain (63). There is also a long-range disulfide bond that exists between a cysteine residue within the extracellular domain and the transmembrane spanning domain (65). There are 5 predicted N-linked glycosylation sites in the extracellular domain of CD47, and one within the transmembrane spanning domains (63, 66). Although glycosylation sites are necessary for CD47 to be expressed at the membrane of yeast cells (67), it has been shown that these glycosylation sites are not necessary for proper CD47 folding (67) nor required for the CD47/SIRP α interaction (68).

1.3.3 E3CaG1

A fragment of TSP-1, called E3CaG1, consists of the third type 2 EGF-like repeat, the calcium binding domain that contains an RGD integrin binding site, and the CD47-binding C-terminal domain (69, 70) (Figure 1.3). E3CaG1 was used to examine the specific effects of CD47 binding without interference from the many other TSP-1-

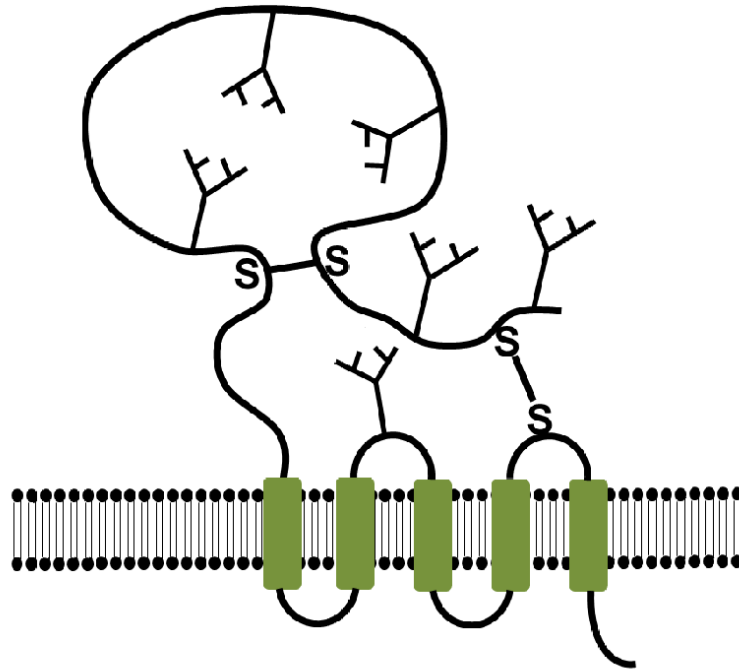


Figure 1.4. Diagram of CD47 structure. CD47 consists of a large, extracellular, IgV-like domain that contains 5 N-linked glycosylation sites. There are 5 predicted transmembrane helices and an alternatively spliced cytoplasmic tail. An additional glycosylation site is predicted to be within the transmembrane domains. CD47 also has two disulfide bonds (S-S), one located within the extracellular domain, and one between the extracellular and transmembrane domains.

binding proteins.

1.4 CD47 associates with other membrane proteins

1.4.1 Integrins

CD47 is widely known to associate with integrin $\alpha_v\beta_3$ on platelets, ovarian OV10 cells, and C32 melanoma cells (59, 71, 72). CD47 has also been shown to physically form a complex with integrin $\alpha_{IIb}\beta_3$ on platelets (73). Binding of the C-terminal domain of TSP-1 to CD47 is known to have an effect on the activity of several integrins, including $\alpha_v\beta_3$, $\alpha_{IIb}\beta_3$, and $\alpha_2\beta_1$ (72, 74, 75). The C-terminal domain of TSP-1 as well as the 4N1K peptide enhances $\alpha_v\beta_3$ mediated melanoma cell spreading, but this enhancement is blocked by an anti-CD47 antibody (72). Binding of the 4N1K peptide, which is derived from the C-terminal domain of TSP-1, to CD47 is also known to activate platelet aggregation through integrin $\alpha_{IIb}\beta_3$ via recruitment of focal adhesion kinase (FAK) (74). Peptide 4N1K was also shown to induce vascular smooth muscle cell chemotaxis, and this response was inhibited by the addition of anti-CD47 and anti- α_2 antibodies (75).

1.4.2 VEGFR2

CD47 has been recently shown to have a constitutive association with the vascular endothelial growth factor receptor 2 (VEGFR2) (76). VEGFR2 is a receptor tyrosine kinase located in endothelial cell membranes. Binding of the ligand VEGF to VEGFR2 is associated with vascular development as well as angiogenesis of blood vessels through the PI3 kinase/Akt signaling pathway (77, 78). Activation of VEGFR2 through the binding of its ligand VEGF results in increased expression and activity of endothelial

nitric oxide synthase (eNOS), thus leading to increased circulating nitric oxide levels (79, 80). However, binding TSP-1 to CD47 causes a disruption of the CD47/VEGFR2 association and results in a dephosphorylation of VEGFR2 (76). Additionally, TSP-1 was shown to inhibit Akt activation through binding to CD47, thus resulting in inhibition of the nitric oxide pathway (76). CD47 is involved with multiple signaling pathways and regulates many cellular functions, as evidenced by its binding to a variety of receptors including integrins, VEGFR2, and SIRP α . Although the ligands of CD47 can bind to it in complex with other receptors (i.e. VEGFR2), the extracellular domain of SIRP α can bind to CD47 alone, and CD47 is present on erythrocytes, which contain no integrins (81). Therefore, CD47 is the receptor of signaling pathways that may or may not involve association with other intracellular membrane proteins.

1.5 TSP-1 as a nitric oxide regulator

TSP-1 binds to CD47 through its C-terminal domain, leading to inhibition of the nitric oxide-binding enzyme sGC and decreased cGMP production (82-84). TSP-1-induced inhibition of sGC can ultimately lead to multiple physiological effects, including vasoconstriction, decreased angiogenesis, and impaired wound healing (61, 85-87).

1.5.1 TSP-1 binding to CD47 downregulates sGC through a rise in intracellular calcium

It has been shown in endothelial and vascular smooth muscle cells that picomolar levels of TSP-1 binding to CD47 causes a decrease in cGMP levels through the nitric oxide receptor sGC (43, 86). Ligation of CD47 causes a decrease in NO-stimulated responses such as vascular cell adhesion, migration, and proliferation (43). TSP-1 has

been reported to cause a decrease in NO-stimulated tissue perfusion (88). Antibody ligation of TSP-1 or genetic knockdown of CD47 caused an increase in tissue survival (88, 89), indicating TSP-1 binding to CD47 contributed to ischemia in injured tissues. It has been recently shown in our lab that E3CaG1 binding to CD47 causes a rise in $[Ca^{2+}]_i$ in Jurkat T lymphocytes, which in turn decreases cGMP levels (82). Inhibition is through sGC phosphorylation, which reduces the K_m for GTP by 13-fold (82). Therefore, the increase in $[Ca^{2+}]_i$ is the direct link between the anti-angiogenic properties of the C-terminal domain of TSP-1 the inhibition of the nitric oxide signaling pathway through sGC. Angiotensin II (Ang II) is another ligand that inhibits sGC activity through binding to its G protein-coupled AT_1 receptor on endothelial and vascular smooth muscle cells (90, 91). Ang II causes an increase in $[Ca^{2+}]_i$ through activation of phospholipase C (PLC) and extrusion of calcium ions from the sarcoplasmic reticulum. A particular study found the decrease in cGMP levels caused by Ang II was reversed by the calcium/calmodulin-dependent phosphodiesterase inhibitor IBMX (90), and we have shown in our lab that Ang II-induced calcium increases directly inhibited sGC activity (82). This shows that both TSP-1 and Ang II inhibit sGC through an $[Ca^{2+}]_i$ increase.

1.5.2 TSP-1, VEGFR2, and calcium

VEGFR2 can associate with β_1 integrins as well as $\alpha_v\beta_3$ in addition to its association with CD47 and CD36 (45, 92, 93). Integrin $\alpha_v\beta_3$ is a multifunctional signaling molecule that has been shown to have pro-angiogenic as well as anti-angiogenic properties depending on which proteins it binds and associates with (94). For example, VEGF binding to VEGFR2 induces phosphorylation of $\alpha_v\beta_3$ to induce adhesion and

migration of endothelial cells (95). However, TSP-1 can bind directly to $\alpha_v\beta_3$ via an RGD domain (41), and it has been suggested this can cause localization of TSP-1 to cell surfaces to promote its anti-angiogenic effects (94, 96).

TSP-1 can modulate the calcium activity of $\alpha_v\beta_3$. TSP-1 has been shown to cause calcium influxes in IMR-90 fibroblasts, and the process involves binding to both $\alpha_v\beta_3$ and CD47 (97). CD47 was also shown to be necessary for the calcium increase in endothelial cells which involved fibronectin-binding integrins (98). Taken together, these data show that angiogenesis is a multifaceted process involving multiple membrane receptors including integrins, VEGFR2, and CD47, and that TSP-1 can regulate angiogenic physiologic responses depending on the protein complexes to which it binds.

1.6 Research Topic

The goal of this dissertation was to identify possible membrane binding partners that associate with CD47 and are required for the decrease in sGC activity induced by TSP-1 (Figure 1.6). In Chapter 2, I describe how the use of PWR spectroscopy allowed for measurement of dissociation constants for a C-terminal fragment of TSP-1 binding to native cell membranes, and that multiple CD47 complexes exist within these membranes. In Chapter 3, I identify the membrane proteins that are associated with CD47 and involved in TSP-1 binding. I determined that CD47 was associated with both VEGFR2 and integrin $\alpha_v\beta_3$ through PWR spectroscopy. In addition to its association with CD47, I discovered VEGFR2 also formed a complex with $\alpha_v\beta_3$ on native Jurkat T lymphocyte plasma membranes. Our hypothesis was that VEGFR2 was required for TSP-1 binding to CD47, and TSP-1 binding to this complex causes a rise in $[Ca^{2+}]_i$. In Chapter 4, I

show that VEGFR2 is involved in TSP-1-induced calcium increase through the use of a flow cytometry fluorescence-based calcium assay. In Chapter 5, I use HEK 293T cells containing knockouts of both CD47 and VEGFR2 to prove that both proteins are required for the increase in $[Ca^{2+}]_i$ observed upon TSP-1 binding. In Chapter 6, I discuss further experiments that would strengthen the conclusion that the VEGFR2 association with CD47 is required for TSP-1-induced calcium increase. These include purification of cloned CD47 and structural studies by X-ray crystallography, as well as insertion of purified CD47 into a synthetic lipid bilayer and measurement of TSP-1 binding. Critical residues of CD47 involved in TSP-1 binding could also be identified through mutagenesis and subsequent PWR binding studies.

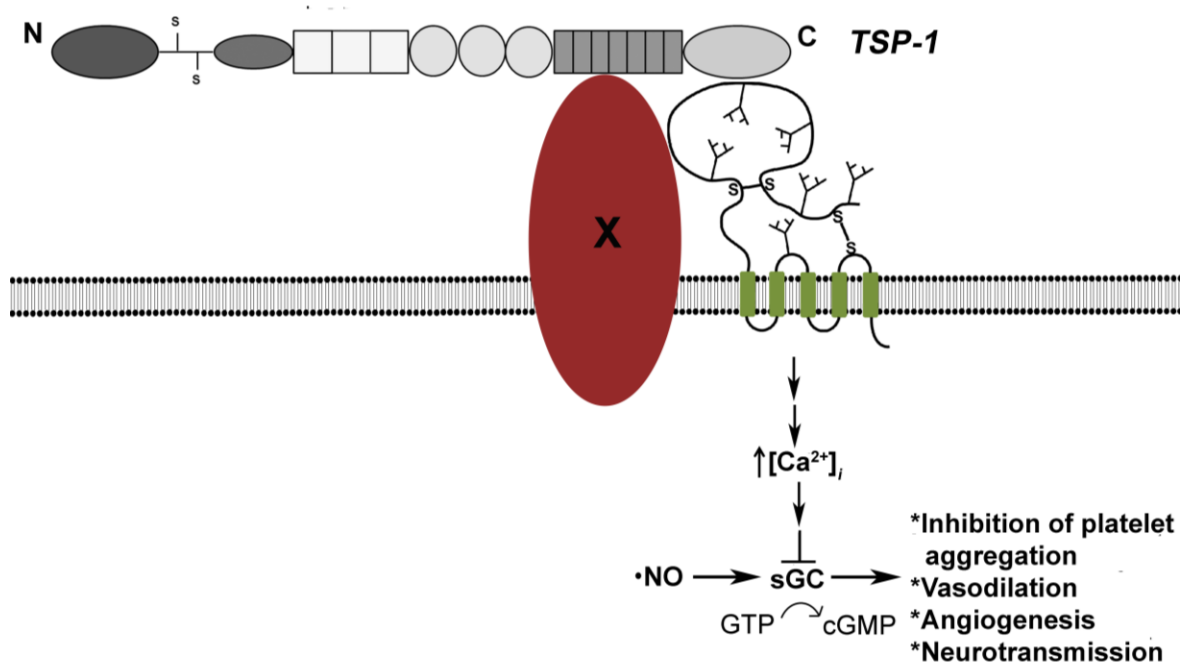


Figure 1.5. Diagram of research goal. TSP-1 binds to CD47 through its C-terminal domain, causing an increase in $[Ca^{2+}]_i$, ultimately causing a decrease in sGC activity and a reduction in cGMP levels. CD47 is known to associate with multiple membrane proteins, including β_1 and β_3 integrins as well as VEGFR2. The goal of my work was to determine if other membrane proteins were required for TSP-1 induced inhibition of sGC.

CHAPTER 2

. DEVELOPMENT OF PLASMON-WAVEGUIDE RESONANCE (PWR) SPECTROSCOPY FOR MEASUREMENT OF THROMBOSPONDIN-1 BINDING TO NATIVE JURKAT MEMBRANES

2.1 Introduction to PWR

Plasmon-waveguide resonance spectroscopy is an optical technique that can be used to measure binding affinities of ligands to membrane receptors as well as give information about structural changes a receptor undergoes upon ligand binding. PWR has been used previously to determine binding constants as well as different conformations due to ligand binding to the human δ -opioid receptor (99, 100). It is important to note that PWR can be used to examine ligand/receptor interactions in a native plasma membrane. This is crucial when determining binding constants to receptors such as CD47, whose ligand binding can involve multiple membrane protein binding partners. Details concerning the theory and analysis of PWR have been described elsewhere (101-107). PWR involves coupling plasmon-generating modes within a metal film to waveguide modes under total internal reflection conditions. Total internal reflection occurs when light traveling through a material with a specific refractive index reaches the interface of a second material with a different refractive index at an incident angle that is greater than critical angle. This only occurs when the refractive index of the light traveling through the first material (n_1) is greater than the refractive index of the second material (n_2), according to Snell's Law ($n_1[\sin\theta_1] = n_2[\sin\theta_2]$). The resonator (or plasmon waveguide), which consists of a glass prism

containing a 50 nm layer of silver beneath a 500 nm layer of silica (n_1), is in contact with an aqueous buffer medium (n_2) and placed on a rotating table to record the PWR spectrum (Figure 2.1). The refractive index of the glass prism substrate (n_3) also has to be less than that of the waveguide in order for total internal reflection to occur between each of the interfaces (108). The silver is responsible for producing plasmon modes, and the dielectric silica acts as a waveguide, in which resonances can be excited at the expense of the incident light energy. Surface plasmon resonance spectroscopy (SPR) does not include the dielectric silica layer on the prism surface, and therefore is less sensitive than PWR. Activation of waveguide modes produces an evanescent electromagnetic field on the surface of the silica that decays exponentially into the adjacent medium. The interaction between the evanescent electromagnetic field and molecules immobilized on the silica surface (such as deposited membrane fragments) allows for changes in optical characteristics to be measured. Under resonance conditions, the electromagnetic wave from the polarized light couples to that of the guided waves in the silica, producing a dramatic decrease in reflected light intensity. Polarized light reflected through the prism excites waveguide modes using both p - and s -polarized light (perpendicular and parallel to the prism surface, respectively) to generate two independent PWR spectra. Changes in the refractive index of both p - and s -polarized light (n_p and n_s , respectively) affect the angle at which the waveguide modes are excited. Since p -polarized light is perpendicular and s -polarized light is parallel to the prism surface, changes in n_p and n_s can give information regarding mass and/or structural changes that occur upon ligand binding. In addition, plotting resonance position shifts as

a function of the amount of ligand added to the prism surface can be used to determine dissociation constants. In this chapter, PWR spectroscopy is used to measure the E3CaG1 binding to Jurkat T cell plasma membranes in order to calculate K_d values. Jurkat cells lose their ability to bind E3CaG1 over time or under high density growth conditions, yet retain CD47 on their membrane. This led to the hypothesis that another membrane protein might be associated with CD47 and involved in E3CaG1 binding, and the presence of this associated protein changes over time. This chapter also describes how PWR spectroscopy was used to identify a possible candidate for the membrane protein in complex with CD47 involved in E3CaG1 binding.

2.2 Materials and Methods

2.2.1 Materials

CD47 monoclonal antibody (B6H12) (1 mg/ml) and an isotype control antibody (IgG₁, κ -FITC) were obtained from eBioscience (San Diego, CA). Anti-Na⁺/K⁺ ATPase antibody (C464.6) was obtained from Millipore (Temecula, CA). Jurkat T cells were purchased from ATCC (T1B-152). Recombinant SIRP α -Fc was a generous gift from Dr. Thomas Miller (NIH). Phosphate-buffered saline (PBS) was prepared as 10 mM KH₂PO₄, 10 mM Na₂HPO₄, 137 mM NaCl, 2.7 mM KCl, pH 7.4. Tris-buffered saline (TBS) was prepared as 10 mM Tris HCl, 150 mM NaCl, pH 7.4. Lysis buffer was prepared as 50 mM Tris-HCl, 100 mM KCl, pH 7.5, supplemented with 4% (v/v) mammalian protease inhibitor cocktail (Sigma, St. Louis, MO). Sucrose solutions were made in 50 mM Tris-HCl, 100 mM KCl, pH 7.5 and filtered using a 0.2 μ m filter (to ensure purity) for use in sucrose gradients. The baculovirus vector pAcGP67.coco was

kindly provided by Dr. Deane Mosher (University of Wisconsin). PWR prisms were coated by Evaporated Coatings, Inc. (Willow Grove, PA). Unless otherwise noted, all other materials were obtained from Sigma.

2.2.2 Cell culture

Sf9 insect cells were grown in Grace's Insect Media (Invitrogen) containing 10% FBS, gentamicin, and fungizone. Jurkat T cells were maintained in RPMI 1640 (Invitrogen) supplemented with 5% - 10% fetal bovine serum (FBS), 5 mg/ml penicillin, and 1 mg/ml streptomycin grown at 37 °C in 5% CO₂. Jurkat T cells considered low-passage were cultured at a density below 2 x 10⁶ cells/ml for less than 3 weeks. Jurkat T cells considered high-passage were cultured for longer than 4 weeks or at a density above 3 x 10⁶ cells/ml. MCF-7 cells were maintained in DMEM supplemented with 10% FBS, 5 mg/ml penicillin, and 1 mg/ml streptomycin grown at 37 °C in 5% CO₂.

2.2.3 Preparation of plasma membrane fragments

Approximately 10⁸ Jurkat T cells were centrifuged at 300 x g in a Dynac centrifuge (Becton Dickinson, Franklin Lakes, NJ) for 5 min to pellet cells. Pellets were washed twice with 5 ml of PBS buffer, frozen quickly in liquid nitrogen and stored at -80 °C until further use. Pellets were lysed by resuspending in 250 µl lysis buffer and disrupted with 25 strokes using a 25 gauge needle. This lysate was centrifuged at 1000 x g at 4 °C for 10 min to remove unbroken cells and nuclei. The supernatants were carefully layered on top of a discontinuous sucrose gradient prepared using 750 µl each of 50%, 45%, 40%, 35%, and 30% sucrose solutions. The gradients were centrifuged at 200,000 x g for 17 h at 4 °C using a SW60 rotor (Beckman, Brea, CA) with acceleration

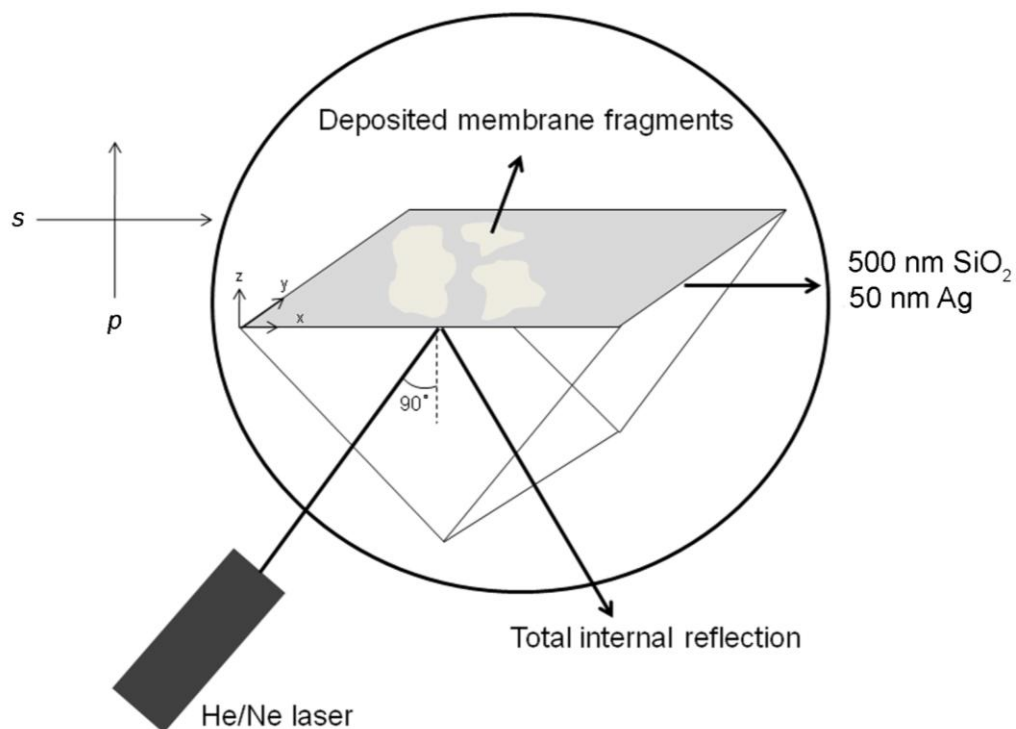


Figure 2.1. PWR instrument setup. Polarized light from a He/Ne laser is totally internally reflected through a glass prism that has a 50 nm layer of Ag overlaid by a 500 nm layer of dielectric SiO₂. The resonator is placed on a rotating table so reflected light intensity is measured as a function of incident angle. Total internal reflection excites waveguide modes using *p*- and *s*-polarized light to generate an evanescent electromagnetic field, producing a decrease in reflected light intensity. Deposition of membrane fragments on the prism surface alters the angle at which resonance occurs and alters the characteristics of the PWR spectrum. Changes in resonance angle as a function of concentration of ligand added can be used to measure K_{ds} .

and deceleration profiles of 7. After centrifugation, a clear band was visible at the 35% interface. 400 μ l fractions were taken from the top of the gradient, and those containing membrane were pooled, diluted 10-fold with 50 mM Tris-HCl, 100 mM KCl, pH 7.5 and centrifuged at 100,000 $\times g$ for 1 h at 4 °C. The pellets were resuspended in 200 μ l of the same buffer, and aliquots were frozen quickly in liquid nitrogen and stored at -80 °C until further use. A BCA assay (Thermo Scientific) was used to determine total protein concentrations using bovine serum albumin (BSA) as the standard.

2.2.4 Purification of E3CaG1

E3CaG1 was purified as described previously (82, 109). Sf9 insect cells at a density of 1×10^6 cells/ml were transferred into serum-free SF900II media (Invitrogen) prior to infection with baculovirus encoding E3CaG1 with a multiplicity of infection of 5. After infecting for 65 hours, media containing secreted E3CaG1 was added to Ni²⁺-NTA beads (Qiagen, Valencia, CA) to purify E3CaG1 using its N-terminal His-tag. Beads were washed with 10 mM Tris-HCl, 150 mM NaCl, 15 mM imidazole, pH 7.2, then eluted with 10 mM Tris-HCl, 150 mM NaCl, 2 mM CaCl₂, 300 mM imidazole, pH 7.2. Purified E3CaG1 was dialyzed into TBS with 2mM CaCl₂ and aliquots were stored at -80 °C until further use. A BCA assay was performed to determine total protein concentration, as described above.

2.2.5 Preparation of prisms for PWR spectroscopy

Before each use, prisms were cleaned in a 1% solution of Tergazyme (Alconox, White Plains, NY) for 30 minutes in a sonicating water bath. Afterwards, 3 washes of 10 min each in Millipore-filtered water were performed with a thorough rinsing of the prism

in Millipore-filtered water between each wash. The prisms were dried with nitrogen gas for immediate use.

2.2.6 Deposition of membrane fragments onto PWR prism

The sample cell was filled with 50 mM Tris-HCl, 100 mM KCl, pH 7.5 and allowed to equilibrate before addition of membrane fragments. After equilibration of the buffer occurred, the prism was separated from the sample cell. A solution of 10 μ l of 100 mM CaCl_2 was deposited onto the silica surface of the prism, followed by 10 μ l of purified plasma membranes and allowed to equilibrate for 25 min at room temperature. Addition of CaCl_2 to membranes allowed for better adherence to the silica surface. The resonator was then placed in the sample compartment of the PWR spectrometer. The prism was washed 4 times with 50 mM Tris-HCl, 100 mM KCl, pH 7.5 at 100 μ l/sec to remove unbound membrane and excess calcium ions. Changes in the PWR spectra were recorded after membrane deposition.

2.2.7 Addition of E3CaG1 to sample cell

Stock solutions of E3CaG1 were used to make 1 μ M, 50 nM, 12.5 nM, 7.5 nM, 2.5 nM, 1.5 nM, and 0.5 nM dilutions. E3CaG1 dilutions for use in PWR were made in TBS supplemented with 2 mM CaCl_2 . Dilutions were added in 1 μ l increments to the 500 μ l PWR sample cell to make the final concentrations indicated and slowly mixed with a Hamiltonian syringe. Changes in the PWR spectra were recorded after ligand addition. PWR spectra were allowed to equilibrate prior to addition of subsequent ligand additions. Equilibration time ranged between 15 and 45 minutes. We approximate the total amount of ligand added is larger than the amount of membrane receptor within the

membrane, given that the sample cell volume is approximately 1000 times larger than the volume of deposited membrane in contact with the sample cell (103). This is to ensure equilibrium dissociation constants are being measured. For example, purified membrane concentrations contained approximately 0.2 mg/ml total protein, and these samples included plasma membranes, membranes from the endoplasmic reticulum, Golgi, lysosomes, etc. Assuming 10% of the sample contained plasma membrane, this would translate into approximately 5 ng of plasma membranes in contact with the sample cell after addition and equilibration. The amount of CD47 could constitute approximately 1 - 5% of the total plasma membrane deposited on the prism surface in order for the amount of ligand added to be sufficiently larger than the amount of receptor, but in actuality the concentration of CD47 within the plasma membrane could be much smaller. This indicates our instrument setup and sample deposition is appropriate for measuring dissociation constants, even at the picomolar level.

2.2.8 Addition of CD47/isotype antibodies to sample cell

Stock solutions of antibody were used to make 50 nM, 12.5 nM, 7.5 nM, 2.5 nM, 1.5 nM, and 0.5 nM dilutions. Antibody dilutions for use in PWR spectroscopy were made in 50 mM Tris-HCl, 100 mM KCl, pH 7.5. Dilutions were added in 1 μ l increments to the 500 μ l PWR sample cell to make the final concentrations indicated, and changes in the PWR spectra were recorded.

2.2.9 PWR instrument

Plasmon waveguide resonance spectroscopy was performed using a Beta PWR

instrument (Proterion Corporation) that measures reflected light intensity from a CW laser (He-Ne; $\lambda = 632.8$ nm) as a function of incident angle. Minimums in reflected light intensity at the resonance angle upon ligand addition were compared to that of the membrane without any ligand added to obtain ligand resonance position shifts (LRS). The resonance angle of the membrane was also compared to that of buffer alone to obtain the membrane resonance position shift (MRS). The ligand resonance position shift was divided by the membrane resonance position shift measured using both *p*- and *s*-polarized light and multiplied by 100 to obtain percent resonance position shifts (% RS = [LRS/MRS] x 100). Binding experiments were repeated at least three times, and the titration curves shown in figures are representative of one experiment.

2.2.10 Data Analysis

Bar graphs depict an average of at least three independent experiments \pm standard error of the mean (SEM). Statistical analysis to determine the significance between data sets was performed using an unpaired Student's *t*-test. Values of $p \leq 0.05$ (*), and $p \leq 0.01$ (**) were considered statistically significant. 2-parameter hyperbolic PWR binding curves were fit using the equation $y = a[x]/(K_d + x)$. 3-parameter hyperbolic PWR binding curves were fit using the equation $y = y_0 + ((a[x])/K_d + x)$. Data sets were fit using 2-parameter hyperbolic functions when the final membrane resonance position after washing was used as the initial zero concentration of ligand/antibody added. A 3-parameter hyperbolic function was used when initial concentrations of ligand/antibody added did not produce significant resonance position shifts, and therefore a zero

concentration was not used as the initial data point. Sigmoidal PWR binding curves were fit using the equation $y = a/(1 + e^{-((x - K_d)/b)})$.

2.3 Results

2.3.1 CD47 is required for E3CaG1 binding

In order to determine the necessary membrane components involved in TSP-1 binding to CD47, PWR spectroscopy was performed using purified Jurkat plasma membranes. Purified Jurkat plasma membranes were placed on the PWR resonator, and a spectral shift was recorded, indicating deposition of the membrane fragments occurred. An increase in resonance position of at least 100 mdeg using *p*-polarized light was recorded for each experiment, which indicated enough membranes were deposited to measure a subsequent ligand spectral shift (Figure 2.2). Prisms were then washed to remove unbound membranes and equilibrated before subsequent ligand/antibody addition. A typical *s:p* ratio ranging from 0.5-0.7 was observed upon membrane addition for experiments, which is similar to previously reported values (*110, 111*). These values indicate resonance position shifts measured using *s*-polarized light are less than resonance position shifts measured using *p*-polarized light. This translates into higher changes in refractive index as measured by *p*-polarized light than by *s*-polarized light. These differences in resonance position depending on the polarization of light used could indicate that membranes maintain a molecular order when deposited upon the prism surface (*111*).

Before we determined TSP-1 could bind to CD47 on Jurkat plasma membranes, it was first determined that CD47 was present on the membrane fragments. Previous flow

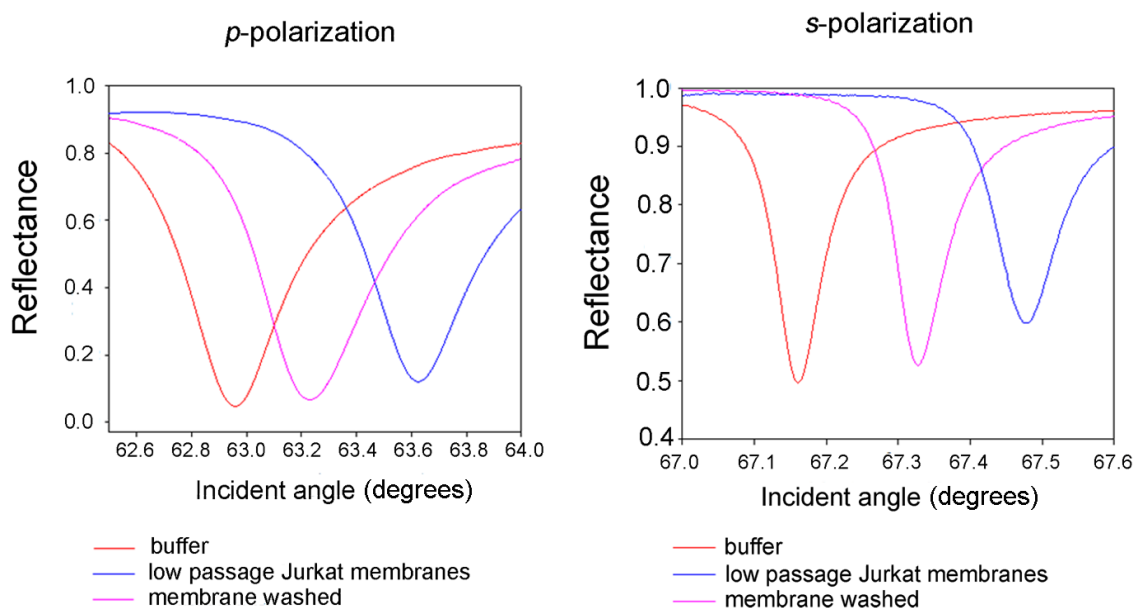


Figure 2.2. Typical PWR spectra observed for *p*- and *s*-polarized light. Red spectra show the resonance angle observed upon addition of buffer (50 mM Tris-HCl, 100 mM KCl, pH 7.5) alone. Blue spectra show the resonance angle measured upon addition of membranes to the prism surface. The resonance position increases dramatically, indicating an increase in refractive index. The pink spectra show the resonance angle upon washing the membrane. The resonance position decreases compared to unwashed membrane, indicating a decrease in refractive index both perpendicular and parallel to the prism surface, which could be explained by removal of some membrane from the prism surface.

cytometry experiments from our laboratory indicate that although Jurkat T lymphocytes retain CD47 on their surface, over time they lose the ability to bind to TSP-1 (82). To observe if the same trend could be measured by PWR spectroscopy, low-passage Jurkat T lymphocyte plasma membranes were placed in a PWR spectrophotometer, and increasing amounts of anti-CD47 antibody was added to determine a dissociation constant (Figure 2.3). An average K_d of 1.3 pM was measured (Table 2.1), indicating CD47 was present on the membranes. When increasing amounts of anti-CD47 antibody were added to high-passage Jurkat plasma membranes, a similar K_d of 1.7 pM was measured (Figure 2.4, Table 2.1), showing CD47 is continuously present.

2.3.1.1 Addition of anti-CD47 antibody inhibits E3CaG1 binding

To measure TSP-1 binding to CD47, a recombinant C-terminal fragment of TSP-1 called E3CaG1 was used. E3CaG1 contains the third type II repeat, the calcium-binding domain, as well as the C-terminal domain known to bind to CD47 (69, 70). This fragment was used in order to avoid complications due to the other domains of TSP-1 binding to their various receptors. It is important to note, however, that E3CaG1 retains an RGD sequence in the last type III repeat that binds to integrin $\alpha_v\beta_3$ (40, 41) in addition to the C-terminal domain that binds to CD47. As a control experiment, E3CaG1 did not significantly bind to the prism surface if no membranes were deposited (Figure 2.5). To determine if E3CaG1 was binding to CD47, a saturating amount of E3CaG1 was added to purified Jurkat plasma membranes followed by 13.3 nM of anti-CD47 antibody (Figure 2.6). Unlike with antibody alone, no significant spectral shifts were observed upon

TABLE 2.1. List of dissociation constants determined by PWR spectroscopy

Ligands/Antibodies added to low-passage purified Jurkat plasma membranes	K_d (pM) \pm SD
E3CaG1 ^a	1.3 \pm 0.65
E3CaG1 ^b	2300 \pm 790
SIRP α ^c	3.1 \pm 1.7
anti-CD47 (B6H12) Ab ^d	1.3 \pm 0.29
anti- α_v (272-17E6) Ab ^e	1.2 \pm 0.7
anti-VEGFR2 (260.4) Ab ^f	2.9 \pm 3.01
anti-CD47 (B6H12) Ab then E3CaG1 ^g	no binding
anti- α_v (272-17E6) Ab then E3CaG1 ^h	retained pM binding, no nM binding
anti-VEGFR2 (260.4) Ab then E3CaG1 ⁱ	no pM binding, reduced nM binding
Ligands/Antibodies added to high-passage purified Jurkat plasma membranes	
SIRP α ^j	1.4 \pm 1.4
anti-CD47 (B6H12) Ab ^k	1.7 \pm 0.71
E3CaG1 ^l	no binding
Ligands/Antibodies added to CD47-JinB8 plasma membranes (expression on)	
E3CaG1 ^m	1.3 \pm 0.85
E3CaG1 ⁿ	1300 \pm 460
anti-VEGFR2 (260.4) Ab then E3CaG1 ^o	no pM binding, no nM binding
anti-CD47 (B6H12) Ab then E3CaG1 ^p	no pM binding, retained nM binding
Ligands added to MCF-7 purified plasma membranes	
E3CaG1 ^q	1.7 \pm 0.77
Ligands added to CD47-JinB8 plasma membranes (expression off)	
E3CaG1 ^r	1800 \pm 1000

^a pM E3CaG1 titration curves (n = 3, ranging from 1 pM to 150 pM)

^b nM E3CaG1 titration curves (n = 3, 200 pM E3CaG1 was added to saturate pM binding sites, then nM E3CaG1 was added, ranging from 1.2 nM to 6 nM)

^c pM SIRP α titration curves (n = 3, ranging from 1 pM to 50 pM)

^d anti-CD47 (B6H12) Ab titration curves (n = 4, ranging from 1 pM to 50 pM)

^e anti- α_v (272-17E6) titration curves (n = 3, ranging from 1 pM to 30 pM)

^f anti-VEGFR2 (260.4) Ab titration curves (n = 3, ranging from 1 pM to 25 pM)

^g anti-CD47 (B6H12) Ab titration curve was performed, then no significant binding occurred upon subsequent addition of 5 nM E3CaG1 (n = 4)

- ^h 13.3 nM anti- α_v (272-17E6) Ab was added to membranes and allowed to equilibrate, followed by the addition of 5 pM E3CaG1, then an additional 5 nM E3CaG1 was added (n = 3)
- ⁱ 50 pM or 10 nM anti-VEGFR2 (260.4) Ab was added to membranes (different amounts did not alter % resonance position shifts because the K_d for antibody binding is low pM) and allowed to equilibrate, followed by the addition of 50 pM E3CaG1, then up to 5 nM E3CaG1 was additionally added (either a single amount was added or a nM titration curve was performed, n = 3)
- ^j SIRP α titration curves (n = 3, ranging from 1 pM to 30 pM)
- ^k anti-CD47 (B6H12) Ab titration curves (n = 3, ranging from 0.5 pM to 75 pM)
- ^l One E3CaG1 titration curve was performed (ranging from 15 nM to 170 nM), and other experiments were performed in which 5 nM E3CaG1 was added to membranes (n = 2, no apparent binding was observed in any case)
- ^m pM E3CaG1 titration curves (n = 3, ranging from 0.5 pM to 5 pM)
- ⁿ nM E3CaG1 titration curves (n = 3, ranging from 1 nM to 5 nM)
- ^o 50 pM anti-VEGFR2 (260.4) Ab was added to membranes and allowed to equilibrate, followed by the addition of 50 pM E3CaG1, then an additional 5 nM E3CaG1 was added (n = 3)
- ^p 13.3 nM anti-CD47 (B6H12) Ab was added to membranes and allowed to equilibrate, followed by the addition of 50 pM E3CaG1, then an additional 5 nM E3CaG1 was added (n = 3)
- ^q pM E3CaG1 titration curves (n = 4, ranging from 0.5 pM to 50 pM)
- ^r nM E3CaG1 titration curves (n = 3, 50 pM E3CaG1 was added to saturate pM binding sites, then additional nM E3CaG1 was added, ranging from 1 nM to 5 nM).

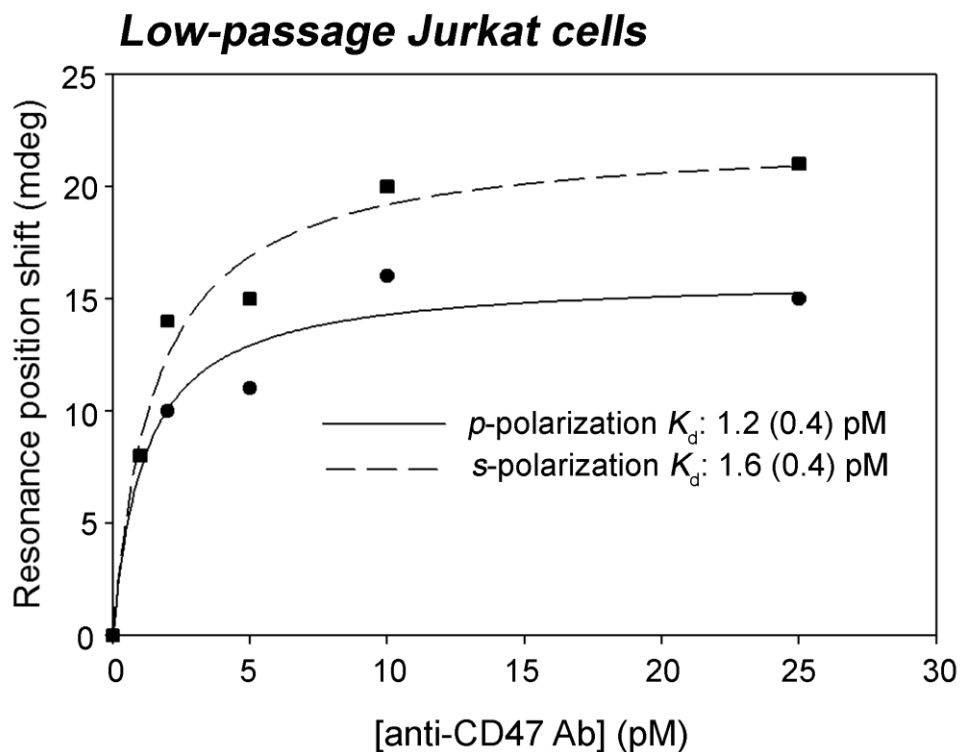


Figure 2.3. CD47 is present on low-passage Jurkat plasma membranes. Representative binding curve of anti-CD47 antibody added to low-passage purified Jurkat plasma membranes. An anti-CD47 Ab (B6H12) was added in increasing concentrations to membranes until saturation was reached. Dissociation constants measured with both p - and s -polarized light were calculated using 2-parameter hyperbolic fits.

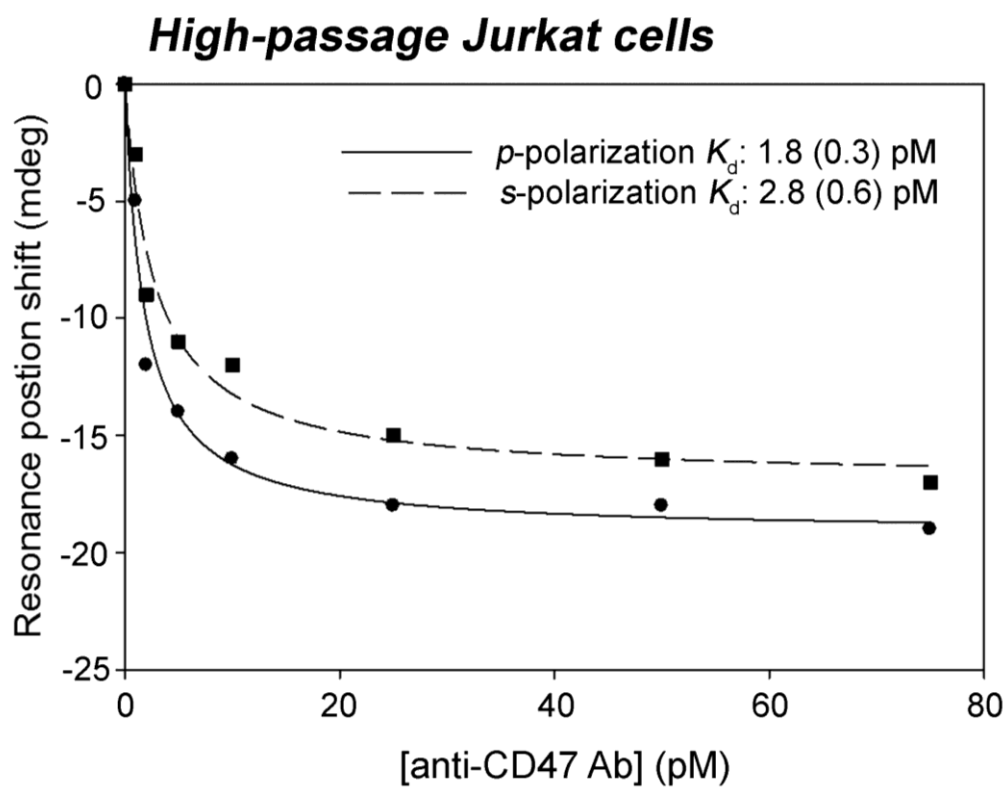


Figure 2.4. CD47 is present on high-passage Jurkat plasma membranes. Representative binding curve of anti-CD47 Ab to young purified Jurkat plasma membranes.

Experiments were performed as described for Figure 2.3.

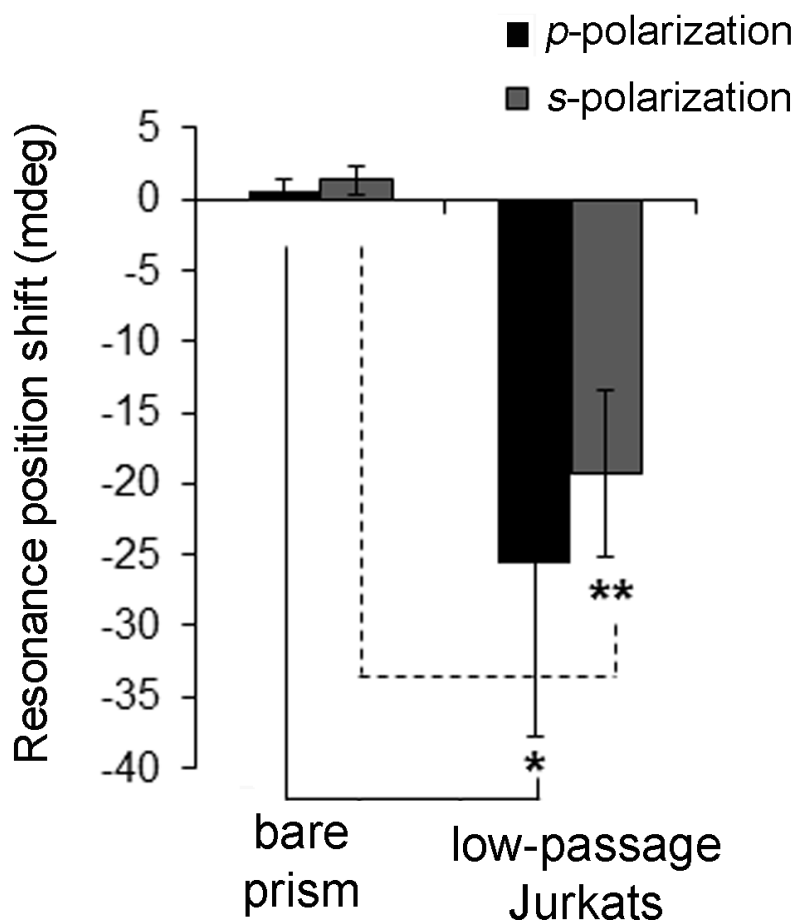


Figure 2.5. E3CaG1 does not bind to the prism surface. Resonance position shifts are shown from addition of E3CaG1 to a bare prism in contact with buffer, as well as from addition of E3CaG1 to low-passage Jurkat plasma membranes ($n = 3$ for each condition). There are minimal resonance position shifts observed from addition of E3CaG1 to the bare prism, indicating E3CaG1 does not bind to the silica of the prism surface.

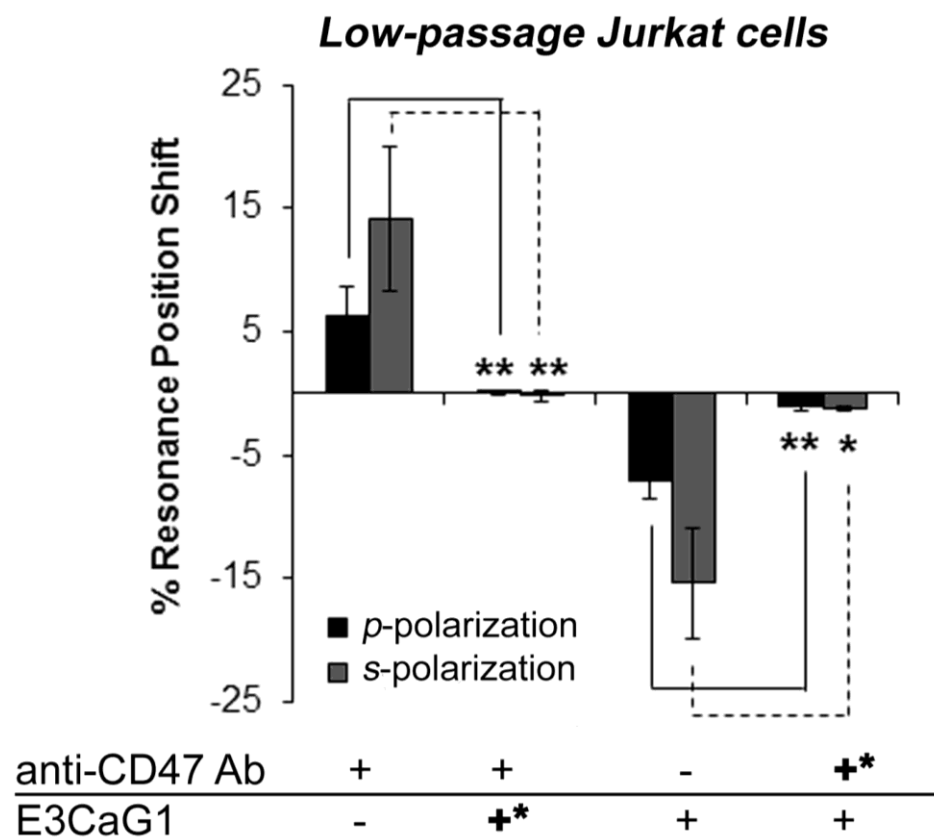


Figure 2.6. E3CaG1 binds to CD47. Bar graphs depicting PWR percent resonance position shifts of anti-CD47 (B6H12) Ab, with and without prior E3CaG1 incubation. +* indicates the ligand/antibody that was first added. – indicates no second protein was added to the membrane. For experiments where both antibody and E3CaG1 were added, the data shown are for the second protein. The expected shift for the addition of the first protein was observed in all cases. E3CaG1 additions show total percent resonance position shifts after pM titration curves were performed (up to 150 pM added). 13.3 nM anti-CD47 Ab was added after E3CaG1 titration curves or after one large amount of E3CaG1 (2 nM) was added to the membrane. Anti-CD47 Ab additions show total

percent resonance position shifts after pM titration curves were performed (up to 13.3 nM added). 5 nM E3CaG1 was added after CD47 Ab titrations. The graph also shows percent resonance position shift caused by E3CaG1, with and without prior anti-CD47 antibody incubation. anti-CD47 Ab binding is inhibited by the presence of E3CaG1, and vice versa.

addition of the anti-CD47 antibody, indicating E3CaG1 was indeed binding to its membrane receptor CD47. Purified Jurkat plasma membranes were also pre-incubated with a saturating amount of anti-CD47 antibody prior to 5 nM E3CaG1, and the latter produced no further significant resonance position shifts, confirming the specificity of E3CaG1 binding (Figure 2.6).

The negative resonance position shift observed upon E3CaG1 binding is indicative of a decrease in refractive index, which could be caused by a decrease in mass. To ensure addition of E3CaG1 was not removing membranes from the prism surface, a Na^+/K^+ ATPase antibody was added to purified MCF-7 plasma membranes, followed by the addition of anti-VEGFR2 antibody. The Na^+/K^+ ATPase antibody produced a decrease in resonance position, mimicking the negative resonance position shift of E3CaG1. Binding of this antibody should not affect the subsequent binding of the anti-VEGFR2 antibody if the membranes were still adhered to the prism surface, and we indeed observed that binding of the Na^+/K^+ ATPase antibody did not prevent the subsequent positive resonance position shift from anti-VEGFR2 antibody binding (Figure 2.7). Therefore, the decrease in resonance position from E3CaG1 binding is possibly due to a large conformational change that results in a decrease in refractive index or a rearrangement within the membrane that causes a mass decrease.

2.3.1.2 Addition of an isotype antibody and Angiotensin II do not inhibit E3CaG1 binding

To ensure the anti-CD47 antibody was not nonspecifically binding to Jurkat membranes, an anti-mouse isotype antibody was added to low-passage Jurkat plasma

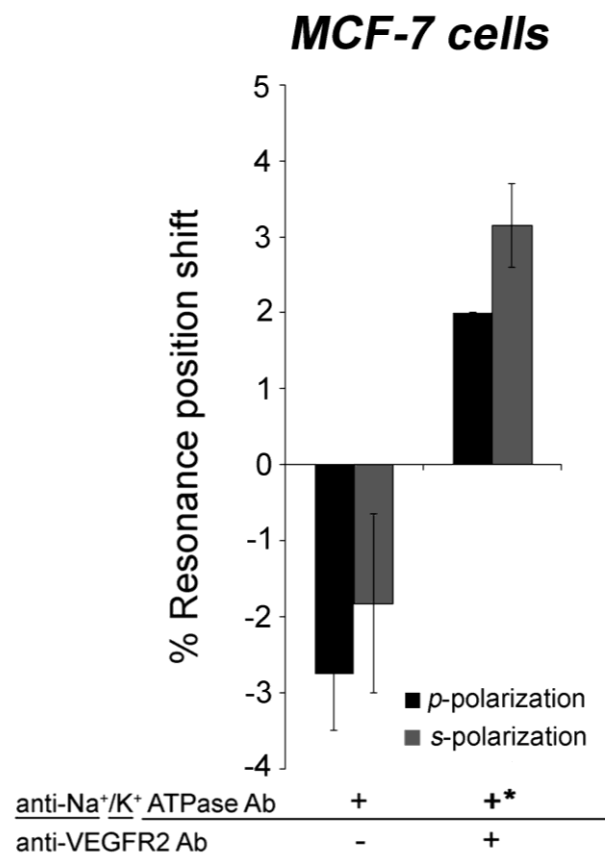


Figure 2.7. Negative resonance position shifts do not inhibit subsequent antibody binding. PWR bar graph showing addition of anti-Na⁺/K⁺ ATPase Ab (C464.6) followed by anti-VEGFR2 (55B11) Ab. +* indicates the ligand/antibody first added. – indicates no second protein was added to the membrane. For experiments where both proteins were added, the data shown are for the second protein. Addition of 13.3 nM anti-Na⁺/K⁺ ATPase Ab produced a decrease in refractive index using both *p*- and *s*-polarized light, which did not prevent the subsequent increases in refractive index caused by addition of a 1:250 dilution of anti-VEGFR2 Ab. This suggests negative resonance position shifts do not indicate removal of membrane from the prism surface, but rather a possible

conformational change that causes a decrease in the refractive index of the light interacting with material on the prism surface. Error bars are representative of the range of 2 independent experiments.

membranes prior to the addition of E3CaG1. Addition of 1 nM isotype antibody did not produce significant spectral shifting upon addition to low-passage Jurkat plasma membranes, indicating minimal binding occurred (Figure 2.8). In addition, the presence of the isotype antibody did not inhibit subsequent resonance position shifts upon 5 nM E3CaG1 addition, which demonstrated the anti-CD47 antibody inhibition of E3CaG1 was specific and that membranes remain functional throughout the experiment. The accuracy of our PWR measurements were substantiated by adding Angiotensin II (Ang II), to purified Jurkat plasma membranes. An average K_d of 0.56 nM was measured (Figure 2.9), which is similar to reported values that range between 0.2-1.0 nM (112-114).

2.3.2 E3CaG1 binds to CD47 on purified Jurkat plasma membranes with picomolar and nanomolar dissociation constants

After determining E3CaG1 was binding to CD47, increasing amounts of E3CaG1 were added to determine the K_d . Two distinct dissociation constants were observed. Higher affinity binding occurred with an average K_d of 1.3 pM, and lower affinity binding occurred with an average K_d of 2.3 nM (Figures 2.10 and 2.11). This indicates multiple CD47 complexes are present within Jurkat plasma membranes.

The expected binding curve for a simple system is increasing resonance position shift for added mass. Neither pM nor nM binding displayed this behavior: both gave a negative resonance position shift, and nM binding produced a sigmoidal curve. This behavior was saturable and reproducible. While the full reason for this is not yet apparent, similar observations have been made by adding the antagonist naltrindole (NTI) to the human brain δ -opoid receptor (103). Addition of NTI caused decreases in

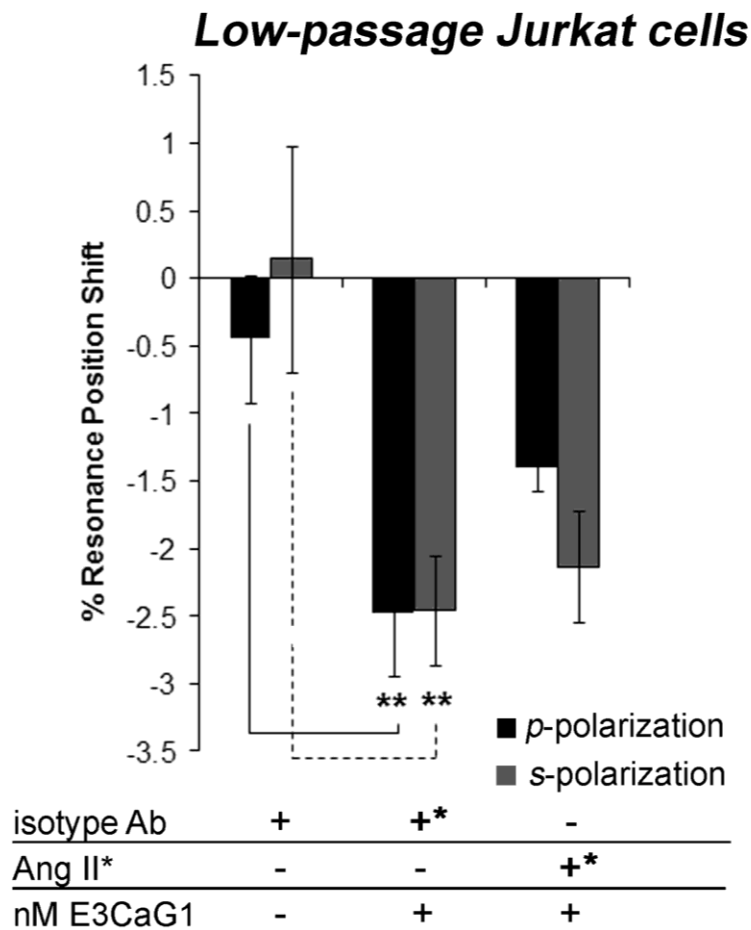


Figure 2.8. Addition of an isotype Ab does not inhibit E3CaG1 binding. Bar graph depicting PWR percent resonance position shifts from the addition of an isotype Ab followed by 5 nM E3CaG1. +* indicates the ligand/antibody first added. For experiments where two proteins were added, the data shown are for the second protein. There is minimal isotype Ab binding (1 nM added), and this does not inhibit subsequent binding of 5 nM E3CaG1. This shows inhibition of E3CaG1 binding by anti-CD47 Ab is specific. The graph also shows comparable percent resonance position shifts from 5 nM E3CaG1 after membranes were incubated with Ang II, as compared to E3CaG1 percent

resonance position shifts after membranes were incubated with an isotype Ab. *Ang II
p- and *s*-polarization error bars represent a range over 2 independent experiments.

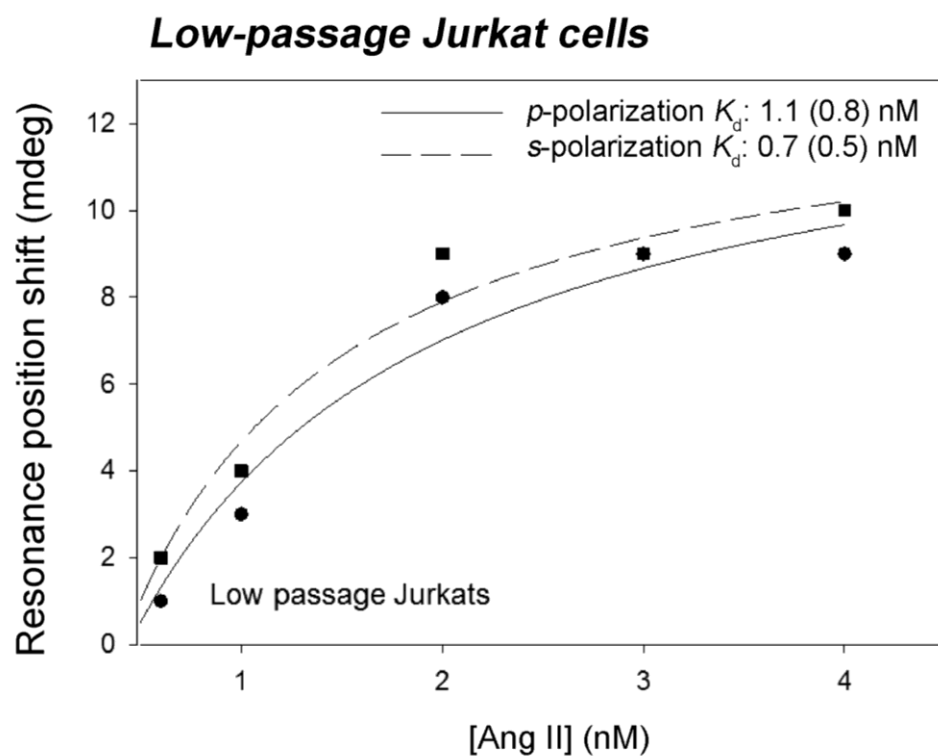


Figure 2.9. Angiotensin II binds to low-passage Jurkat membranes with a nM K_d . Binding curve showing resonance position shifts upon addition of Angiotensin II. The curve was fit using a 3-parameter hyperbolic function. Both p - and s -polarization curves show low nanomolar dissociation constants, which are similar to reported values.

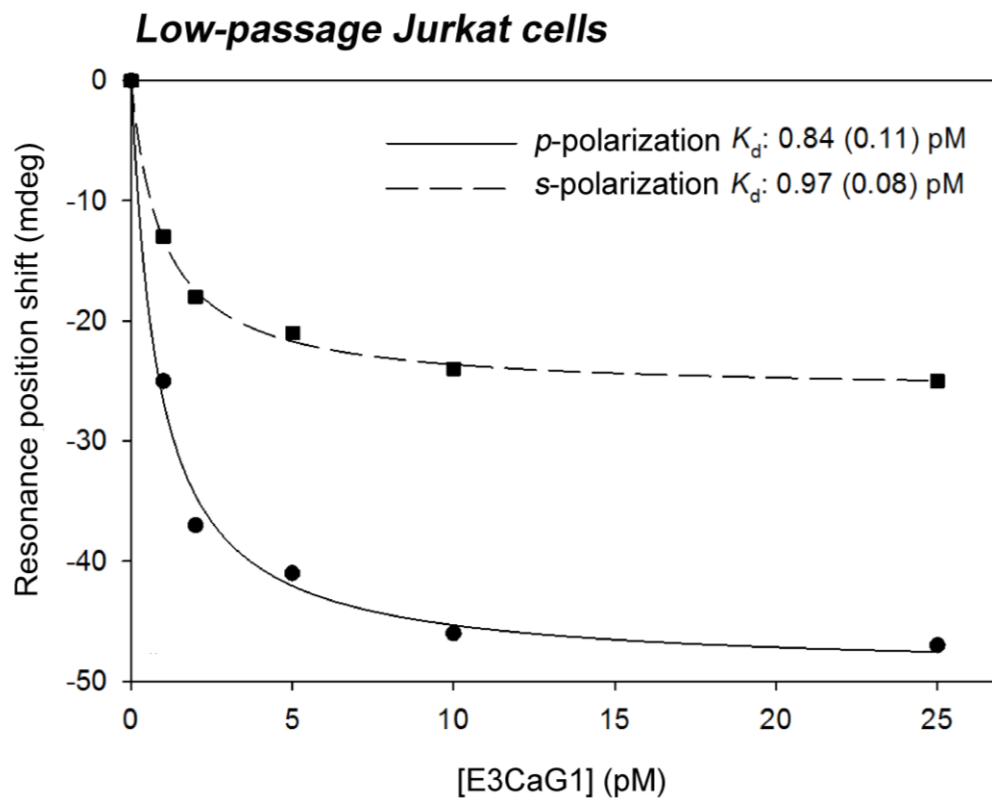


Figure 2.10. E3CaG1 binds to low-passage Jurkat plasma membranes with a pM K_d . Representative pM binding curve of E3CaG1 to young purified Jurkat plasma membranes. E3CaG1 was added in increasing concentrations to low-passage purified Jurkat plasma membranes until saturation was reached. E3CaG1 binds to young purified Jurkat plasma membranes with a pM K_d .

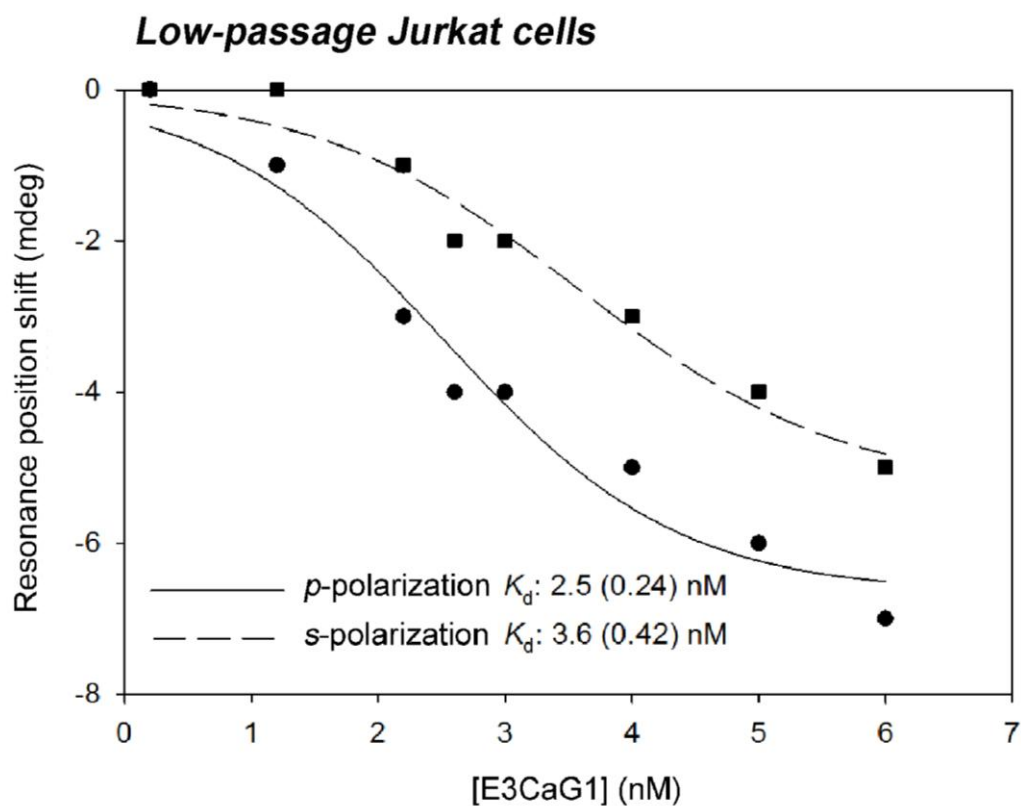


Figure 2.11. E3CaG1 binds to low-passage Jurkat plasma membranes with a nM K_d . Representative PWR binding curve of nM E3CaG1 binding to low-passage Jurkat membranes. Picomolar binding sites were saturated (using 200 pM E3CaG1) before increasing nanomolar concentrations of E3CaG1 were added. Curves were fit using a 3-parameter sigmoidal function.

resonance position using both *p*- and *s*-polarized light, and smaller resonance angles were attributed to decreases in mass density (103). Sigmoidal curves that showed decreases in resonance position have also been observed during incorporation of the cytochrome *b₆f* protein complex into a phosphatidylcholine membrane (115). It was suggested that one possibility for this observation was the dissociation of a dimeric complex upon membrane incorporation (115). The fact that we observed a sigmoidal curve produced from negative resonance position shifts upon E3CaG1 binding suggests cooperativity occurred when nM amounts of E3CaG1 were added to the membrane surface, and the binding of one molecule of E3CaG1 influenced the binding of another. The fact that the resonance position shifts are negative (compared to the resonance position of the membrane alone) upon both pM and nM E3CaG1 binding, could indicate the dissociation of a receptor complex, which would explain the observation of a refractive index decrease upon ligand binding. An example of a PWR spectra recorded upon increasing pM concentrations of E3CaG1 added to low-passage purified Jurkat plasma membranes is shown in Figure 2.12.

2.3.3 Determining the measurement of equilibrium dissociation constants

To ensure equilibrium dissociation constants were being measured rather than simply titrating receptors on the membrane surface, I compared the magnitude of E3CaG1 resonance position shifts to resonance position shifts that occurred upon deposition of membrane fragments. If equilibrium dissociation constants were being measured, a similar K_d should be measured regardless of the amount of receptor present. Greater receptor concentration, as indicated by greater percentage of resonance shifts

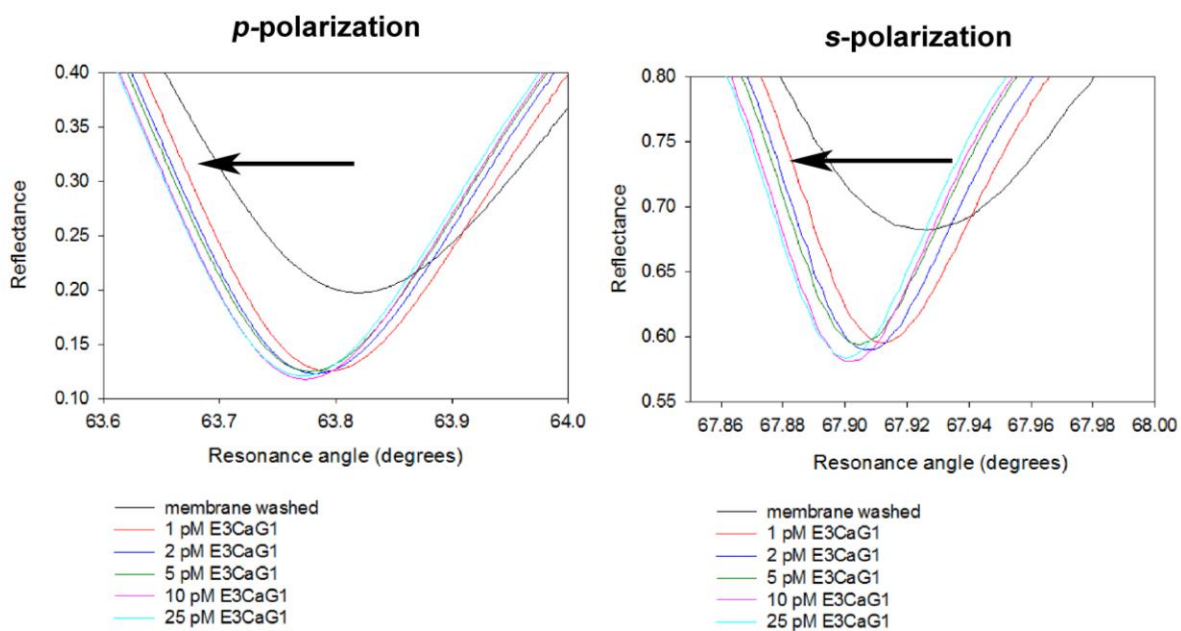


Figure 2.12. Example of PWR spectra upon pM E3CaG1 addition to low-passage Jurkat plasma membranes. Increasing amounts of pM E3CaG1 were added to low-passage Jurkat plasma membranes, and the resonance angle decreased with each addition (compared to the resonance angle of the membrane without prior ligand addition).

from the membrane, should not alter the value found for K_d . This is what was found, as shown in Table 2.2. For example, when more membrane fragments adhered onto the prism surface, indicated by a higher membrane resonance position shift, a higher spectral shift from the bound ligand was recorded (Table 2.2). This suggests more receptor was present to bind ligand due to the larger amount of membrane available for binding. Although total resonance position shifts resulting from the bound ligand varied, similar dissociation constants were calculated, indeed showing equilibrium dissociation constants were being measured.

2.3.4 E3CaG1 binds to CD47 on purified MCF-7 plasma membranes

To confirm the higher binding affinity of E3CaG1 to CD47 in a cell line other than Jurkat cells, an increasing amount of E3CaG1 was added to purified MCF-7 (breast cancer epithelial cell) plasma membranes. A similar K_d of 1.65 pM was observed, indicating E3CaG1 binding is similar in both lymphocytes and epithelial cells (Figure 2.13). On MCF-7 plasma membranes, addition of E3CaG1 produced a decrease in the resonance position compared to the resonance position of membrane fragments alone, which is a similar trend observed using Jurkat plasma membrane fragments.

2.3.5 CD47 is not sufficient for E3CaG1 binding

Since our laboratory previously found that CD47 was necessary but insufficient for E3CaG1 binding, I hypothesized that a second protein was required. When E3CaG1 was added in increasing amounts to high-passage purified Jurkat plasma membranes, little changes in resonance position were observed, even up to concentrations of 170 nM (Figure 2.14). Therefore, additions of E3CaG1 using high-passage Jurkat membranes

TABLE 2.2. List of *p*- and *s*-polarization resonance position shifts from addition of membrane and E3CaG1 to the PWR prism surface. Increasing pM amounts of E3CaG1 were added to the membrane, and total percent resonance position shifts are listed. Increasing resonance position shifts correlate to increasing ligand resonance position shifts, but similar dissociation constants were calculated, as listed in Table 2.1 (under low-passage Jurkat plasma membranes E3CaG1^a).

<i>p</i> -polarization Jurkat membrane resonance position shifts (mdeg)	<i>p</i> -polarization E3CaG1 resonance position shifts (mdeg)	Percent E3CaG1 shifts
286	-12	4.2%
327	-18	5.5%
489	-47	9.6%
<i>s</i> -polarization Jurkat membrane resonance position shifts (mdeg)	<i>s</i> -polarization E3CaG1 resonance position shifts (mdeg)	
161	-9	5.6%
198	-24	12.1%
278	-25	9.0%

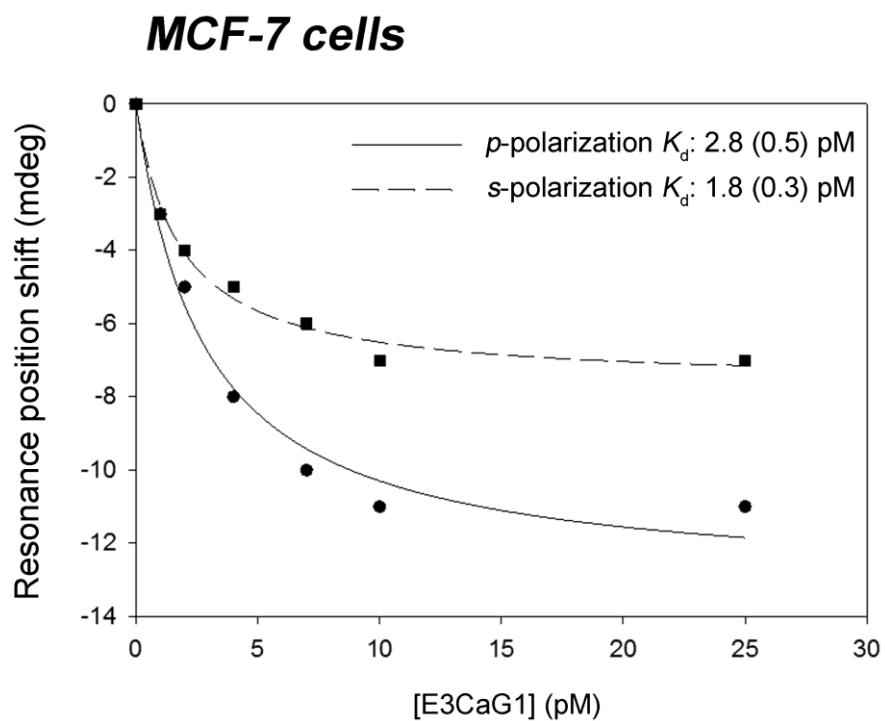


Figure 2.13. E3CaG1 binds to purified MCF-7 plasma membranes with a pM K_d . PWR binding curve showing resonance position shifts upon E3CaG1 binding to purified MCF-7 membranes. Both p - and s -polarization curves indicate pM binding with similar values for K_d to those measured with Jurkat plasma membranes.

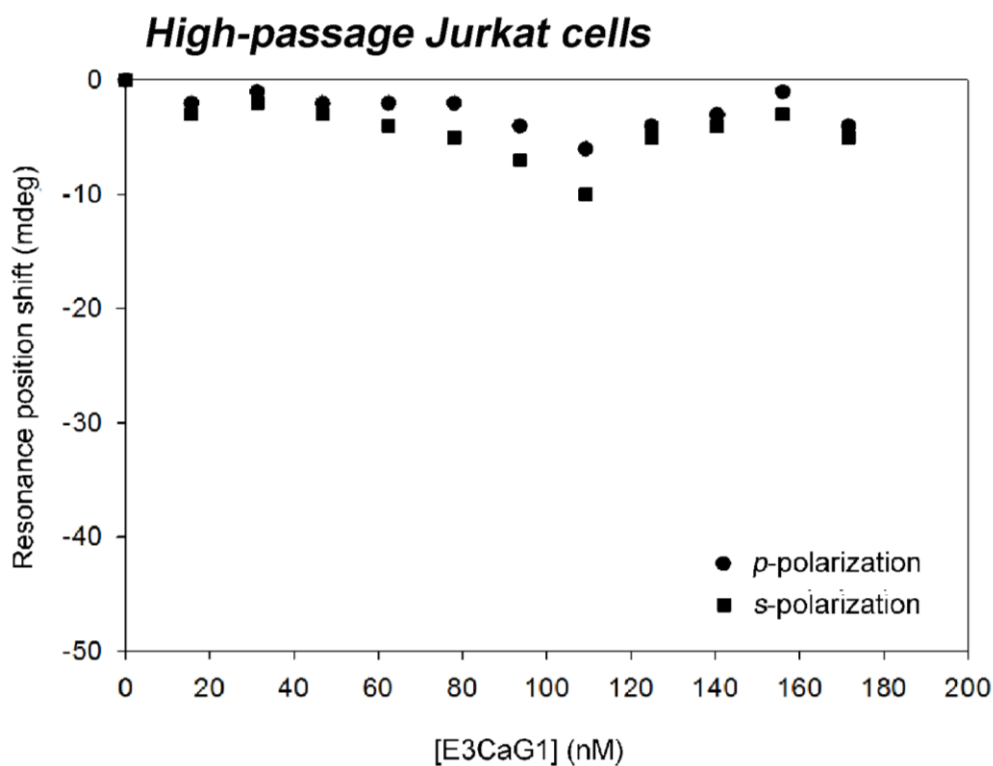


Figure 2.14. E3CaG1 does not appear to bind to high-passage Jurkat membranes.

Increasing concentrations of E3CaG1 were added to high-passage Jurkat membranes and no significant changes in resonance position were observed compared to low passage Jurkat plasma membranes (Figure 2.10). This indicates CD47 is not sufficient for E3CaG1 binding. Two other experiments were performed in which 5 nM E3CaG1 was added to high-passage Jurkat membranes, and no significant binding was observed in either case.

produced significantly less refractive index changes compared to low-passage purified Jurkat plasma membranes, even when concentrations of E3CaG1 were 1000-fold higher. This confirms results from previous flow cytometry experiments that show E3CaG1 cannot bind to Jurkat T lymphocytes that have been in cell culture for long periods (82). Therefore, although CD47 is present on Jurkat T-lymphocytes regardless of passage number, Jurkat cells cultured over 4 weeks can no longer bind E3CaG1. This is perhaps due to a change in a CD47 signaling complex that no longer allows for E3CaG1 to bind, and may involve another membrane protein associated with CD47. This change in phenotype that occurs within Jurkat cells over time may be used to identify the proposed CD47 complex that is involved in the reduction of sGC activity upon TSP-1 binding. In this and future chapters, experiments are performed that search for this unknown component of the CD47 complex.

2.3.6 SIRP α binds to CD47 on Jurkat plasma membranes

SIRP α is the other known ligand of CD47, and it has been shown to bind to the CD47 extracellular domain with μ M affinity (58). SIRP α was added to both low and high-passage purified Jurkat plasma membranes and found to bind to both samples (Figure 2.15, 2.16). The average K_d observed when SIRP α bound to low-passage purified Jurkat plasma membranes was 3.1 pM (Table 2.1) and when bound to high-passage purified Jurkat plasma membranes was 1.4 pM (Table 2.1). Furthermore, SIRP α addition to both low-passage and high-passage Jurkat plasma membranes produced decreases in resonance position compared to membrane alone, which is similar to that observed when E3CaG1 was added to low-passage Jurkat membranes. Although both CD47 ligands

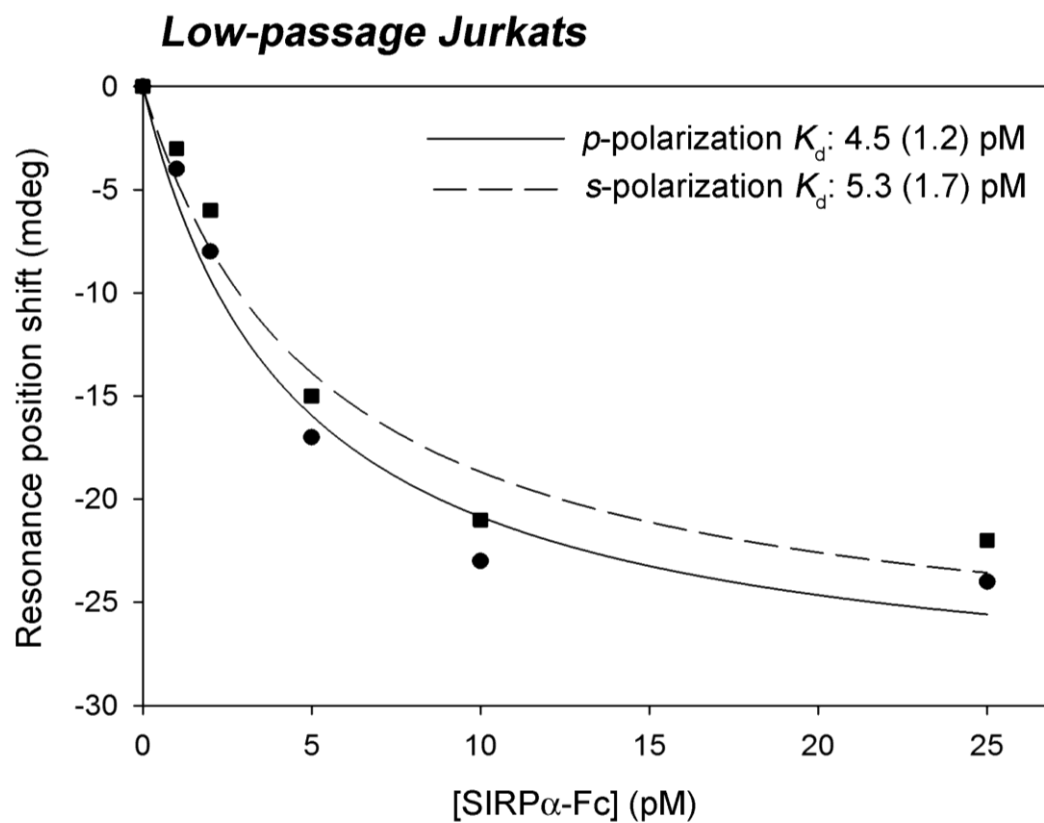


Figure 2.15. SIRP α -Fc binds to CD47 on low-passage Jurkat membranes.

Representative PWR binding curve of SIRP α -Fc added to low-passage purified Jurkat plasma membranes. Increasing concentrations of SIRP α -Fc was added to membranes until saturation was reached. A pM dissociation constant was measured for both p - and s -polarizations.

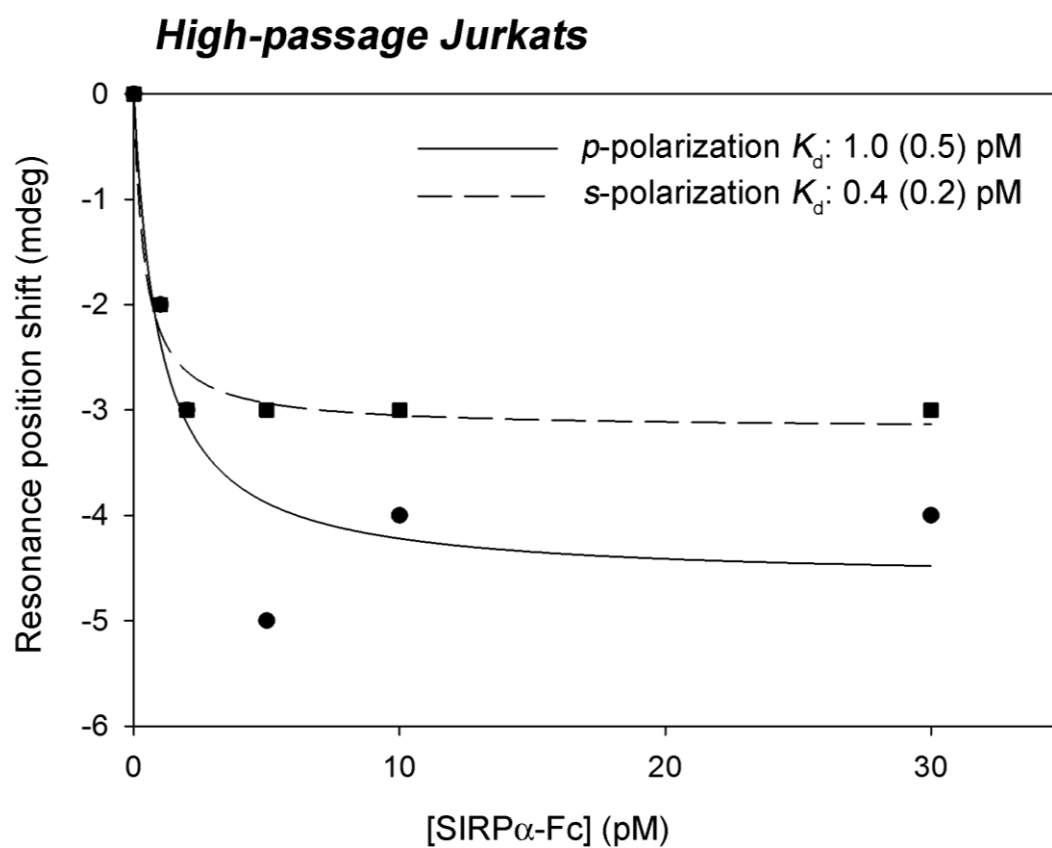


Figure 2.16. SIRP α -Fc binds to CD47 on high-passage Jurkat membranes. Experiment setup is the same as described in Figure 2.12. SIRP α -Fc binds to high-passage Jurkat plasma membranes with a pM K_d similar to that observed on low-passage purified Jurkat plasma membranes.

caused decreases in refractive index upon addition to the membrane surface, E3CaG1 binding was lost over time, whereas SIRP α binding was retained. Therefore, SIRP α binding to CD47 does not change over time, whereas E3CaG1 binding does. This suggests SIRP α does not bind to CD47 in the same manner as E3CaG1. This also gives support to previous evidence that SIRP α can bind to CD47 alone, without the presence of binding partners. It is also possible SIRP α binds tightly to a CD47 complex that differs from that which binds E3CaG1.

2.4 Discussion

Nitric oxide, produced from NOS, regulates multiple physiologic processes through binding to its receptor sGC, including angiogenesis, blood pressure and neurotransmission. Thrombospondin-1 is a multifunctional extracellular matrix protein that has a multitude of domains that bind a variety of receptors, including the integrin-associated protein CD47 (39). Through PWR spectroscopy, I have shown a C-terminal fragment of TSP-1 called E3CaG1 binds to CD47 with both pM and nM affinities, suggesting other possible membrane proteins are involved in E3CaG1 binding to CD47. The Roberts group has also shown picomolar levels of TSP-1 (10 - 100 pM) is sufficient to inhibit sGC activity (43, 86). Also, circulating levels of TSP-1 are reported to be low, approximately 50 - 200 pM (116), which supports a low picomolar dissociation constant of TSP-1 binding to its receptor CD47. We observed decreases in both *p*- and *s*-polarized light upon the addition of E3CaG1 to purified Jurkat plasma membranes, which indicated decreases in refractive index upon ligand binding. This could be explained by the dissociation of a receptor complex. One possibility, explored in the next chapter, is that

E3CaG1 binds to CD47 in complex with VEGFR2 on Jurkat T cells since previous work has shown CD47 and VEGFR2 dissociate upon TSP-1 binding (76). I have also shown E3CaG1 loses the ability to bind to CD47 over time by PWR spectroscopy, confirming previous findings from our lab (82). Therefore, it is possible the expression of specific membrane proteins associated with CD47 change over time, decreasing E3CaG1 binding.

I have also found that the other known ligand of CD47, SIRP α , binds with a picomolar dissociation constant. The previously reported K_d of SIRP α is 1.2 μ M (58), but this value was found using surface plasmon resonance (SPR) spectroscopy and adding the extracellular domain of CD47 to an immobilized extracellular domain of SIRP α . Also, the K_d was found only using extracellular domains of both SIRP α and CD47 and it has been reported CD47 needs a long-range disulfide bond between one of its transmembrane domains and its extracellular domain in order to function properly and bind SIRP α efficiently (65). The fact that the previously reported K_d was not found using full-length CD47 could explain the discrepancy between it and the low picomolar K_d reported here, measured with full-length CD47.

CHAPTER 3

. IDENTIFICATION OF MEMBRANE PROTEINS IN COMPLEX WITH CD47 INVOLVED IN THROMBOSPONDIN-1 BINDING

3.1 Introduction

Work done up to this point suggested another membrane protein is involved in E3CaG1 binding to CD47. CD47 is widely known to associate with integrins such as $\alpha_v\beta_3$, and since E3CaG1 contains a β_3 binding site in the last type 2 repeat, I hypothesized E3CaG1 could bind to a CD47/ $\alpha_v\beta_3$ complex. The decrease in resonance position shifts that were observed upon E3CaG1 binding using PWR spectroscopy are reflective of refractive index decreases. One possibility for this observation is a decrease in mass that could result from a dissociation of a receptor complex, and it has been previously shown TSP-1 causes a dissociation of CD47 in complex with VEGFR2. These observations also led to the possibility that E3CaG1 bound to CD47 in complex with VEGFR2. In the previous chapter, I found E3CaG1 to specifically bind to CD47 on Jurkat T cells using PWR, and that binding is lost after long periods of growth in tissue culture. E3CaG1 was also shown to bind specifically to CD47 on Jurkat T cells through PWR spectroscopy. CD47 was also shown to remain on Jurkat cells while E3CaG1 binding decreases over time. This, coupled with the fact that SIRP α binding does not decrease over time, all pointed toward E3CaG1 binding to a CD47 complex whose expression might be altered with cellular age. Therefore, I next examined candidate proteins associated with CD47 that were involved in E3CaG1 binding through experiments involving PWR spectroscopy, flow cytometry, shRNA inhibition, and lentiviral expression.

3.2 Materials and Methods

3.2.1 Materials

Integrin α_v monoclonal antibody 272-17E6 was obtained from abcam (Cambridge, MA). VEGFR2 monoclonal antibodies 55B11 and 260.4 were obtained from Cell Signaling Technology (Danvers, MA) and Sigma (St. Louis, MO), respectively. Anti-mouse AlexaFluor 647 secondary antibody was obtained from Invitrogen (Grand Island, NY). Goat anti-His-FITC antibody was obtained from QED Biosciences (San Diego, CA). Jurkat JinB8 cells were a generous gift from Dr. Thomas Miller (NIH). The CD47-pEGFP-N3 vector was a generous gift from Dr. David Roberts (NIH). Lenti-X HEK 293T cells were purchased from Clontech (Mountain View, CA). Stain/wash buffer was prepared as PBS containing 0.2% (v/v) BSA, and 0.02% (v/v) sodium azide. pLVX-Tight-pURO and pLVX-tet-off Advanced vectors were obtained from Clontech. Xfect reaction buffer, Lenti-X HTX packaging mix, and Xfect polymer were also obtained from Clontech. Krebs buffer was prepared as 25 mM HEPES, 120 mM NaCl, 4.75 mM KCl, 1.44 mM MgSO₄, 11 mM glucose, pH 7.4.

3.2.2 Cell culture

JinB8 cells were maintained in RPMI 1640 (Invitrogen) supplemented with 5% - 10% fetal bovine serum (FBS), 5 mg/ml penicillin, and 1 mg/ml streptomycin. CD47- JinB8 cells were maintained in RPMI supplemented with 10% tetracycline-free FBS, 5 mg/ml penicillin, 1 mg/ml streptomycin, 0.25 μ g/ml puromycin, 100 μ g/ml G418, and 500 ng/ml doxycycline. Lenti-X HEK 293T cells (Clontech) were maintained in high-glucose DMEM (4.5g/L glucose) supplemented with 10% tetracycline-free FBS, 5 mg/ml

penicillin, and 1 mg/ml streptomycin. All cell lines were grown at 37 °C in 5% CO₂.

3.2.3 Cloning of CD47-eGFP

The CD47-pEGFP-N3 vector was used for cloning into the lentiviral pLVX-Tight-pURO vector. This vector contains human CD47 isoform 2 (NM_198793.2) with a C-terminal eGFP tag and a BamHI restriction site between them. The BamHI site was mutated using the Stratagene QuikChange Lightning Mutagenesis kit (Agilent Technologies, Santa Clara, CA). PCR amplification was performed on the mutated CD47-pEGFP-N3 vector introducing 5' BamHI and 3' MluI restriction sites using the 5' AACTCGGATCCATGTGGCCTCTAGTAGCA 3' (forward) and 5' AGTTCACGCGTTTACTTGTACAGCTCGTCCATG 3' (reverse) primers. The DNA was ligated into the pGEM-T-easy vector per manufacturer's instructions (Promega, Madison, WI). CD47-eGFP was then transferred to the pLVX-Tight-pURO vector through double digestion with fast digest BamHI and MluI (Fermentas, Waltham, MA) and ligation with the rapid DNA ligation kit (Thermo Scientific). DNA sequencing showed the correct nucleotide sequence except for a single point mutation at position 545 (NM_198793.2) that resulted in a glycine instead of a glutamate residue. This mutation did not affect fluorescence of the protein or E3CaG1 binding as confirmed by confocal microscopy and PWR spectroscopy.

3.2.4 Generation of lentivirus

CD47-eGFP and Tet-off lentivirus were produced using the Cloneteck Lenti-X Tet-Off advanced inducible expression system according to manufacturer's instructions (Cloneteck). Lenti-X HEK 293T cells were plated in a 10 cm tissue culture dish so they

were 80 - 90% confluent at the time of transfection. CD47-eGFP within the pLVX-Tight-pURO vector as well as the pLVX-Tet-Off Advanced vector were transfected separately into the Lenti-X cells using Xfect reaction buffer, Lenti-X HTX packaging mix and Xfect polymer. The media was changed 24 hours later, and cells were incubated an additional 48 hours so cells could secrete the virus. The supernatant was then collected, centrifuged at $500 \times g$ for 10 min to remove debris, then frozen at -80°C until further use. Viral titers were determined using the Lenti-X p24 rapid titer kit (Clonetechn).

3.2.5 Stable transduction of cells

0.5×10^6 JinB8 cells were washed twice in PBS and once in RPMI supplemented with 10% tetracycline-free FBS, 5 mg/ml penicillin, and 1 mg/ml streptomycin before transduction. Cells were then co-transduced with Tet-off and CD47-eGFP lentivirus at a 2:1 ratio with a multiplicity of infection of 2 by centrifugation for 2 hours at $1000 \times g$ at room temperature. Cells were then transduced for 24 hours at 37°C in 5% CO_2 before being put in RPMI supplemented with 10% FBS, 5 mg/ml penicillin, 1 mg/ml streptomycin, 2 $\mu\text{g}/\text{ml}$ puromycin, and 500 $\mu\text{g}/\text{ml}$ G418, and 500 ng/ml doxycycline. The puromycin and G418 antibiotics were used to select for cells containing both the CD47-eGFP (puromycin resistance) and Tet-off (G418 resistance) vectors. Cells were maintained in selection media for 11 days until cells started to multiply (cells were centrifuged at $100 \times g$ every 2-3 days to remove dead cells before resuspension in fresh media). After JinB8 cells transduced with CD47-eGFP began to multiply, the concentration of antibiotics was reduced to 0.25 $\mu\text{g}/\text{ml}$ puromycin and 100 $\mu\text{g}/\text{ml}$ G418

and cells were maintained in this concentration from this point forward. Expression of protein was turned on by centrifugation of cells at $180 \times g$ for 5 min at room temperature, washing 2x in PBS, then resuspending cells in RPMI supplemented with 10% tetracycline-free FBS, 5 mg/ml penicillin, 1 mg/ml streptomycin, 0.25 $\mu\text{g/ml}$ puromycin and 100 $\mu\text{g/ml}$ G418. Cells were maintained in this media for at least 48 hours prior to experiments.

3.2.6 Confocal microscopy

35 mm live-cell dishes were used for confocal microscopy (MatTek, Ashland, MA). JinB8 cells stably transduced with CD47-eGFP were washed and resuspended in Krebs buffer before being incubated on coverslips for 1 hour at 37 °C in 5% CO₂. To prepare coverslips for confocal microscopy, 0.01% poly-l-lysine was added to 1.5 glass coverslips for 1 h at room temperature. The poly-l-lysine was then removed and the coverslips washed twice in nuclease-free water (Invitrogen). Cells were imaged on a Nikon C1si scanning confocal microscope using an excitation wavelength of 488 nm and a 525/50 detector. A 60x, 1.4 NA oil-immersion objective and Nikon CCD camera were used to view confocal images. At least three random fluorescence images were recorded for each sample. Nikon EZ-C1 version 3.8 software was used to acquire images.

3.2.7 Flow cytometry binding studies

For E3CaG1 binding studies, 2×10^6 Jurkat cells per condition were serum starved 48 hours prior to the experiment. Cells were centrifuged at $180 \times g$ for 5 min at room temperature and washed once in PBS and once in stain/wash buffer at 4 °C. Cells were incubated with 10 nM anti-VEGFR2 (260.4) antibody or anti-CD47 (B6H12) antibody

for 30 min at 4 °C, washed in stain/wash buffer, and fixed with 2% (v/v) PFA (paraformaldehyde) for 15 min at 4 °C. Cells were washed in stain/wash buffer before being incubated with 25 nM E3CaG1 for 1 h at 4 °C. A FITC-conjugated anti-His antibody was added and cells were incubated for an additional 30 min at 4 °C. The cells were washed as described and fixed again with 2% (v/v) PFA. In experiments determining VEGFR2 levels over time, 0.5×10^6 cells per condition were used. Cells were washed once in PBS, and once in stain/wash buffer before being incubated with 10 nM anti-VEGFR2 (260.4) antibody for 30 min at 4 °C. Cells were centrifuged at $200 \times g$ for 5 min at 4 °C, and resuspended in stain/wash buffer. 5 µg anti-mouse AlexaFluor 647 secondary antibody was added for 30 min at 4 °C. Cells were washed as described, and resuspended in stain/wash buffer with 2% PFA until acquisition. Fluorescence was measured using a Becton Dickinson LSR II flow cytometer with an excitation wavelength of 488 nm and a 525/50 nm emission filter or with a Guava easyCyte 8HT flow cytometer (Millipore, Billerica, MA) using a 40 mW red laser with an excitation wavelength of 635 nm and a 661/19 nm emission filter. On the LSR, 10,000 cells were counted and gated on live cells using forward and side scatter fluorescence. On the Guava easyCyte 8HT, 5,000 cells were counted and gated on live cells using forward and side scatter fluorescence. The same gate was applied for each sample measured. A gate was also created on the population of cells fluorescent at 525 nm or 661 nm, and the same gate was applied for each sample measured. Cells without any fluorophore and those incubated with secondary antibody alone were used as controls. Total mean/median fluorescence (MFI) was calculated by multiplying the fluorescence of the gated

population at 525 nm or 661 nm by the percentage of cells within the gate (MFI x % cells) (117). Relative MFI was calculated as $(\text{total MFI})_{\text{sample}} - (\text{total MFI})_{\text{secondary Ab}}$. Data analysis was performed using FloJo or Millipore InCyte software (Billerica, MA).

3.3 Results

3.3.1 E3CaG1 binds to CD47 in complex with VEGFR2 with a picomolar K_d

To further investigate VEGFR2 as the possible membrane complex that binds E3CaG1 and regulates the production of cGMP, increasing amounts of anti-VEGFR2 (260.4) antibody was added to purified Jurkat plasma membranes to determine if this receptor was present. Addition of the anti-VEGFR2 antibody bound with an average K_d of 2.9 pM (Figure 3.1, Table 2.1), confirming the presence of VEGFR2. When membranes were pre-incubated with anti-VEGFR2 antibody, picomolar binding of E3CaG1 was significantly reduced, suggesting E3CaG1 bound to a CD47/VEGFR2 complex with pM affinity (Figure 3.2). Measurement of E3CaG1 binding to Jurkat cells by flow cytometry was also shown to be reduced when anti-CD47 or anti-VEGFR2 antibodies were added (Figure 3.3 and Figure 3.4). However, when low-passage Jurkat membranes were pre-incubated with anti-VEGFR2 antibody, nM E3CaG1 binding was still observed. Levels of nM E3CaG1 binding were slightly, but not significantly lower than those observed without pre-incubation of anti-VEGFR2 antibody (Figure 3.2). These results indicated VEGFR2 did not play a significant role in E3CaG1 binding to CD47 with a nM K_d .

3.3.2 E3CaG1 binds to CD47 in complex with integrin $\alpha_v\beta_3$ with a nanomolar K_d

Since E3CaG1 was shown to bind to CD47/VEGFR2 with high affinity, I

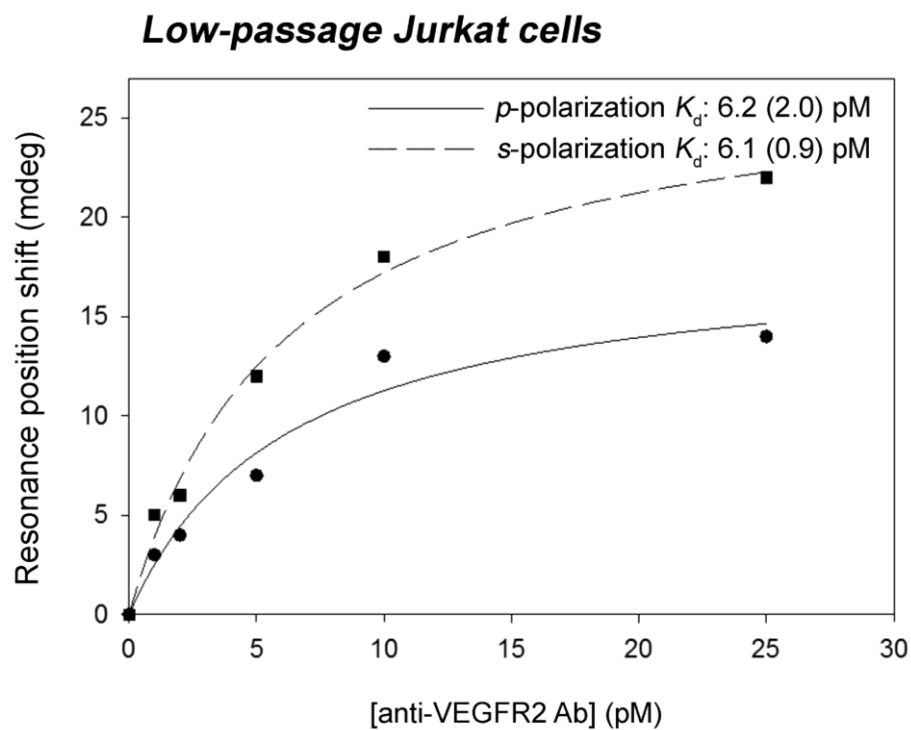


Figure 3.1. VEGFR2 is present on low-passage Jurkat plasma membranes.

Representative PWR binding curve resulting from addition of increasing concentrations of anti-VEGFR2 (260.4) Ab to low-passage Jurkat membranes. A pM K_d was measured.

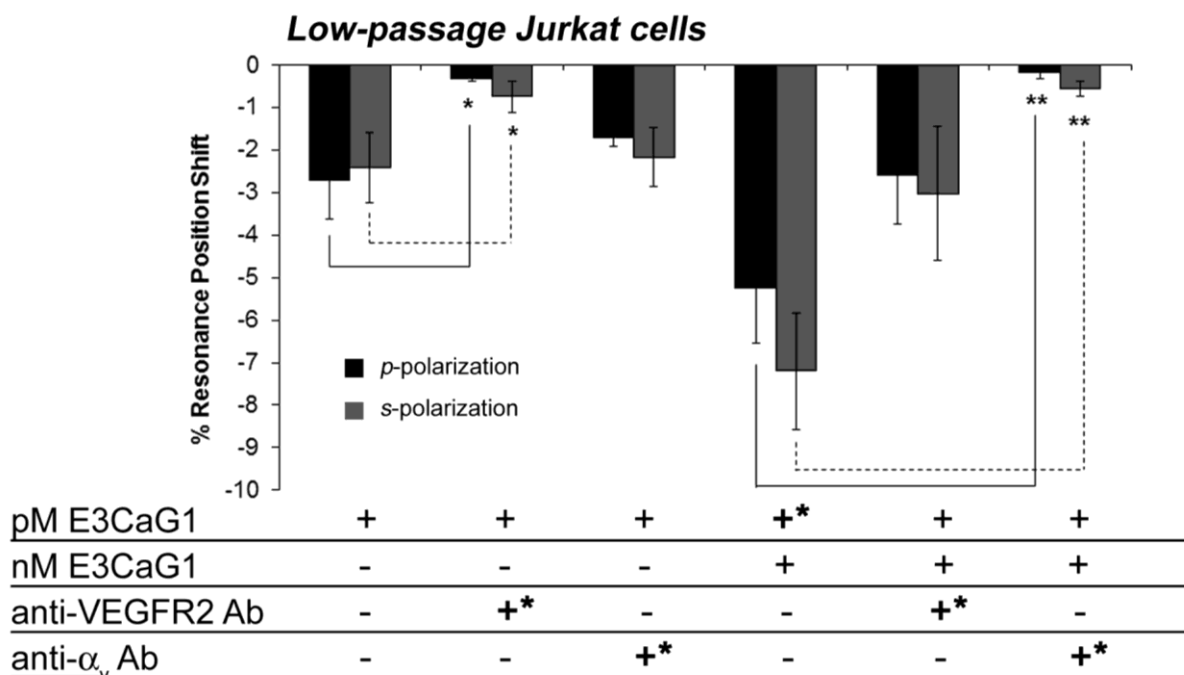


Figure 3.2. E3CaG1 binds to CD47/VEGFR2 with a pM K_d and CD47/ $\alpha_v\beta_3$ with a nM K_d on low-passage Jurkat plasma membranes. Bar graphs depicting PWR percent resonance positions shifts on low-passage purified Jurkat plasma membranes upon pM and nM E3CaG1 binding, with or without prior incubation of anti-VEGFR2 (260.4) Ab or anti- $\alpha_v\beta_3$ (272-17E6) Ab. **+** indicates the ligand/antibody first added. **-** indicates the protein was not added to the membrane. For experiments where two proteins were added, the data shown are for the second protein. For experiments where three proteins were added, pM E3CaG1 sites were saturated prior to the addition of nM E3CaG1, and resulting percent resonance position shifts shown are those resulting only from nM addition of E3CaG1. The expected shift for the addition of the first protein was observed in all cases. The presence of anti-VEGFR2 Ab (50 pM or 10 nM) inhibited 50 pM but not 5 nM concentrations of E3CaG1 binding. 5 nM E3CaG1 was added either in one large

amount or through titration. Prior addition of 13.3 nM anti- $\alpha_v\beta_3$ Ab inhibited 5 nM but not 50 pM binding of E3CaG1. E3CaG1 additions were added through one addition to the sample cell. This indicates E3CaG1 binds to CD47 in complex with VEGFR2 with a pM K_d and CD47 in complex with $\alpha_v\beta_3$ with a nM K_d .

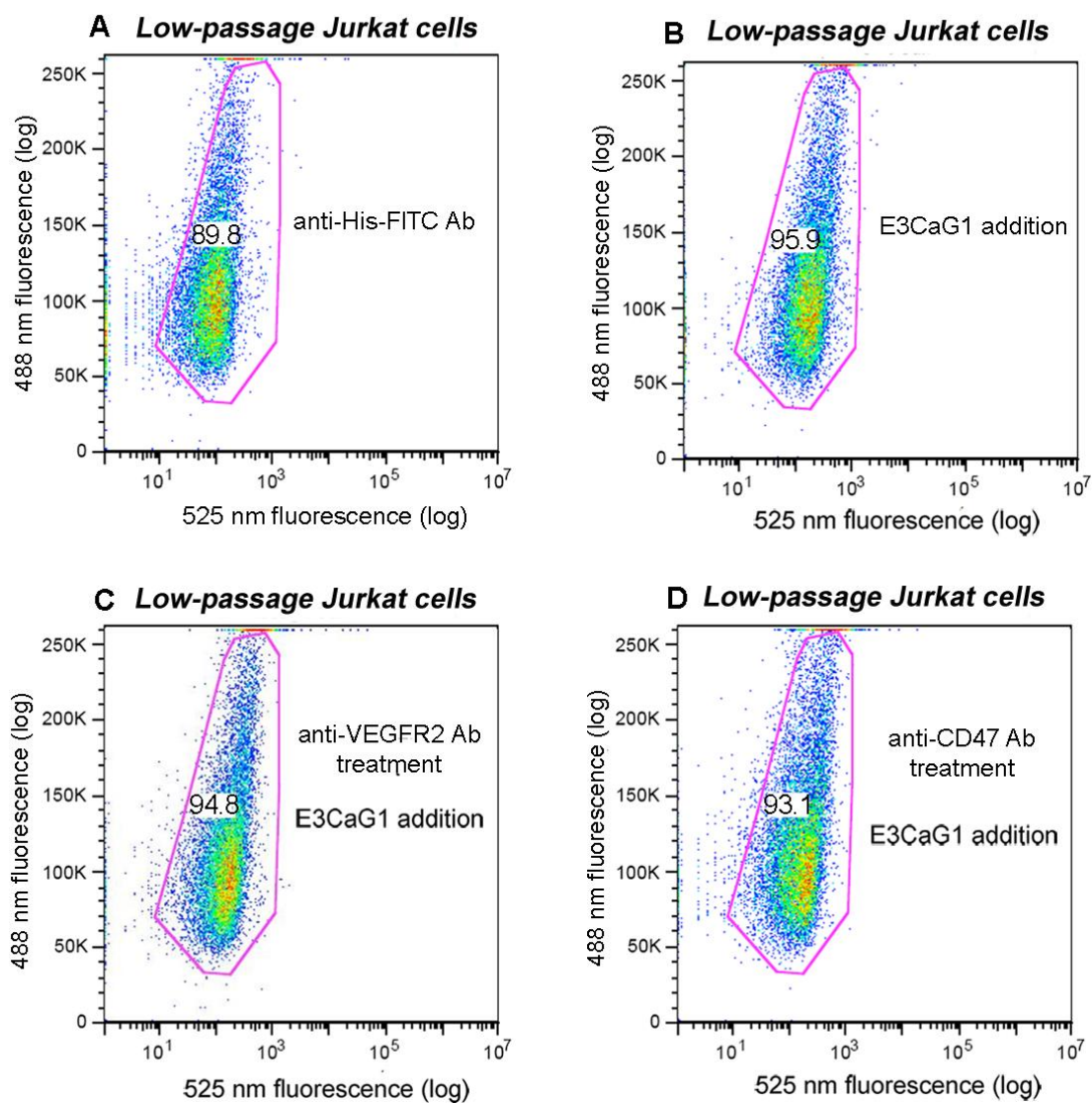


Figure 3.3. Dot plots showing fluorescence from anti-His-FITC secondary Ab bound to E3CaG1, with and without prior incubation of anti-VEGFR2 (260.4) and anti-CD47 (B6H12) antibodies. Fluorescence at 525 nm is shown on the x-axis. Numbers within the cell populations represent the percentage of cells within the gate. *A*. Fluorescence from addition of anti-His-FITC Ab alone. *B*. Fluorescence from addition of 25 nM

E3CaG1 prior to addition of anti-His-FITC secondary Ab. *C.* Same as *B*, except cells were previously incubated with 10 nM anti-VEGFR2 Ab. *D.* Same as *B*, except cells were previously incubated with 10 nM anti-CD47 Ab. Dot plots show an increase in fluorescence upon E3CaG1 addition compared to secondary Ab alone, indicating binding. However, prior incubation with either anti-VEGFR2 or anti-CD47 antibodies decreased fluorescence compared to that caused by E3CaG1 addition.

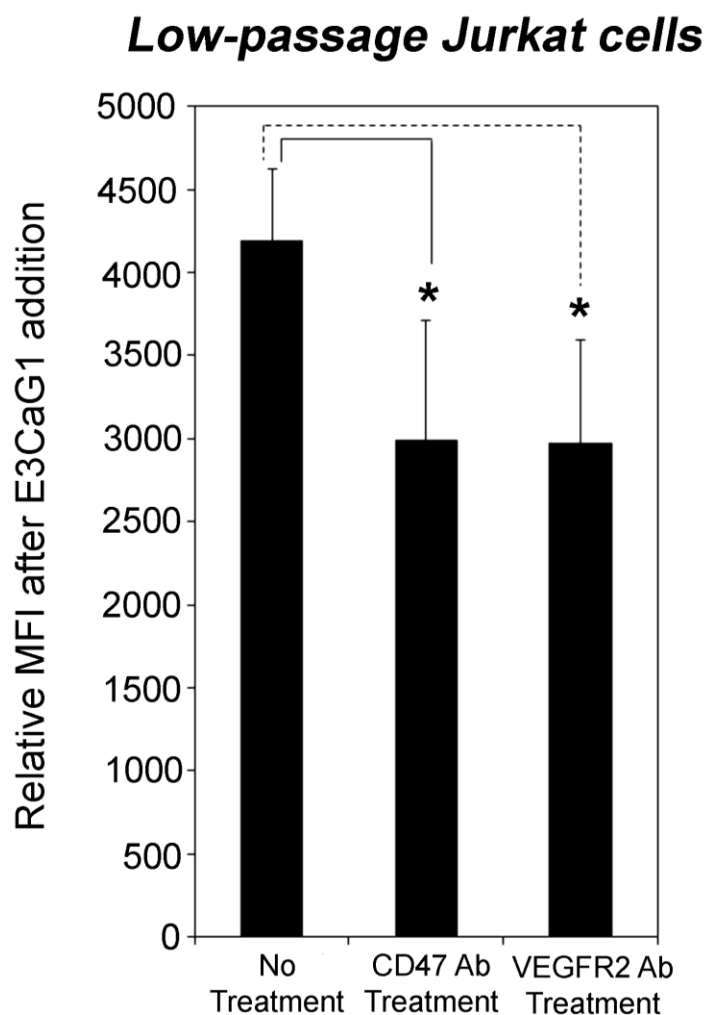


Figure 3.4. E3CaG1 binds to CD47 in complex with VEGFR2 by flow cytometry.

Graphical representation of Figure 3.3. Flow cytometry experiment showing relative MFI after 25 nM E3CaG1 addition (compared to MFI of anti-His-FITC Ab alone) to Jurkat cells. Incubation with anti-CD47 (B6H12) Ab or anti-VEGFR2 (260.4) Ab significantly decreased E3CaG1 binding, indicating E3CaG1 was binding to a complex involving CD47 and VEGFR2. $n = 3$.

wanted to identify if E3CaG1 bound to CD47 in complex with another membrane protein to produce the second, nanomolar K_d . PWR experiments showed incubation with anti-VEGFR2 antibody did not inhibit spectral shifting caused by nM E3CaG1 addition to membranes, indicating E3CaG1 was binding to a CD47 complex not involving VEGFR2 with a nanomolar K_d on Jurkat cells (Figure 3.2). To investigate the possibility of E3CaG1 binding to a CD47 complex involving integrin $\alpha_v\beta_3$, we first examined if $\alpha_v\beta_3$ was present on Jurkat plasma membranes. An anti- α_v antibody was added to purified Jurkat plasma membranes and produced spectral shifting, which indicated binding. The resulting binding curve showed an average K_d of 1.2 pM (Figure 3.5, Table 2.1). This dissociation constant was similar to that for anti-CD47 (B6H12) antibody, the strength of binding coming from the high affinity and avidity for antibody-antigen interactions. Knowing that α_v was present within the membrane, a saturating amount anti- α_v antibody was added, followed by a saturating amount of pM E3CaG1 (50 pM). Resonance position shifts were observed similar to those seen without prior incubation of antibody, but no further spectral shifts were observed after subsequent 5 nM E3CaG1 addition. This showed E3CaG1 was binding to CD47 in complex with integrin α_v with nanomolar affinity (Figure 3.2). Our lab has previously shown E3CaG1 binding to CD47 causes a decrease in NO-stimulated sGC activity in Jurkat T cells, and this reduction is reversed by incubation with an anti-CD47 antibody (82). We have also shown that addition of an anti- $\alpha_v\beta_3$ as well as anti- α_v antibody to Jurkat cells prior to E3CaG1 does not inhibit E3CaG1-induced reduction of cGMP (82). This suggests although there is a $\alpha_v\beta_3$ /CD47 complex on the cell membrane, it is not involved in the nitric oxide signaling

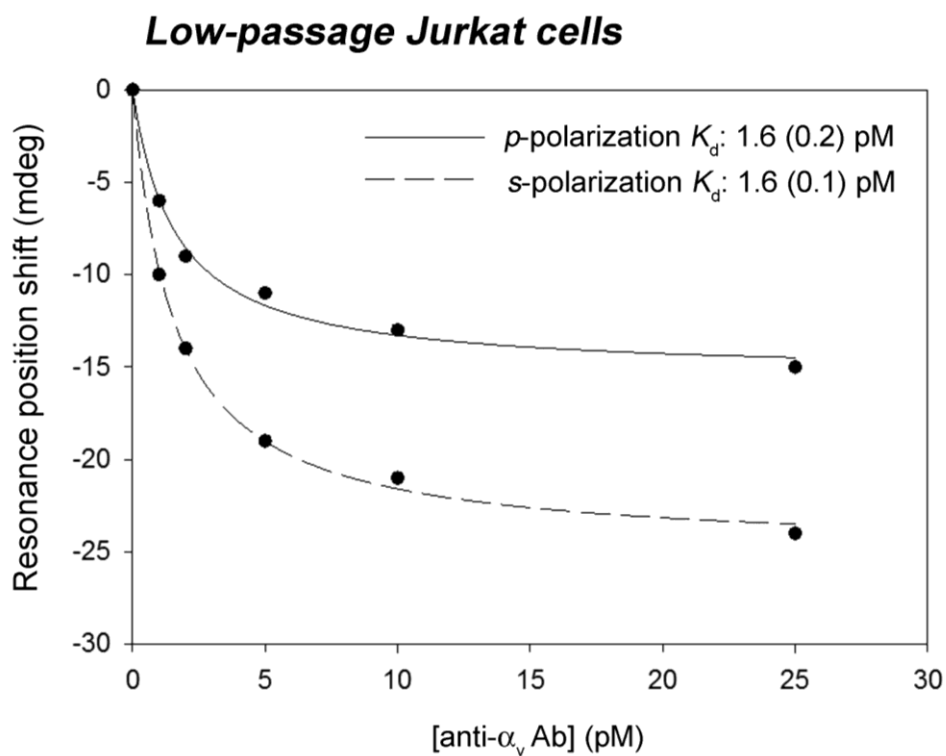


Figure 3.5. Integrin α_v is present on low-passage Jurkat plasma membranes.

Representative PWR binding curves resulting from addition of increasing concentrations of anti- α_v (272-17E6) Ab to low-passage Jurkat membranes. A pM K_d was measured.

pathway.

3.3.3 The loss of E3CaG1 binding correlates to a decrease in VEGFR2 expression

Since CD47/ $\alpha_v\beta_3$ was not the complex involved in E3CaG1-induced sGC inhibition, I examined whether VEGFR2 in complex with CD47 was involved in regulating the NO signaling pathway. Flow cytometry experiments were done to determine if VEGFR2 levels changed with Jurkat cell time in tissue culture and could possibly correlate to the loss of E3CaG1 binding. The presence of VEGFR2 was significantly reduced on high-passage Jurkat cells compared to low-passage Jurkat cells as shown by flow cytometry and PWR spectroscopy (Figure 3.6, 3.7, and 3.8). Since E3CaG1 could not bind to high-passage cells, this suggested VEGFR2 was needed for E3CaG1 binding.

3.3.4 Expression of CD47-eGFP in CD47-null (JinB8) cells using a lentiviral transduction system

Native Jurkat T cells contain the protein receptor CD47 on their membrane (82, 118, 119). A mutated Jurkat cell line called JinB8, however, does not contain CD47 (119). I generated a cell line called CD47-JinB8 in which human CD47 with a C-terminal enhanced green fluorescent protein (eGFP) tag was stably put back into JinB8 cells through lentiviral transduction. Expression of CD47-eGFP was under control of a tetracycline regulator, with addition of doxycycline turning off expression of the protein. This cell line was generated to determine if E3CaG1 binding to and functionality of CD47 could be restored. Additionally, CD47-JinB8 cells were made in order to produce large amounts of properly glycosylated recombinant CD47 for future purification and

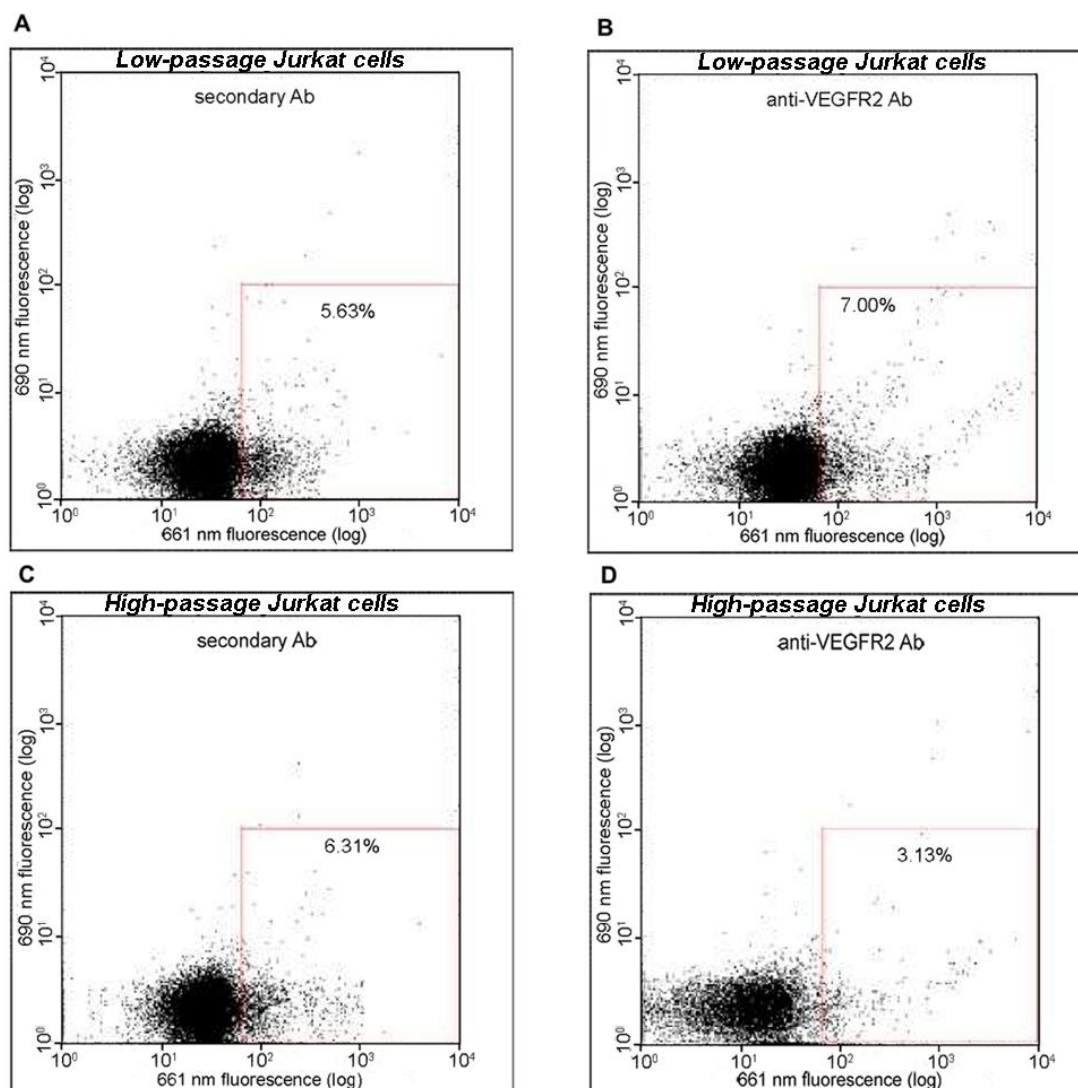


Figure 3.6. Dot plots showing fluorescence upon anti-VEGFR2 (260.4) Ab addition to low and high-passage Jurkat cells. Fluorescence emitted at 661 nm is shown on the x-axis. *A.* Low-passage Jurkat cells incubated with anti-mouse AlexaFluor 647 secondary Ab alone. *B.* Low-passage Jurkat cells incubated with anti-VEGFR2 Ab prior to the addition of anti-mouse AlexaFluor 647 secondary Ab. *C.* Same as *A*, only done with high-passage Jurkat cells. *D.* Same as *B*, only done with high-passage Jurkat cells.

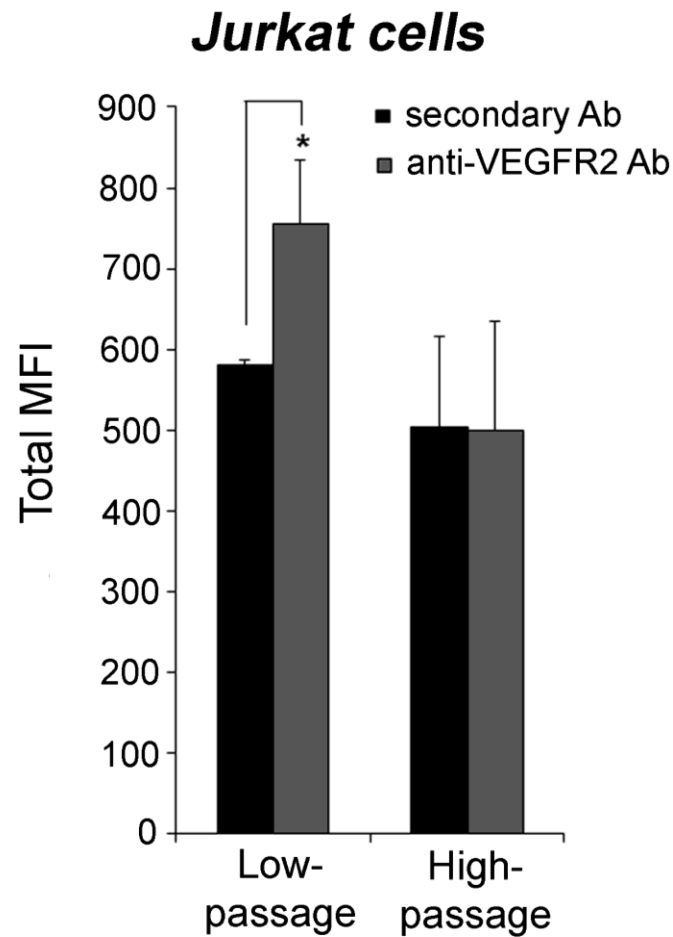


Figure 3.7. VEGFR2 levels decrease on Jurkat cells over time. Graphical representation of Figure 3.6. Low and high-passage Jurkat cells were incubated with anti-VEGFR2 (260.4) Ab prior to incubation with anti-mouse AlexaFluor 647 secondary Ab and fluorescence was measured. There was a significant increase in fluorescence in low-passage Jurkat cells when they were incubated with anti-VEGFR2 Ab compared to those incubated with secondary Ab alone. There was no significant difference in high-passage Jurkat cells treated with anti-VEGFR2 Ab compared to those treated with secondary Ab alone. $n = 3$.

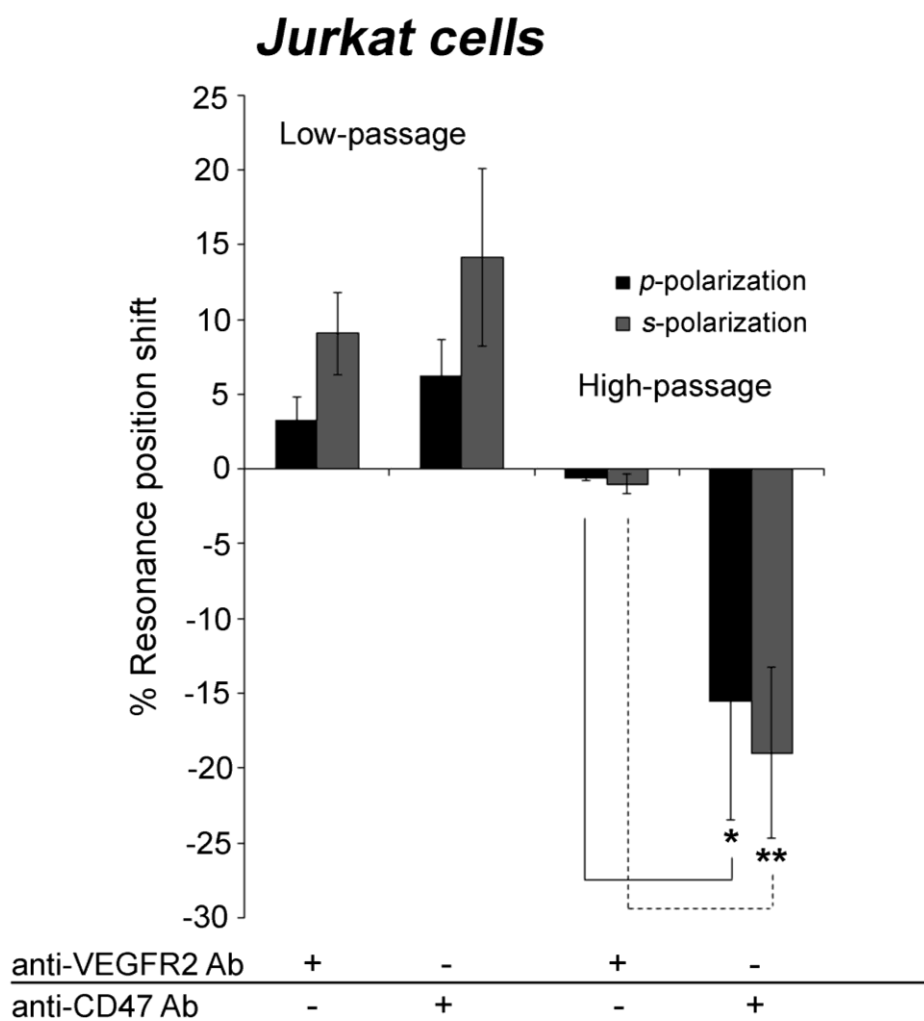


Figure 3.8. There is a significant decrease in anti-VEGFR2 Ab binding in high-passage Jurkat membranes compared to anti-CD47 Ab binding. PWR bar graph showing percent resonance position shifts upon anti-VEGFR2 Ab and anti-CD47 Ab addition to both low-passage and high-passage Jurkat cells. – indicates the protein was not added to the membrane. There is no significant difference between anti-VEGFR2 (260.4) Ab and anti-CD47 (B6H12) Ab binding to low-passage Jurkat cells (data shown are from independent titration curves that range from 1 pM to 50 pM). However, there is minimal

anti-VEGFR2 (55B11) Ab binding to high-passage Jurkat membranes (a single amount of a 1:250 dilution was added) and a significant difference between anti-VEGFR2 Ab and anti-CD47 (B6H12) Ab binding (data shown are from independent titration curves ranging from 1 pM to 75 pM) was observed.

structural studies.

3.3.4.1 Determination of transduction by PWR spectroscopy and confocal microscopy

To determine if CD47-JinB8 cells behaved in a similar manner to Jurkat cells, we first examined whether CD47-eGFP was expressed properly in the cell membrane.

Purified CD47-JinB8 membranes with expression turned on and off (by withdrawal and maintenance in doxycycline, respectively) were deposited on the surface of the PWR prism followed by addition of anti-CD47 (B6H12) antibody. There was a significant difference in CD47 expression between JinB8 cells and CD47-JinB8 cells maintained without doxycycline, with the latter showing a much higher percent resonance position shift from the addition of the B6H12 antibody than the former (Figure 3.9).

To confirm the expression of CD47-eGFP on CD47-JinB8 cells, confocal microscopy was done to show the distribution of fluorescence on live cells. CD47-JinB8 cells were maintained with and without doxycycline, then placed on poly-L-lysine coated coverslips for imaging. Poly-L-lysine was used to help the cells adhere to the coverslips for imaging due to Jurkat T lymphocytes being a suspension cell line. There was more fluorescence observed from cells with CD47-eGFP expression turned on than from cells with CD47-eGFP fluorescence turned off (Figure 3.10). Fluorescence was distributed evenly throughout cells maintained without doxycycline (expression turned on), and fluorescence was also observed on these cell membranes. This supports the PWR data where anti-CD47 (B6H12) antibody bound to purified CD47-JinB8 plasma membranes.

3.3.5 A CD47-null Jurkat cell line in which CD47 is re-introduced behaves similarly to native Jurkat T cells

negative resonance position shift upon addition of anti-CD47 Ab on CD47-JinB8 (expression on) membranes was observed as compared to native high-passage Jurkat cells.

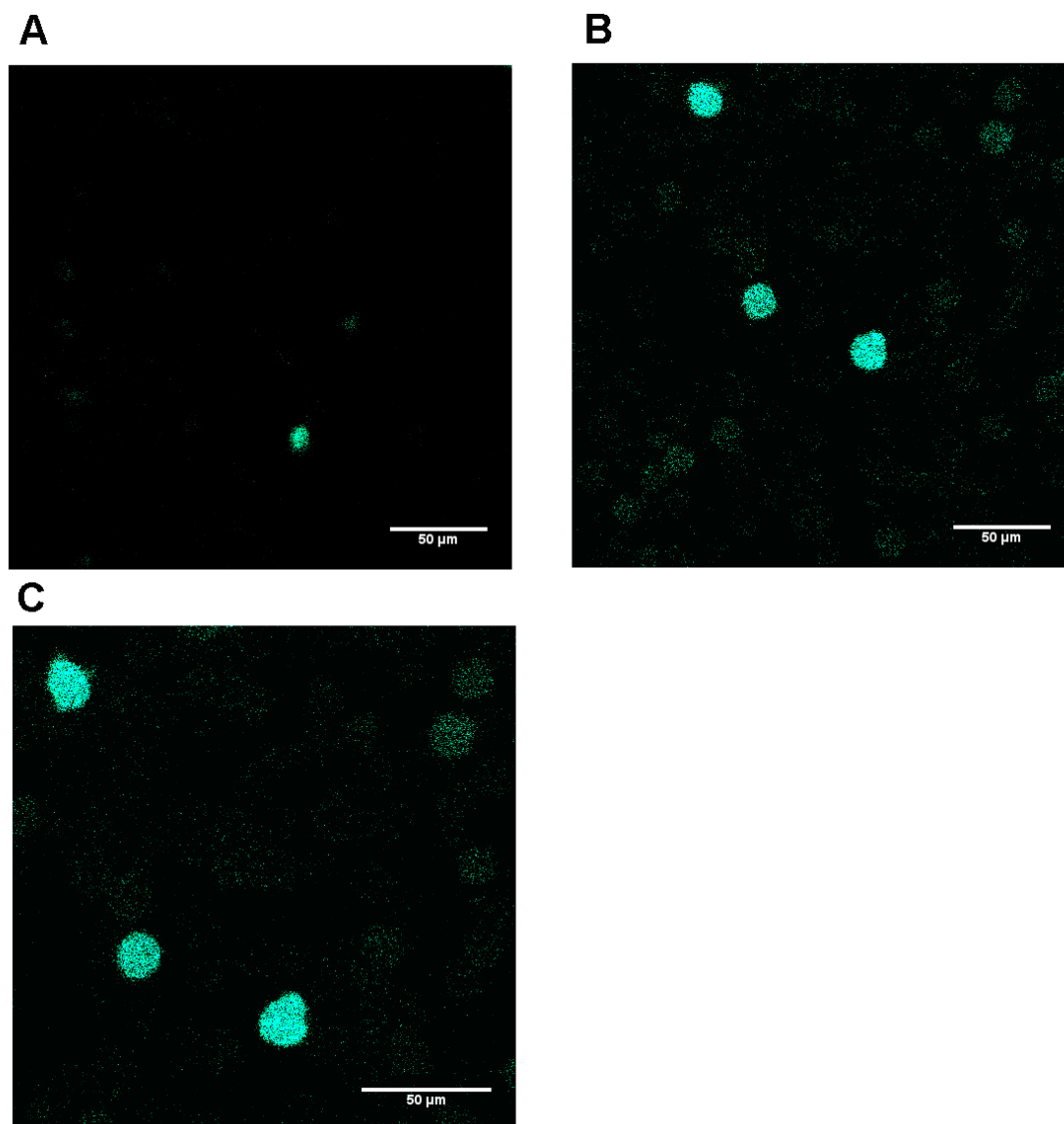


Figure 3.10. CD47 is expressed on CD47-JinB8 cells by confocal microscopy. Images were taken at 10.6% laser power. *A*. Confocal microscopy image of CD47-JinB8 cells (expression off). Image size: 258.3 μm. *B*. Same as *A*, except done with CD47-JinB8 cells (expression on). Image size: 258.3 μm. There are more fluorescent cells in the CD47-JinB8 (expression on) image than the CD47-JinB8 (expression off) image. *C*. Image *B*, only zoomed in. Image size: 193.2 μm.

3.3.5.1 E3CaG1 binds to CD47 in complex with VEGFR2 with a picomolar K_d on JinB8 cells stably transduced with CD47-eGFP and another complex involving VEGFR2 with a nM K_d

To see if E3CaG1 bound to its receptor CD47 on CD47-eGFP-JinB8 cells, increasing concentrations of pM E3CaG1 were added, and a K_d of 1.3 pM was observed (Figure 3.11), which is the same as the 1.3 pM K_d measured for native Jurkat T cells (Figure 2.8). To observe if E3CaG1 bound to CD47/VEGFR2 with pM affinity on CD47-JinB8 membranes, anti-VEGFR2 antibody was incubated on membranes prior to the addition of E3CaG1. The anti-VEGFR2 antibody inhibited pM E3CaG1 binding on CD47-JinB8 membranes in addition to native Jurkat membranes, showing the same CD47 complex was occurring on both cell lines (Figure 3.13).

A second, weaker K_d of 1.3 nM was also measured on the CD47-JinB8 purified plasma membranes (Figure 3.12). I have also shown that this occurs on purified plasma membranes from native Jurkat cells, from binding to CD47 in complex with integrin $\alpha_v\beta_3$. On low-passage Jurkat membranes, it was also observed that incubation with anti-VEGFR2 antibody slightly reduced, but did not significantly inhibit, nM binding of E3CaG1 to the membrane. However, when the same experiment was performed on CD47-JinB8 cells, the presence of anti-VEGFR2 antibody caused a significant decrease in both pM and nM E3CaG1 binding (Figure 3.13). This suggested that on this cell line, VEGFR2 was involved in both pM and nM E3CaG1 binding. This suggested E3CaG1 was binding to another complex involving VEGFR2 with nM affinity, and that there was much more of this complex present on CD47-JinB8 cells than native Jurkat cells.

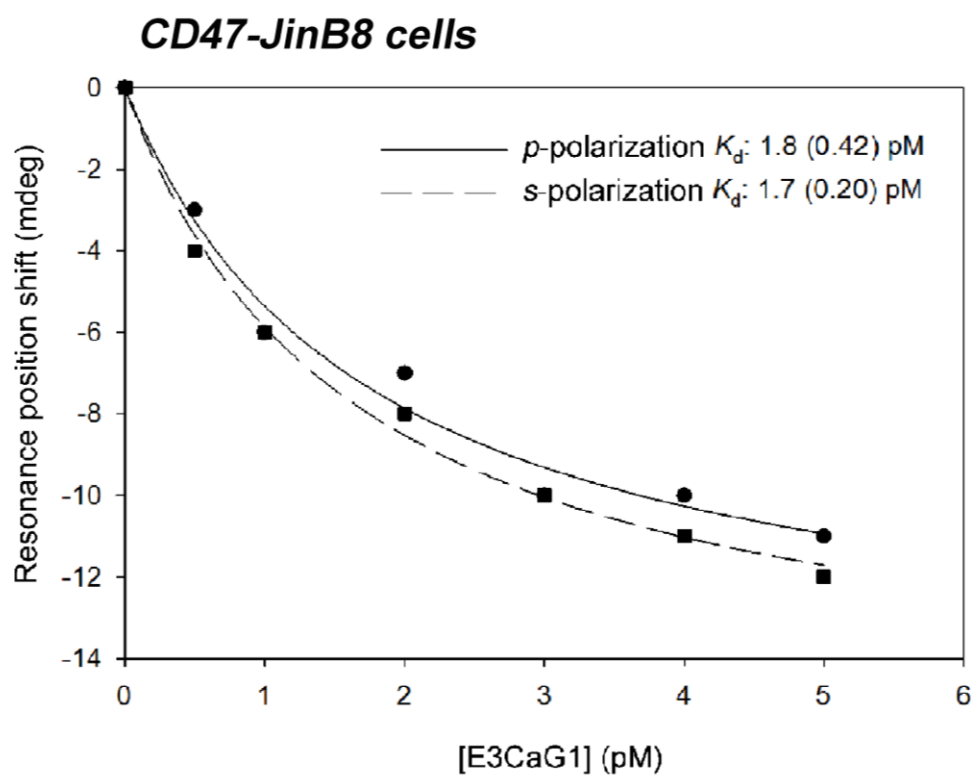


Figure 3.11. E3CaG1 binds to CD47-JinB8 plasma membranes with a pM K_d . The same experimental setup was done as described in Figure 2.10, only performed using CD47-JinB8 membranes.

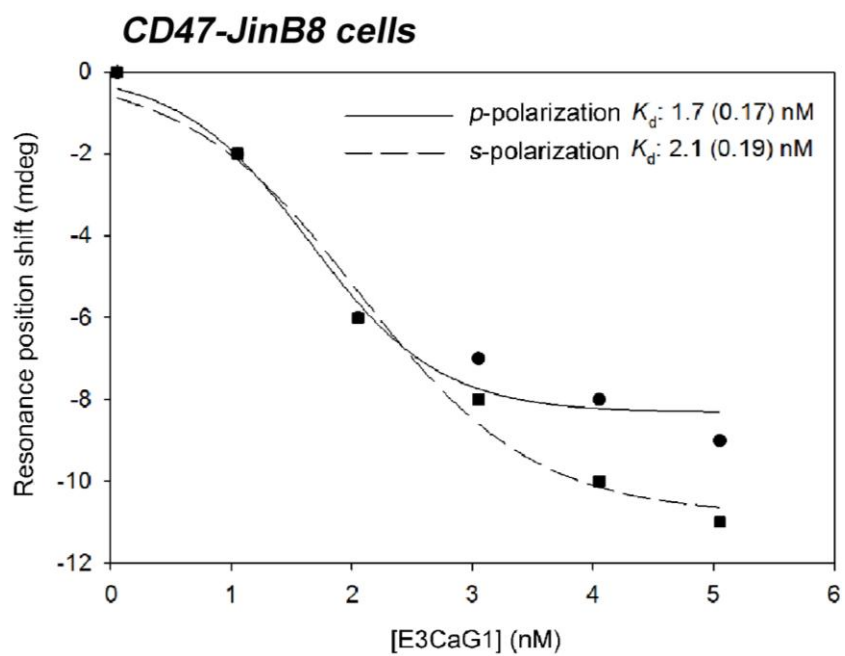


Figure 3.12. E3CaG1 binds to CD47-JinB8 plasma membranes with a nM K_d . The same experimental setup was done as described in Figure 2.11, only performed with CD47-JinB8 membranes.

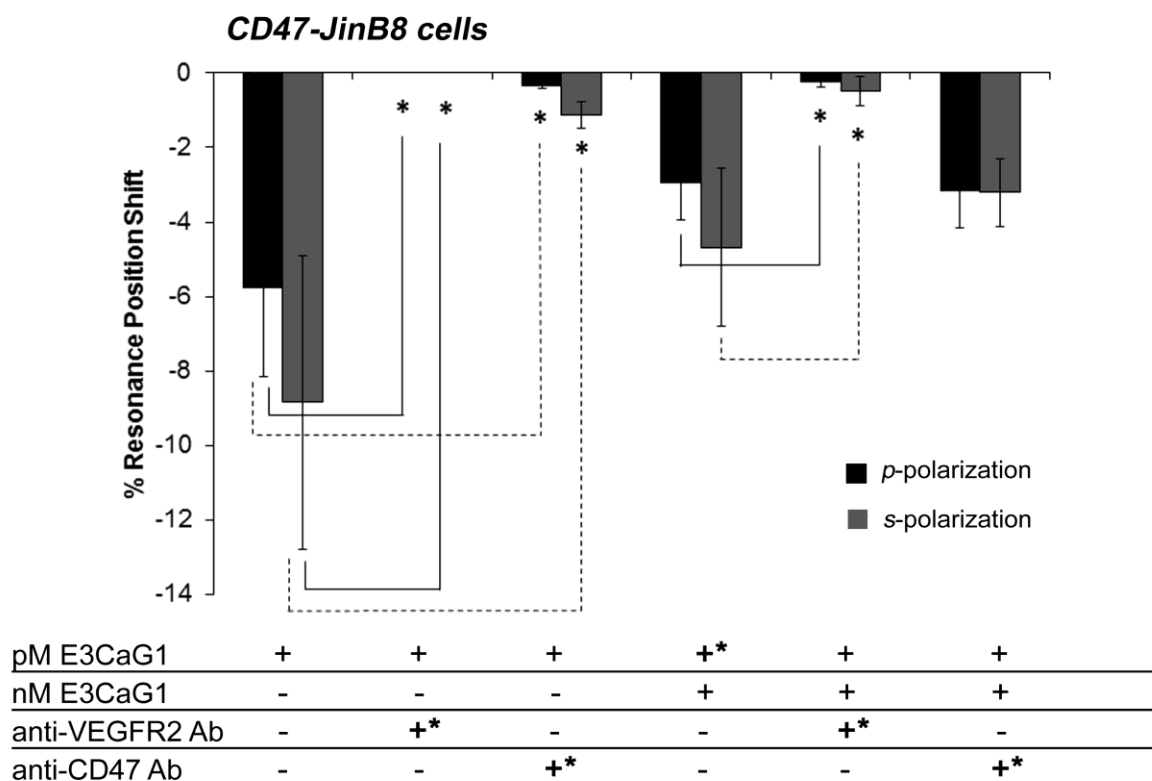
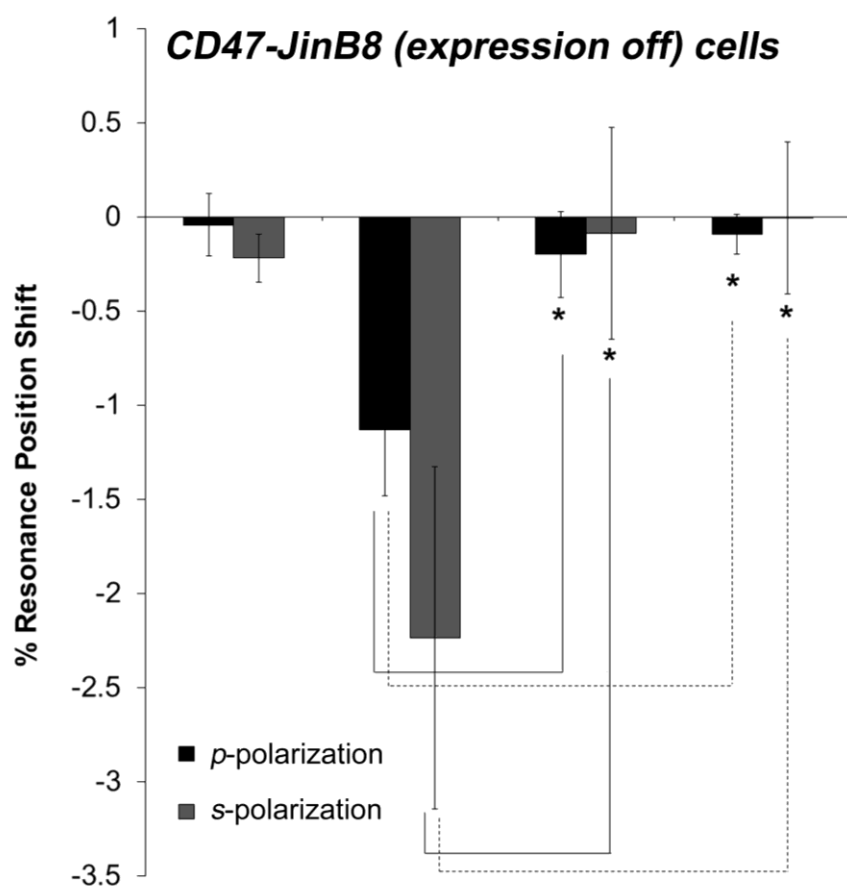


Figure 3.13. E3CaG1 binds to CD47/VEGFR2 with a pM affinity and another VEGFR2 complex with a nM affinity on CD47-JinB8 plasma membranes. Bar graphs depicting PWR percent resonance positions shifts on CD47-JinB8 plasma membranes upon pM and nM E3CaG1 binding, with or without prior incubation of anti-VEGFR2 (260.4) Ab or anti-CD47 (B6H12) Ab. +* indicates the ligand/antibody first added. – indicates the protein was not added to the membrane. For experiments where two proteins were added, the data shown are for the second protein. For experiments where three proteins were added, pM E3CaG1 sites were saturated prior to the addition of nM E3CaG1, and resulting percent resonance position shifts shown are those resulting only from nM addition of E3CaG1. Anti-VEGFR2 (260.4) antibody (a single amount of 50 pM was

added to membranes) inhibits both 50 pM and subsequent 5 nM E3CaG1 binding, indicating VEGFR2 is involved in binding to both complexes. Prior addition of anti-CD47 Ab (a single amount of 13.3 nM was added to membranes) inhibited 50 pM but not subsequent 5 nM binding of E3CaG1. Taken together, these results indicated on CD47-JinB8 membranes, E3CaG1 can bind to a CD47/VEGFR2 complex with pM affinity and a separate VEGFR2 complex not involving CD47 with nM affinity.

3.3.6 E3CaG1 binds to VEGFR2 in complex with integrin $\alpha_v\beta_3$ with a nM K_d

To further investigate this complex, E3CaG1 was added to CD47-JinB8 cells in which expression of CD47 had been turned off as well as JinB8 cells that did not contain CD47 (Figure 3.14 and 3.15). No significant pM E3CaG1 binding was observed on either cell line, which was expected since we have shown E3CaG1 binds to CD47 in complex with VEGFR2 with pM affinity. However, nM E3CaG1 binding was still observed on both cell lines (Figure 3.14 and 3.15). These data indicated E3CaG1 was binding to a complex not involving CD47 with nM affinity. E3CaG1 is known to have a β_3 integrin binding site in its third type II repeat, so we hypothesized that E3CaG1 was binding to VEGFR2 in complex with $\alpha_v\beta_3$ on CD47-JinB8 membranes. To test this hypothesis, anti- α_v as well as anti-VEGFR2 antibodies were added to CD47-JinB8 (expression off) membranes prior to the addition of E3CaG1. Both antibodies inhibited E3CaG1 resonance position shifts (Figure 3.14). In addition, no binding of anti- α_v nor anti-VEGFR2 antibodies was observed on purified JinB8 plasma membranes after addition of nM E3CaG1 (Figure 3.15). Therefore, we concluded E3CaG1 was binding to a VEGFR2/ $\alpha_v\beta_3$ complex. In addition, when anti-CD47 antibody was pre-incubated on CD47-JinB8 (expression on) membranes, pM E3CaG1 binding was retained whereas nM binding was not (Figure 3.13). This confirmed E3CaG1 was binding to a VEGFR2 complex not involving CD47 with a nM K_d on JinB8 and derivations of JinB8 cell lines. The presence of a limited amount of VEGFR2/ $\alpha_v\beta_3$ complex could also explain the slight reduction in nM E3CaG1 binding on low-passage Jurkat membranes upon prior incubation with anti-VEGFR2 antibody. In spite of the identification of VEGFR2/ $\alpha_v\beta_3$



pM E3CaG1	+	++	-	-
nM E3CaG1	-	+	+	+
anti-VEGFR2 Ab	-	-	++	-
anti- α_v Ab	-	-	-	++

Figure 3.14. E3CaG1 binds to VEGFR2/ $\alpha_v\beta_3$ on CD47-JinB8 (expression off membranes). PWR bar graph depicting percent resonance position shifts upon E3CaG1 addition on CD47-JinB8 (expression off) membranes. ++ indicates the ligand/antibody first added. - indicates the protein was not added to the membrane. For experiments where two proteins were added, the data shown are for the second protein. No significant shifts were observed upon 50 pM E3CaG1 binding due to the fact that no CD47 was

present. However, subsequent 5nM E3CaG1 binding was observed (nM E3CaG1 was titrated on the membrane ranging from 1 nM to 5 nM). nM E3CaG1 binding was inhibited by pre-incubation of either 6.65 nM anti- α_v (272-17E6) or 50 pM anti-VEGFR2 (260.4) Ab (single amounts of the antibodies were added to the membrane prior to addition to a single amount of 5 nM E3CaG1).

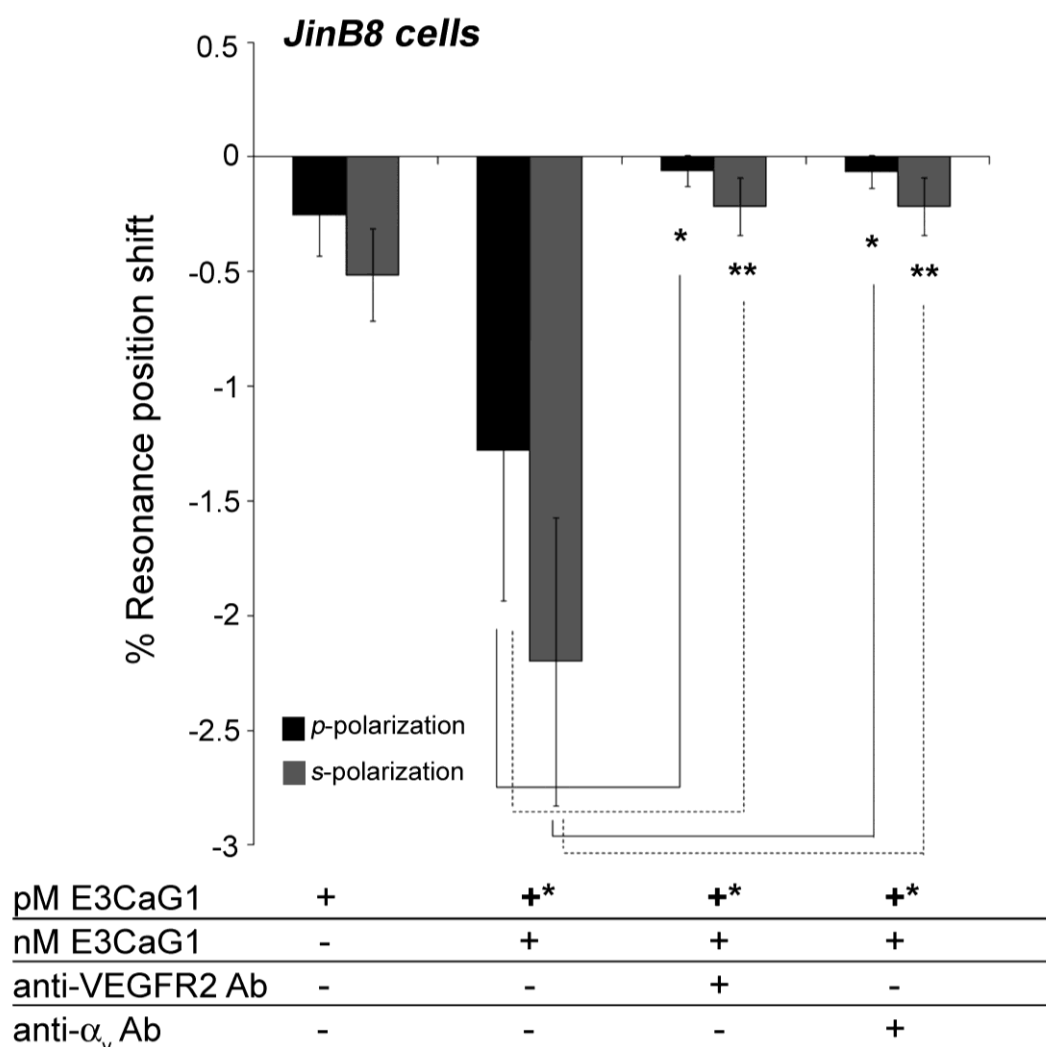


Figure 3.15. E3CaG1 inhibits anti- α_v and anti-VEGFR2 Ab binding to JinB8 plasma membranes. PWR bar graph showing percent resonance position shifts upon E3CaG1 addition to JinB8 membranes. **+** indicates the ligand/antibody first added. **-** indicates the protein was not added to the membrane. For experiments where two proteins were added, the data shown are for the second protein. For experiments where three proteins were added, pM E3CaG1 was added prior to the addition of nM E3CaG1, and resulting

percent resonance position shifts shown are those resulting only from subsequent antibody addition. The same trend was observed on JinB8 membranes as on CD47-JinB8 (expression off) membranes. No pM E3CaG1 binding was observed, but subsequent nM E3CaG1 binding was measured (a single amount of 50 pM E3CaG1 was added to the membranes, followed by a single amount of 5 nM E3CaG1). Subsequent addition of 6.65 nM anti- α_v (272-17E6) or 50 pM anti-VEGFR2 (260.4) Ab (added in single amounts) did not produce significant resonance position shifts, indicating the presence of E3CaG1 inhibited antibody binding to their receptors.

on the CD47-JinB8 cell line, the presence of a CD47/ $\alpha_v\beta_3$ complex cannot be excluded, since incubation with anti-CD47 antibody did seem to slightly reduce the *s*-polarization percent resonance position shift caused by nM E3CaG1 addition. Therefore, it is possible a small amount of CD47/ $\alpha_v\beta_3$ resides within CD47-JinB8 membranes, and the sigmoidal E3CaG1 nM binding curve (Figure 3.12) could be representative of E3CaG1 binding to this complex, VEGFR2/ $\alpha_v\beta_3$, or perhaps represents E3CaG1 binding to a combination of the two. When E3CaG1 was added to CD47-JinB8 (expression off) membranes, a K_d of 1.8 nM was measured for binding to the VEGFR2/ $\alpha_v\beta_3$ complex through addition of increasing amounts of nM E3CaG1 (Figure 3.16, Table 2.1). This curve was hyperbolic, and differed from the nM E3CaG1 binding curve observed on CD47-JinB8 (expression on) membranes, giving support to the presence of a small amount of CD47/ $\alpha_v\beta_3$ complex on CD47-JinB8 membranes in addition to the larger amount observed on low-passage Jurkat membranes. This data could suggest the sigmoidal curve observed when nM E3CaG1 was added to CD47-JinB8 (expression on) membranes could be a combination of two hyperbolic curves, measuring binding to both CD47/ $\alpha_v\beta_3$ and VEGFR2/ $\alpha_v\beta_3$.

3.4 Discussion

In this chapter, I have shown that the transmembrane protein CD47 associates with other membrane proteins such as vascular endothelial growth factor receptor 2 and integrin $\alpha_v\beta_3$ on native Jurkat T cell plasma membranes. Since CD47 associates with multiple binding partners, precise measurement of dissociation constants to particular CD47 complexes is complicated, and is further made difficult by determination of K_d values within the native membrane environment. However, PWR spectroscopy allowed

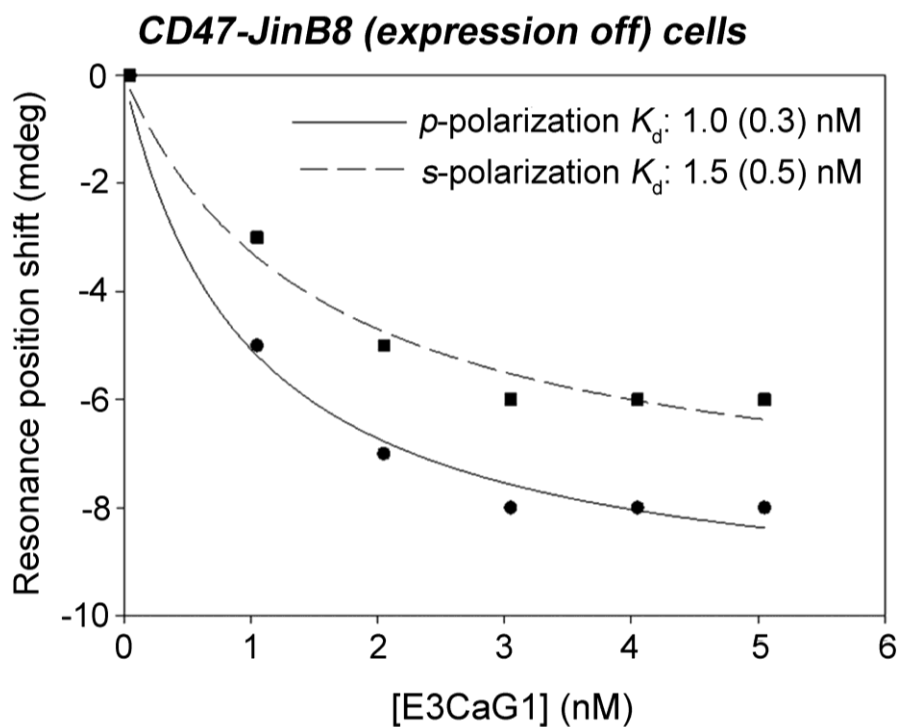


Figure 3.16. E3CaG1 binding curve to CD47-JinB8 (expression off) plasma membranes. E3CaG1 was added in increasing amounts to purified CD47-JinB8 (expression off) plasma membranes, and a representative set of p - and s -polarization binding curves are shown. E3CaG1 bound with a nM K_d .

for precise measurement of dissociation constants of multiple CD47 complexes through changes in refractive index upon ligand binding. Through PWR spectroscopy, I have shown E3CaG1 binds to CD47 in complex with VEGFR2 with a picomolar dissociation constant on both Jurkat and CD47-JinB8 cell lines (Figure 3.2 and 3.12). The identification of a CD47/VEGFR2 complex by PWR spectroscopy is consistent with immunoprecipitation experiments showing the association of CD47 with VEGFR2 on HUVEC cells (76). This is not the first evidence of a picomolar dissociation constant between a ligand and its receptor. For example, transforming growth factor beta-1 (TGFB-1) has been reported to bind to the TGFB receptor with a 50 pM K_d (120), and antibody-antigen interactions also range from pM to low nM (121). Biotin binds to avidin with an even higher affinity, on the order of 4×10^{-14} M (122). Tumor necrosis factor (TNF) can bind to the TNF receptor-1 (TNF-R1) with high affinity (19 pM K_d) while binding to the TNF receptor-2 (TNF-R2) with lower affinity (420 pM K_d), and the higher affinity binding has been attributed to the higher stability of the TNF/TNF-R1 interaction (123). Therefore, E3CaG1 binding to CD47 in complex with VEGFR2 creates a stable interaction strengthened by multiple intermolecular forces in order for the ligand to bind with such high affinity.

CD47 is also widely known to associate with integrin $\alpha_v\beta_3$ on platelets, ovarian OV10 cells, and C32 melanoma cells (59, 71, 72), so it is not surprising that I have shown this interaction to occur on Jurkat T lymphocytes as well. E3CaG1 was determined to bind to a second CD47 complex involving $\alpha_v\beta_3$ with approximately 1000-fold less affinity than the CD47/VEGFR2 complex. E3CaG1 was also shown to bind to a

protein complex involving VEGFR2 and integrin $\alpha_v\beta_3$ on JinB8 cells and derivations of this cell line (Fig 3.13). It is possible that when CD47 is not available, VEGFR2 associates with $\alpha_v\beta_3$, which forms a complex that is known to exist (92, 93). For example, it was shown that the α_v as well as the β_3 domain of integrin $\alpha_v\beta_3$ were both required for VEGFR2 association, and this association was not dependent upon the growth factor activation of the VEGFR2 receptor (93). This evidence supports the binding of E3CaG1 to VEGFR2/ $\alpha_v\beta_3$ in our PWR experiments, which involve native membranes without the presence of VEGF.

CHAPTER 4

APPLICATION OF A FLUORESCENCE-BASED CALCIUM ASSAY AS A FUNCTIONAL READOUT FOR THROMBOSPONDIN-1 BINDING TO CD47

4.1 Introduction

In this chapter, I describe the use of a flow cytometry calcium assay to determine which of the identified CD47 complexes bind E3CaG1 and cause a rise in intracellular calcium. Our laboratory recently demonstrated that E3CaG1 binding leads to a rise in $[Ca^{2+}]_i$ to ~250 uM, and that this rise was required for inhibition of sGC (82). Monitoring of E3CaG1-dependent increases in $[Ca^{2+}]_i$ therefore provides a convenient readout for functional binding. Since it has already been shown $\alpha_v\beta_3$ is not involved in the E3CaG1-induced decrease in sGC activity, the next step was to test if a VEGFR2/CD47 complex was required. Flow cytometry proved to be useful as a functional assay for E3CaG1 because after a fluorescence calcium indicator was added to cells, sub-populations that responded to E3CaG1 by showing an increase in fluorescence could be identified. This is an advantage when compared to measurement of fluorescence by a spectrophotometer, which only provides an average fluorescence of the population and small changes are difficult to detect. Detection is additionally complicated by the transient nature and high fluctuations in calcium mobilization. I therefore used flow cytometry to measure calcium changes in both suspension and adherent cells before and after treatment with antibodies to determine if the VEGFR2/CD47 complex was functionally significant in regulating the NO pathway.

4.2 Materials and Methods

4.2.1 Materials

Ionomycin and Fluo-3-AM were obtained from Invitrogen (Grand Island, NY).

Other materials used are described in previous chapters.

4.2.2 Cell culture

Cells were maintained as described in previous chapters.

4.2.3 Flow cytometry calcium assay

0.5×10^6 Jurkat, CD47-JinB8, or JinB8 cells per condition were serum starved for 48 hours prior to the experiment. Suspension cells were centrifuged at $180 \times g$ for 5 min at room temperature before being loaded with 2.5-5 μM Fluo-3-AM for 30 min at room temperature. Cells were washed twice with Krebs buffer, and resuspended in 400 μl Krebs buffer per condition. Cells were put in a Greiner 96-well round-bottom polystyrene plate, then incubated with 10 nM anti-VEGFR2 (260.4), anti- α_v (272-17E6), or anti-CD47 (B6H12) antibodies for 20 min at room temperature. E3CaG1 or buffer alone (TBS supplemented with 2 mM CaCl_2) was added to the wells. Fluorescence was measured using a Guava easyCyte 8HT flow cytometer in plate format. A 75 mW blue laser with an excitation wavelength of 488 nm was used to excite fluorophores and fluorescence was collected using a 525/30 nm emission filter. 5000 cells were counted for each condition, and were gated on live cells using forward and side scatter fluorescence. Cells were treated with 15 μM ionomycin and 750 μM CaCl_2 as a positive control and all populations were gated on this condition to determine which cells showed an increase in intracellular calcium. The MFI at 525 nm was multiplied by the percentage of cells within the positive gate (of the total population), which resulted in the

total MFI. Cells without Fluo-3-AM showed no fluorescence under these gating conditions. Total MFI from addition of buffer alone was subtracted from each well to calculate relative MFI. Data analysis was performed using Millipore InCyte software.

4.3 Results

4.3.1 Measurement of TSP-1 induced intracellular calcium increase by flow cytometry

To determine if the increase in $[Ca^{2+}]_i$ caused by E3CaG1 could be observed by flow cytometry, Jurkat cells were loaded with Fluo-3-AM, a fluorescent dye that is converted to Fluo-3 by esterases once inside the cell. Fluo-3 is the form that readily binds to calcium. Fluorescence of Fluo-3 increases once bound to calcium, and can thus be used as an assay for calcium levels in live cells. In Jurkat cells, E3CaG1 caused an increase in fluorescence when treated with 10 pM, 1 nM, and 25 nM E3CaG1 as measured by flow cytometry compared to buffer alone (Figure 4.1). There were no significant differences in calcium increases between the three concentrations, showing that treatment with pM E3CaG1 saturates the CD47/VEGFR2 complex and supports a pM K_d .

4.3.2 Anti-VEGFR2 antibody inhibits E3CaG1-induced $[Ca^{2+}]_i$ in Jurkat cells

Due to the reported constitutive VEGFR2 association with CD47 in endothelial cells and that addition of an anti-VEGFR2 antibody inhibited pM E3CaG1 binding by PWR spectroscopy, we wanted to determine if addition of anti-VEGFR2 antibody affected E3CaG1-induced calcium levels within the NO pathway. Addition of E3CaG1 caused increases in $[Ca^{2+}]_i$ as shown by flow cytometry. However, pre-incubation with an anti-VEGFR2 antibody inhibited this increase in fluorescence at all three E3CaG1

concentrations (Figure 4.1 and Figure 4.2). This suggests VEGFR2 in complex with CD47 is involved in the E3CaG1-induced rise in intracellular calcium in Jurkat cells.

4.3.3 E3CaG1 binds to CD47 in complex with VEGFR2 to cause an increase in intracellular calcium in JinB8 cells stably transduced with CD47-eGFP

Since E3CaG1 produces a rise in $[Ca^{2+}]_i$ in Jurkat T cells, and this calcium increase involves VEGFR2, I wanted to determine if CD47-eGFP was functional in CD47-JinB8 cells and if the same trend was observed. Cells were loaded with Fluo-3-AM, washed to remove excess dye, and incubated with E3CaG1 or buffer alone. 10 pM, 1 nM, and 25 nM E3CaG1 all caused increases in calcium compared to buffer alone (Figure 4.3 and Figure 4.4). However, anti-VEGFR2 (260.4) antibody added to cells prior to E3CaG1 inhibited the increase in $[Ca^{2+}]_i$, which was also observed in native Jurkat T cells. This suggests CD47-eGFP is functional and associates with VEGFR2 to cause a rise in calcium upon E3CaG1 binding.

4.3.4 E3CaG1 binds to VEGFR2 in complex with $\alpha_v\beta_3$ to cause a decrease in intracellular calcium in CD47-null cells

VEGFR2 activation can result in phospholipase C (PLC) activation, producing inositol triphosphate (IP3) and leading to release of intracellular calcium stores (124, 125). Since our data suggests VEGFR2 associates with $\alpha_v\beta_3$ on CD47-JinB8 cells, and intracellular calcium levels are affected by VEGFR2 phosphorylation, we asked whether E3CaG1 binding to VEGFR2/ $\alpha_v\beta_3$ affected intracellular calcium levels. CD47-null JinB8 cells were used for a calcium assay as was done with CD47-JinB8 cells. Fluo-3-AM-loaded JinB8 cells were incubated with E3CaG1 or buffer, with and without prior

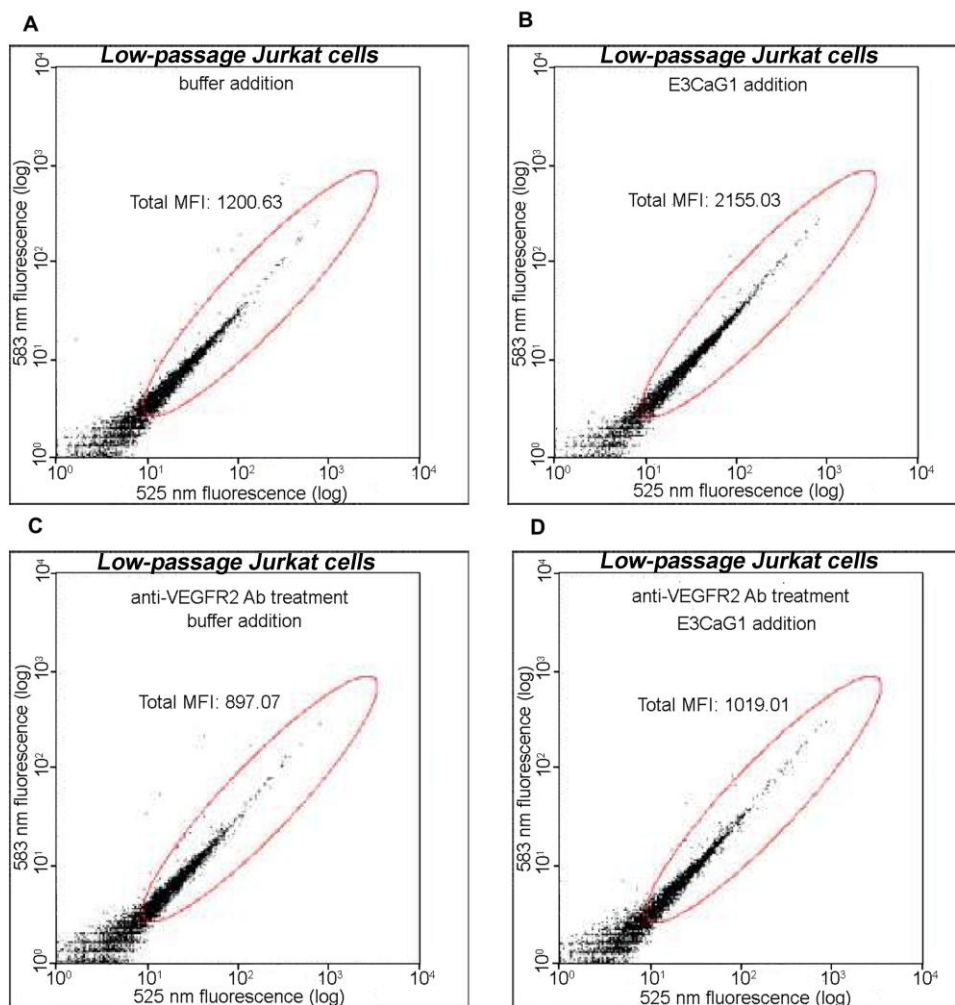


Figure 4.1. Dot plots showing calcium fluorescence upon addition of E3CaG1 in low-passage Jurkat cells. Incubation with anti-VEGFR2 Ab inhibited the calcium increase caused by E3CaG1. Fluorescence at 525 nm is shown on the x-axis. *A*. Fluorescence produced by background $[Ca^{2+}]_i$ (from the Fluo-3-AM indicator) shown from addition of buffer alone. *B*. Fluorescence increase shown from addition of 25 nM E3CaG1. *C*. Same as *A*, only cells were pre-incubated with anti-VEGFR2 Ab prior to buffer addition. *D*. Same as *B*, only cells were pre-incubated with anti-VEGFR2 Ab prior to E3CaG1 addition.

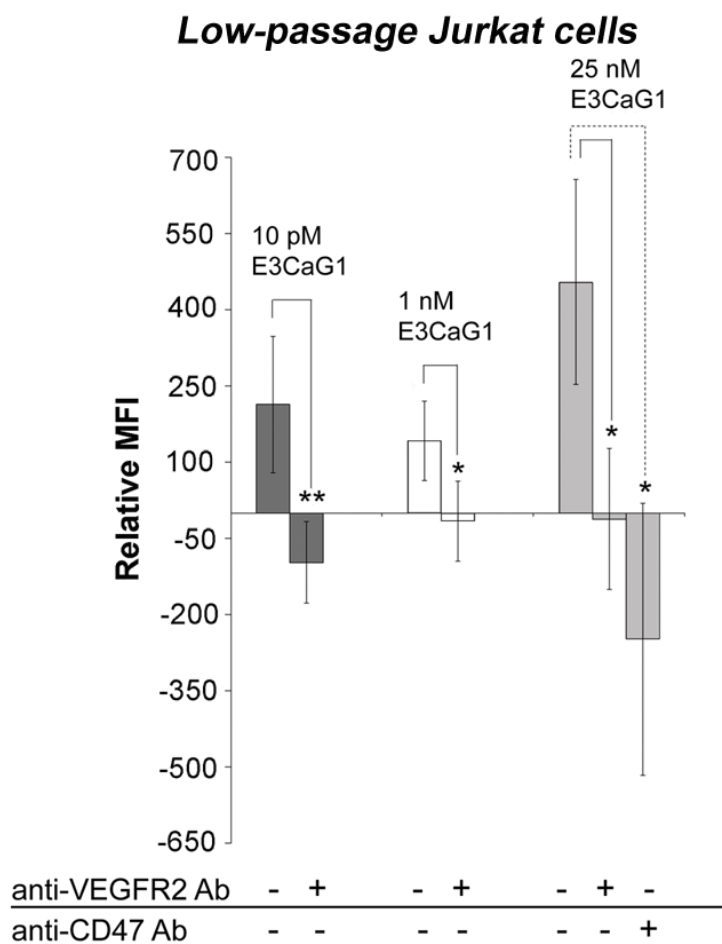


Figure 4.2. CD47 associates with VEGFR2 to produce an E3CaG1-induced rise in $[Ca^{2+}]_i$ in Jurkat cells. Graphical representation of Figure 4.1. Low-passage Jurkat cells were loaded with Fluo-3-AM, followed by addition of 10 pM, 1 nM, or 25 nM E3CaG1 for 10 min. Flow cytometry was used to measure the increase in fluorescence at 488 nm (compared to addition of buffer alone). Relative MFI: $(MFI \times \% \text{ gated cells})_{\text{sample}} - (MFI \times \% \text{ gated cells})_{\text{buffer}}$. Relative MFI was calculated in order to normalize cells to background levels of calcium. Cells were incubated with 10 nM anti-VEGFR2 (260.4) Ab for 20 min prior to the addition of E3CaG1 to observe the effect of the antibody on

E3CaG1-induced calcium release. As a negative control, cells were also incubated with anti-CD47 (B6H12) Ab prior to the addition of 25 nM E3CaG1. E3CaG1 produced a rise in intracellular calcium at all three concentrations, but prior incubation of cells with both the anti-VEGFR2 and anti-CD47 antibodies inhibited this increase.

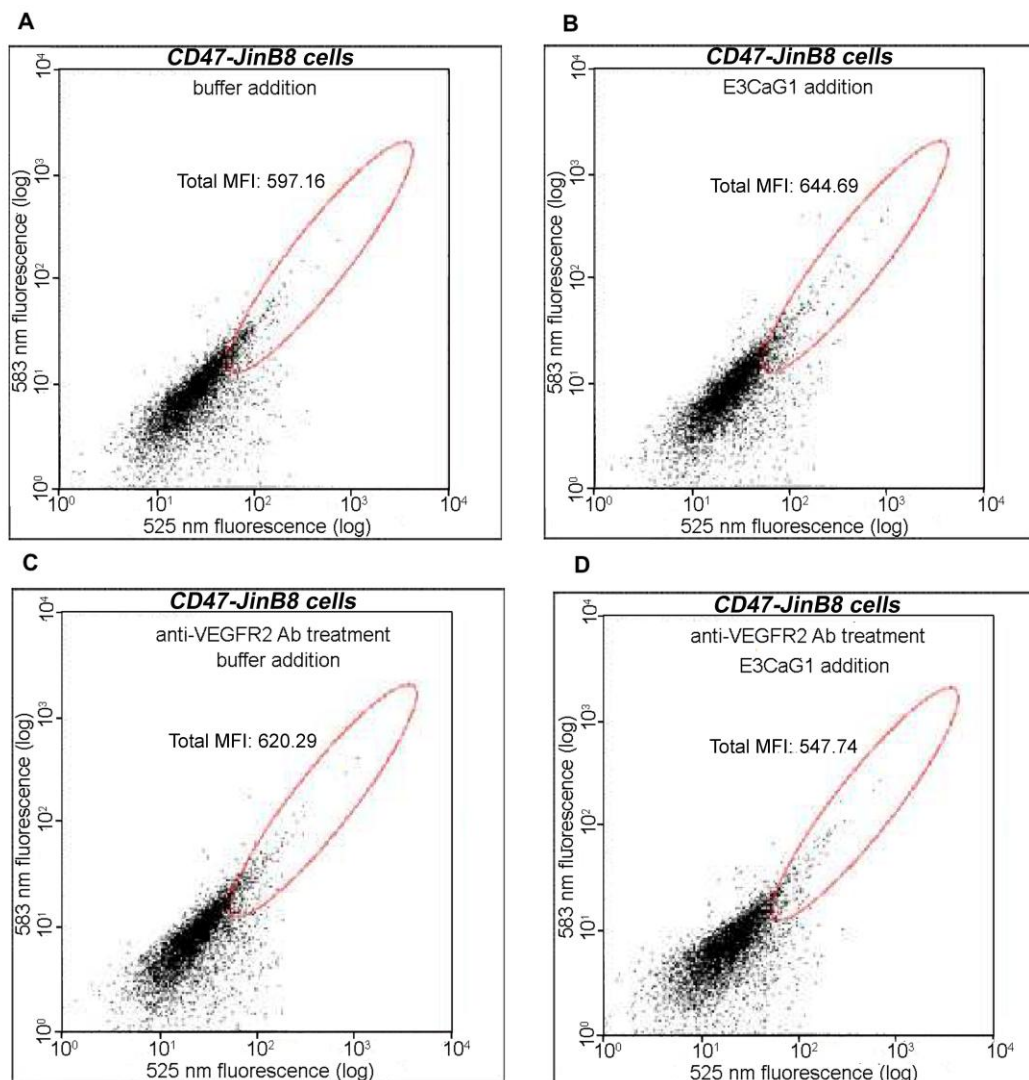


Figure 4.3. Dot plots showing E3CaG1-induced calcium increase in CD47-JinB8 cells. Incubation with anti-VEGFR2 Ab inhibited the calcium increase caused by E3CaG1. Fluorescence emitted at 525 nm is shown on the x-axis. *A.* Cells incubated with buffer alone. *B.* Cells incubated with 25 nM E3CaG1. *C.* Same as *A*, only cells were previously incubated with 10 nM anti-VEGFR2 (260.4) Ab. *D.* Same as *B*, only cells were previously incubated with 10 nM anti-VEGFR2 (260.4) Ab.

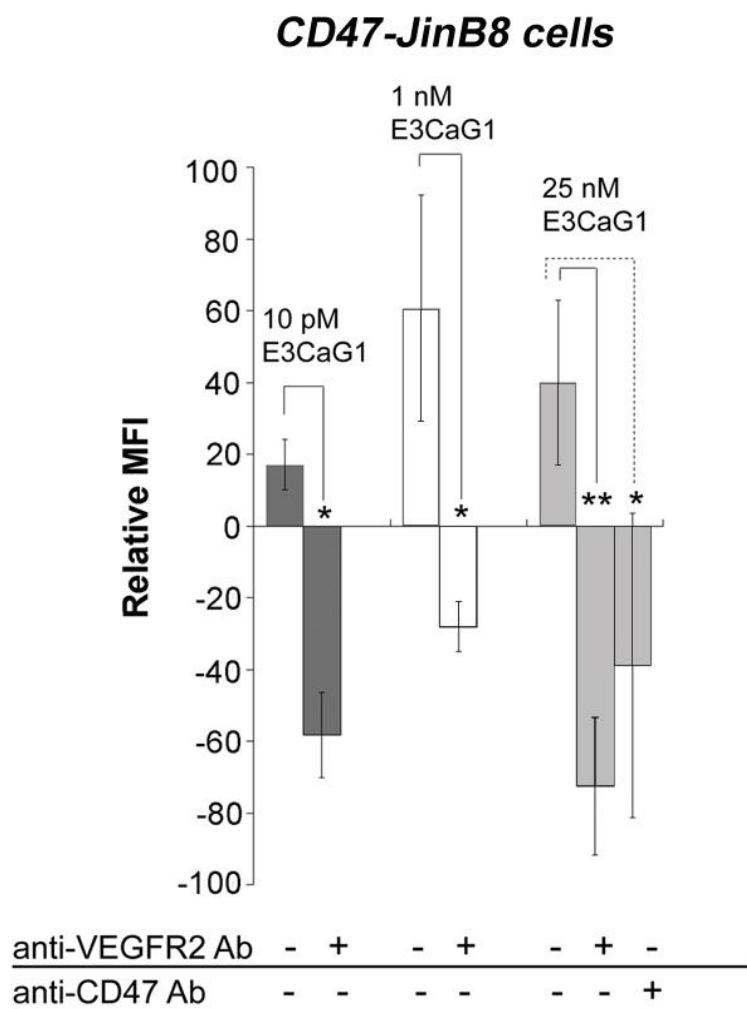


Figure 4.4. CD47 associates with VEGFR2 to produce an E3CaG1-induced rise in $[Ca^{2+}]_i$ in CD47-JinB8 cells. Graphical representation of Figure 4.3. The experimental setup was done as described in Figure 4.2, except for using CD47-JinB8 cells. The same trend observed in Jurkat cells was also seen using CD47-JinB8 cells.

incubation of anti-VEGFR2 or anti- α_v antibodies. Surprisingly, increasing concentrations of E3CaG1 caused a decrease in $[Ca^{2+}]_i$ compared to buffer alone (Figure 4.5 and Figure 4.6). Pre-incubation with either α_v or VEGFR2 antibodies significantly inhibited the 1 nM and 25 nM E3CaG1-induced calcium decrease. There was not a significant difference between calcium levels upon 10 pM E3CaG1 addition with and without prior incubation of α_v or VEGFR2 antibodies, which is probably due to the fact that E3CaG1 binds to VEGFR2/ $\alpha_v\beta_3$ with a nM K_d . Therefore, E3CaG1 binds to VEGFR2/ $\alpha_v\beta_3$ to decrease intracellular calcium levels. Addition of anti-CD47 antibody to both Jurkat and CD47-JinB8 cells caused a decrease in $[Ca^{2+}]_i$ (Figure 4.2 and Figure 4.4), which is explained by E3CaG1 binding to VEGFR2/ $\alpha_v\beta_3$. As mentioned in chapter 3, E3CaG1 binding to VEGFR2/ $\alpha_v\beta_3$ also explains why incubation of Jurkat cells with anti-VEGFR2 antibody slightly reduced nM E3CaG1 binding. There is possibly a small amount of the VEGFR2/ $\alpha_v\beta_3$ complex on Jurkat plasma membranes, but not enough to significantly contribute to E3CaG1 binding, as shown in Figure 2.5. E3CaG1 can therefore cause increases and decreases in calcium based upon the VEGFR2 complexes to which it binds.

4.4 Discussion

E3CaG1 binds to CD47 to increase $[Ca^{2+}]_i$ on both live Jurkat T cells and CD47-JinB8 cells. This calcium increase occurs upon pM addition of E3CaG1 to both cell lines, and the increase is inhibited by prior addition of anti-VEGFR2 antibody. This not only shows CD47-eGFP is active within CD47-JinB8 cells, but, in combination with PWR binding studies, shows that E3CaG1 binds to a CD47/VEGFR2 complex to increase intracellular calcium levels. I also examined whether calcium levels were

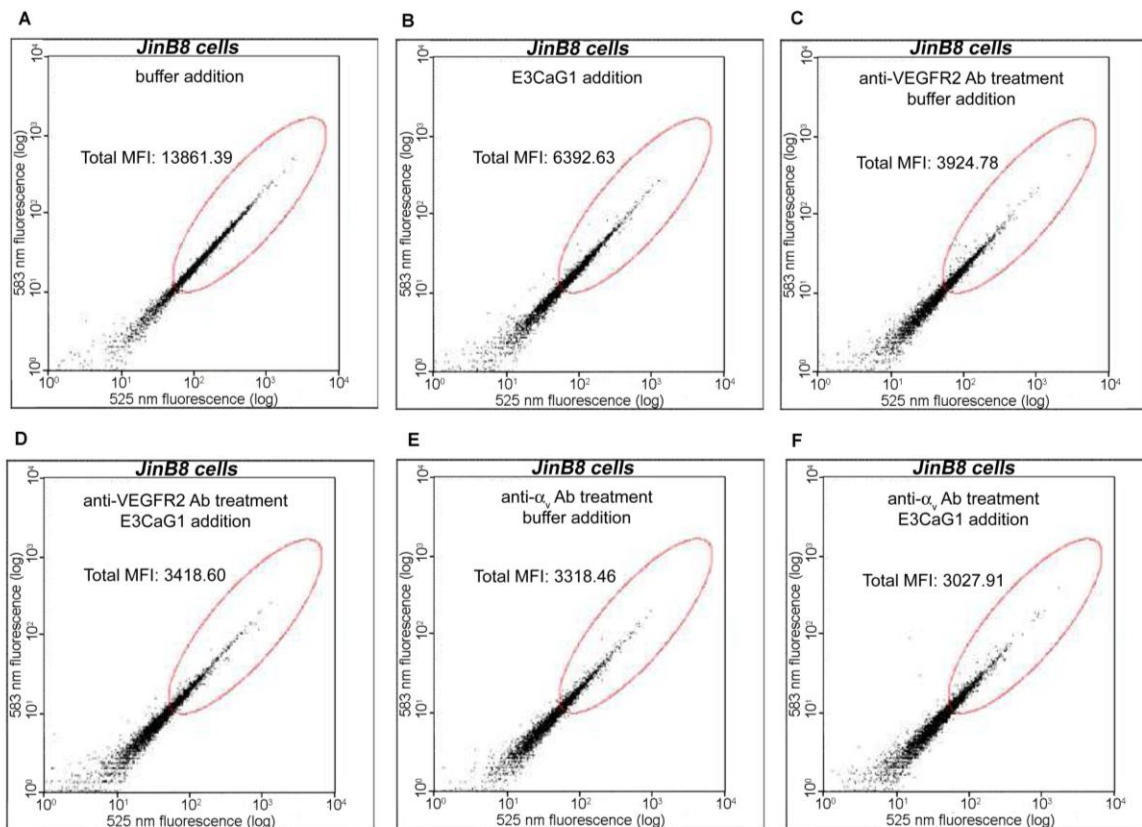


Figure 4.5. Dot plots showing changes in intracellular calcium fluorescence upon E3CaG1 binding to JinB8 cells. Fluorescence emitted at 525 nm is shown on the x-axis. A. Fluorescence from addition of buffer alone. B. Fluorescence from addition of 25 nM E3CaG1. C. and D. Same as A, and B, respectively, except cells were pre-incubated with 10 nM anti-VEGFR2 (260.4) Ab. E. and F. Same as A, and B, respectively, except cells were pre-incubated with 10 nM anti- α_v (272-17E6) Ab.

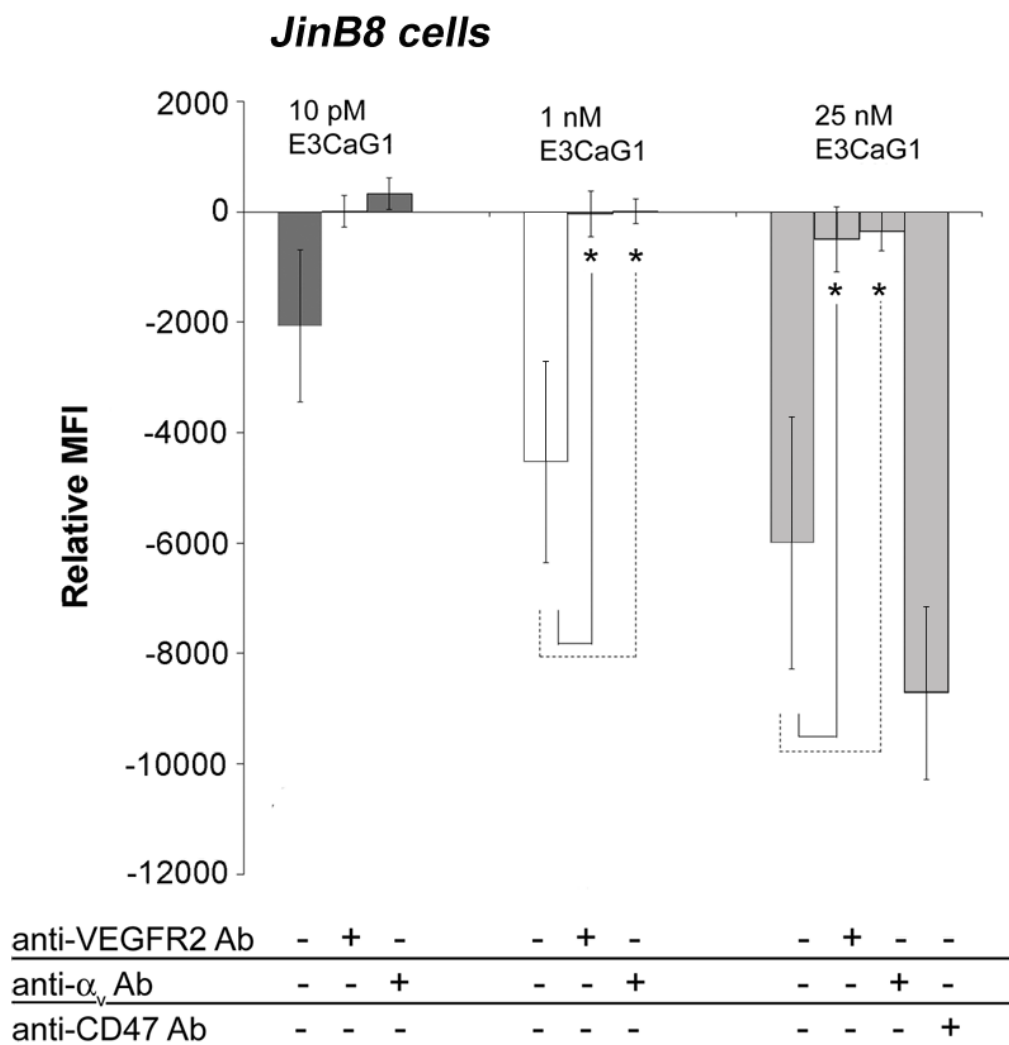


Figure 4.6. E3CaG1 binds to VEGFR2/ $\alpha_v\beta_3$ to decrease $[Ca^{2+}]_i$. Graphical representation of Figure 4.5. Experimental setup is the same as described in Figure 4.2, except done using JinB8 cells. In addition to anti-VEGFR2 (260.4) Ab, anti- α_v (272-17E6) Ab was also added to cells prior to the addition of E3CaG1. Both antibodies inhibited E3CaG1-induced calcium decrease at 1 nM and 25 nM.

affected by E3CaG1 binding to the VEGFR2/ $\alpha_v\beta_3$ complex that was shown to exist on JinB8 cell lines and their derivations. Unexpectedly, addition of E3CaG1 to VEGFR2/ $\alpha_v\beta_3$ was shown to cause a decrease in $[Ca^{2+}]_i$ on CD47-null JinB8 cells. Although VEGF binding to VEGFR2 is known to increase $[Ca^{2+}]_i$ to ultimately lead to an increase in eNOS activity and activation of sGC, eNOS activation requires phosphorylation through Akt (126). The increase in $[Ca^{2+}]_i$ alone does not increase sGC activity, so E3CaG1 binding to CD47/VEGFR2 to increase $[Ca^{2+}]_i$ to ultimately inhibit sGC activity is not a direct contradiction. Additionally, the mechanism of VEGFR2 activation in relation to inhibition of NO signaling in Jurkat cells is unclear. Therefore, it is possible E3CaG1 can inhibit the angiogenic effects of VEGF in Jurkat cells through different mechanisms: by binding to CD47 in complex with VEGFR2 to decrease sGC activation as well as binding to $\alpha_v\beta_3$ in complex with VEGFR2 to directly lower $[Ca^{2+}]_i$ levels. This can be yet another example of cellular cross-talk within signaling pathways to regulate the effects of nitric oxide.

CHAPTER 5

IDENTIFICATION OF MEMBRANE PROTEINS REQUIRED FOR THROMBOSPONDIN-1 INDUCED CALCIUM SIGNALING

5.1 Introduction

Up to this point, I have shown evidence suggesting CD47 in complex with VEGFR2 is involved in the regulation of the NO signaling pathway through an E3CaG1-induced $[Ca^{2+}]_i$ increase. To confirm the roles for VEGFR2 and CD47 in E3CaG1-dependent $[Ca^{2+}]_i$ increase, I used shRNA to knockdown each receptor and measure calcium mobilization. I then replaced each gene and examined recovery of activity. By re-introducing CD47, VEGFR2, or both and performing a flow cytometry calcium assay, I could determine if one or both receptors were required for the $[Ca^{2+}]_i$ increase normally observed upon E3CaG1 binding. The same lentiviral transduction system described in Chapter 3 was used to deliver CD47 and VEGFR2 shRNA into HEK293T cells. Flow cytometry was used to determine if expression of these receptors were removed from the cell surface, and then CD47 with a C-terminal eGFP tag, VEGFR2 with a C-terminal mCherry tag, or both were transiently transfected into the knocked down HEK 293T cells. E3CaG1 was added to cells, and increases in calcium were compared to mock transfected cells to determine which receptors were required for increases in $[Ca^{2+}]_i$.

5.2 Materials and Methods

5.2.1 Materials

HEK293T cells were a gift from Dr. Roger Meisfeld (University of Arizona). Plasmids encoding human CD47 with a C-terminal eGFP tag and VEGFR2 with a C-

terminal mCherry tag were generous gifts from Dr. David Roberts (NIH). Other materials used were the same as described in previous chapters.

5.2.2 Cell culture

HEK293T cells were maintained in DMEM (Invitrogen) supplemented with 10% FBS, 5 mg/ml penicillin, and 1 mg/ml streptomycin. Other cell lines used in this chapter were maintained as described in previous chapters.

5.2.3 Flow cytometry binding studies

For adherent cells, HEK 293T and HEK 293T (CD47- /VEGFR2-null) cells, approximately 75% confluent cells grown in a 2 cm² area were used for each condition. The cells were washed once in PBS and once in stain/wash buffer and pipetted up and down to remove the cells from the wells. The cells were transferred to 1.5 ml Eppendorf tubes and incubated for 30 min on ice with anti-CD47 (B6H12) or anti-VEGFR2 (260.4) antibodies. Cells were resuspended in stain/wash buffer and fixed with 2% (v/v) PFA for 15 min at 4 °C. Cells were centrifuged as described, resuspended in stain/wash buffer, and incubated with 0.2 µg anti-mouse AlexaFluor 647 secondary antibody for 30 min at 4 °C. The cells were fixed again with 2% (v/v) PFA. Cells were analyzed using a LSR II flow cytometer (Becton Dickinson, Franklin Lakes, NJ) with an excitation wavelength of 640 nm and a 670/14 nm emission filter, or analyzed with a Guava easyCyte 8HT flow cytometer using a 40 mW red laser with an excitation wavelength of 635 nm and a 661/19 emission filter. 2,000 cells were counted and gated on live cells using forward and side scatter fluorescence. Cells without any fluorophore and those incubated with secondary antibody alone were used as controls. Total and relative MFI were calculated

as described in 3.2.7 using 670 nm or 661 nm fluorescence. Data analysis was performed using FloJo or Millipore InCyte software.

5.2.4 Confocal microscopy

HEK 293T cells were plated on 1.5 coverlips in live cell dishes (MatTek, Ashland, MA) 24 hours prior to transfection with CD47-eGFP, VEGFR2-mCherry, or both. Cells were washed with Krebs buffer prior to imaging. Images were taken on a Nikon C1si scanning confocal microscope using a 60x, 1.4NA oil-immersion objective and a Nikon CCD camera. To view samples, a 488 nm excitation laser with a 525/50 nm detector was used to view eGFP fluorescence and a 561 nm excitation laser with a 595/50 nm detector was used to view mCherry fluorescence. Each sample was viewed with both lasers to confirm the presence or absence of CD47-eGFP and/or VEGFR2-mCherry. At least three random fluorescence images were recorded for each sample. Nikon EZ-C1 version 3.8 software was used to acquire images.

5.2.5 Generation of lentivirus

The same procedure for generation of lentivirus as described in Chapter 3.2.4 was performed with CD47 shRNA (NM_001777) and KDR shRNA (targeting for VEGFR2, NM_002253) plasmids (Sigma). Viral titers were determined using the Lenti-X p24 rapid titer kit (Clontech).

5.2.6 Stable transduction of cells

HEK293T cells were plated in 10 cm dishes prior to transduction. Cells were then co-transduced with CD47 shRNA and KDR shRNA lentivirus with a multiplicity of infection of 2 for 24 hours. The media was removed and cells were incubated in DMEM

supplemented with 10% FBS, 5 mg/ml penicillin, 1 mg/ml streptomycin, and 3 µg/ml puromycin for 13 days, until cells started growing. The amount of antibiotic was then reduced to 0.25 µg/ml puromycin and cells were maintained at this concentration from this point forward.

5.2.7 Transfection of HEK 293T cells

HEK 293T cells stably transduced with CD47 and KDR shRNA were grown in a 6-well plate 24 hours before the transfection. The cells were 80 - 90% confluent the day of the transfection, and 4 µg of CD47-eGFP, VEGFR2-mCherry, or 4 µg of each were transfected into cells using Turbofect transfection reagent per manufacturer's instructions. Cells were transfected for 42 hours prior to being loaded with Fluo-3-AM and used in a calcium assay. Although cells used for transfection had stable CD47 and VEGFR2 knockdowns, if the amount of DNA re-introduced into the cells by transfection is greater than the capacity of the shRNA, then the protein should still be able to be translated. There have been other successful reports of transfection of presenilin-1 (PS1) and presenilin-2 (PS2) transmembrane receptors which restore expression in knockout mice (127).

5.2.8 Flow cytometry calcium assay

The flow cytometry calcium assay was performed as described in Chapter 4.2.3 with the following changes. HEK 293T cells were placed in a 6-well plate 24 hours prior to the experiment so that they were 80%-90% confluent the day of the experiment. The media was removed and cells were loaded with 5 µM Fluo-3-AM in their wells. For HEK 293T cells stably transduced with CD47-eGFP, VEGFR2-mCherry, or both,

background fluorescence was measured and subtracted from cells that had been treated with E3CaG1 as described in 4.2.3. Data analysis was performed using Millipore InCyte software.

5.3 Results

5.3.1 Determination of relative CD47 and VEGFR2 levels in native HEK 293T cells by flow cytometry

To test the hypothesis that both CD47 and VEGFR2 were required for E3CaG1-induced $[Ca^{2+}]_i$ increase, I generated a cell line that contained neither VEGFR2 nor CD47. However, before this was done, I first confirmed that native HEK 293T cells contained both VEGFR2 and CD47. Anti-CD47 and anti-VEGFR2 antibodies were added to HEK 293T cells, followed by addition of anti-mouse AlexaFluor 647 secondary antibody and fluorescence was determined by flow cytometry. An increase in fluorescence compared to addition of secondary antibody alone was observed in cells treated with anti-CD47 antibody as well as those treated with anti-VEGFR2 antibody, indicating both receptors were present (Figure 5.1 and Figure 5.2).

5.3.2 Determination of CD47 and VEGFR2 levels in CD47- and VEGFR2-null HEK293T cells by flow cytometry

To knock down CD47 and VEGFR2 expression, HEK 293T cells were stably transduced with lentiviral CD47 shRNA and KDR shRNA. To confirm CD47 and VEGFR2 were no longer on the cell surface, HEK 293T (CD47- /VEGFR2- null) cells were incubated with anti-CD47 or anti-VEGFR2 antibodies followed by the addition of anti-mouse AlexaFluor 647 secondary antibody and fluorescence measured at 661 nm.

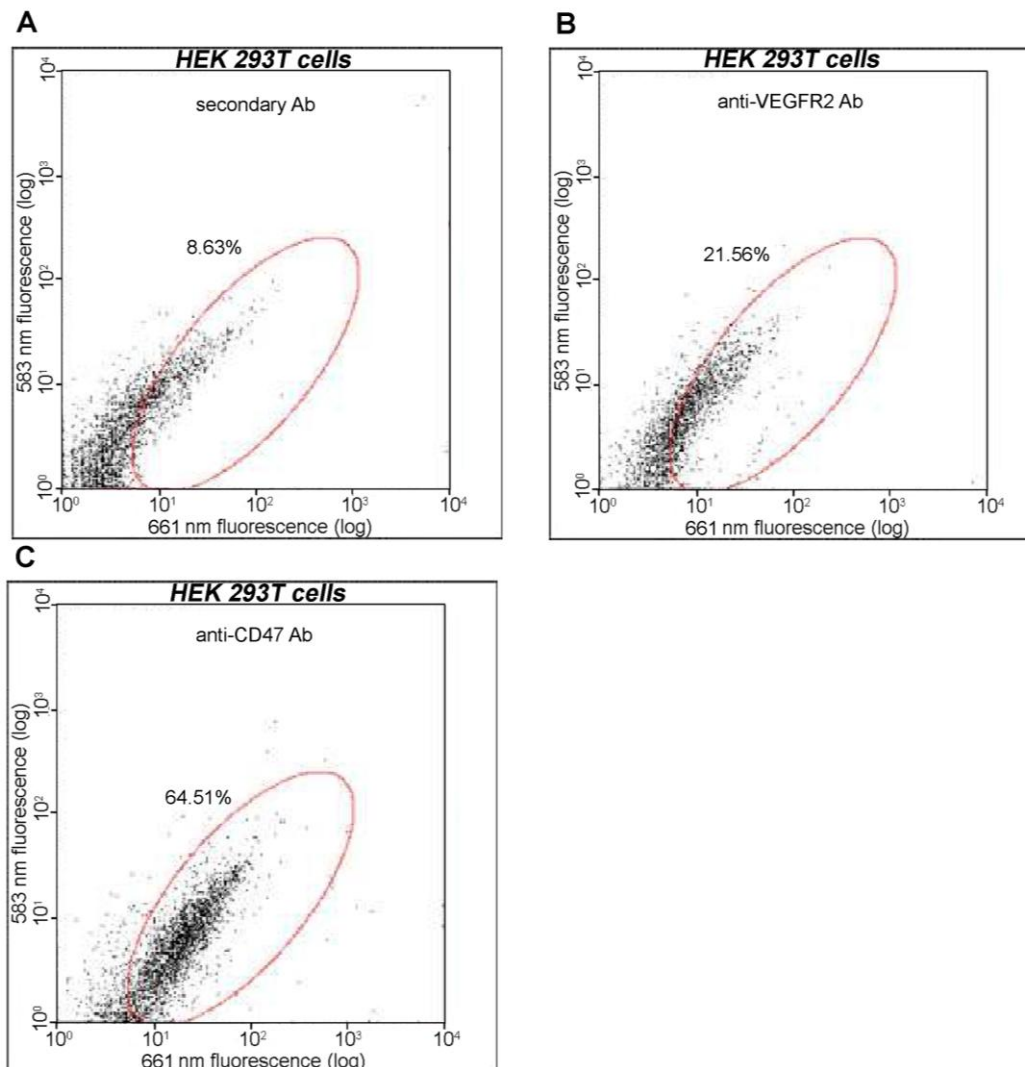


Figure 5.1. Dot plots showing fluorescence upon addition of anti-VEGFR2 (260.4) and anti-CD47 (B6H12) antibodies on native HEK 293T cells. Fluorescence at 661 nm is shown on the x-axis. *A*. Dot plot showing addition of anti-mouse AlexaFluor 647 Ab alone. *B*. Dot plot showing addition of anti-VEGFR2 Ab prior to addition of anti-mouse AlexaFluor 647 Ab. *C*. Dot plot showing addition of anti-CD47 Ab prior to addition of anti-mouse AlexaFluor 647 Ab. Both VEGFR2 and CD47 show an increase in fluorescence compared to addition of secondary Ab alone.

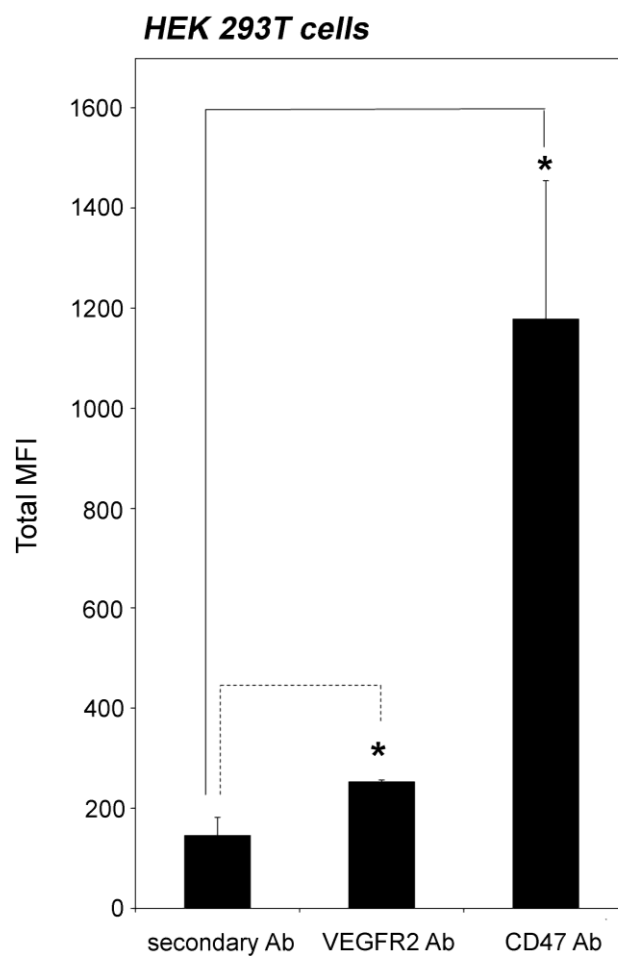


Figure 5.2. CD47 and VEGFR2 are present on HEK 293T cells. Graphical representation of Figure 5.1. Flow cytometry experiment showing total MFI resulting from the addition of anti-mouse AlexaFluor 647 secondary Ab alone, with and without prior addition of anti-VEGFR2 (260.4) Ab or anti-CD47 (B6H12) Ab. There is a significant increase in total MFI upon incubation with both anti-VEGFR2 and anti-CD47 Ab followed by anti-mouse secondary Ab compared to incubation with anti-mouse secondary Ab alone. $n = 3$.

There was not an increase in the fluorescence of the populations of cells treated with CD47 or VEGFR2 antibodies compared to cells treated with secondary antibody alone (Figure 5.3 and Figure 5.4), indicating knockdown HEK 293T cells did not have these receptors.

5.3.3 Determination of re-introduction of CD47-eGFP and VEGFR2-mCherry to CD47- and VEGFR2-null HEK293T cells by confocal microscopy

Confocal microscopy was performed to determine if HEK 293T (CD47- /VEGFR2-null) cells could be successfully transfected with VEGFR2-mCherry and CD47-eGFP. After transfections were performed as described in 5.2.7, fluorescence of cells transfected with VEGFR2-mCherry, CD47-eGFP, or both was observed. Mock transfected cells did not display significant fluorescence using either the 488 laser or the 561 nm laser, which would induce fluorescence of eGFP and mCherry, respectively. Cells transfected with CD47-eGFP were fluorescent upon excitation with the 488 nm laser, but not with the 561 nm laser, indicating eGFP but not mCherry was present. The opposite was observed with cells transfected with VEGFR2-mCherry, with fluorescence only observed when cells were excited with the 561 nm laser. When cells were transfected with both CD47-eGFP and VEGFR2-mCherry, fluorescence was observed using both lasers, although the mCherry fluorescence was less than the eGFP fluorescence. Fluorescence of transfected cells was observed in the cytoplasm and on membranes (Figure 5.5). This showed VEGFR2 and CD47 could be successfully expressed in HEK 293T (CD47- /VEGFR2-null) cells.

5.3.4 VEGFR2 is required for E3CaG1-induced $[Ca^{2+}]_i$ increase in endothelial cells

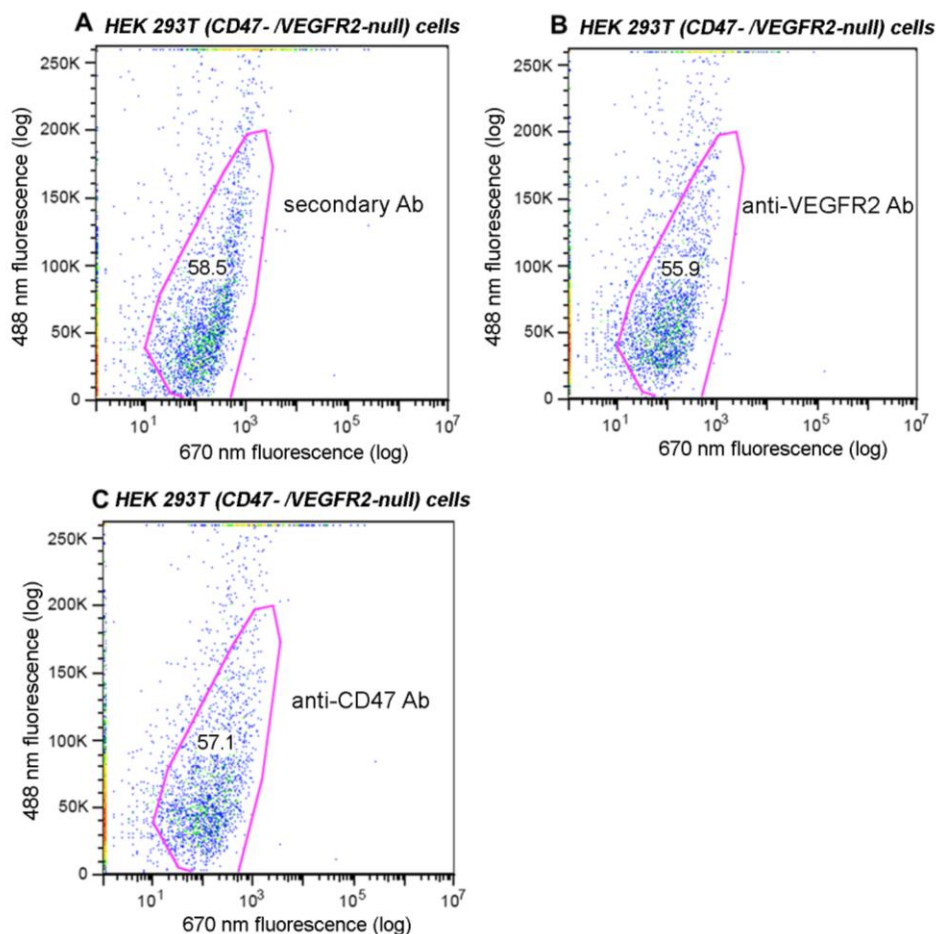


Figure 5.3. Dot plots showing fluorescence of HEK 293T (CD47- and VEGFR2-null) cells upon addition of anti-VEGFR2 (260.4) and anti-CD47 (B6H12) antibodies. Fluorescence at 670 nm is shown on the x-axis. *A.* Fluorescence upon addition of anti-mouse AlexaFluor 647 secondary Ab alone is shown. *B.* Fluorescence upon addition of anti-VEGFR2 Ab prior to addition of anti-mouse AlexaFluor 647 secondary Ab is shown. *C.* Fluorescence upon addition of anti-CD47 Ab prior to addition of anti-mouse AlexaFluor 647 secondary Ab is shown. No increase in fluorescence is observed for either antibody compared to secondary Ab alone, indicating these receptors were not present.

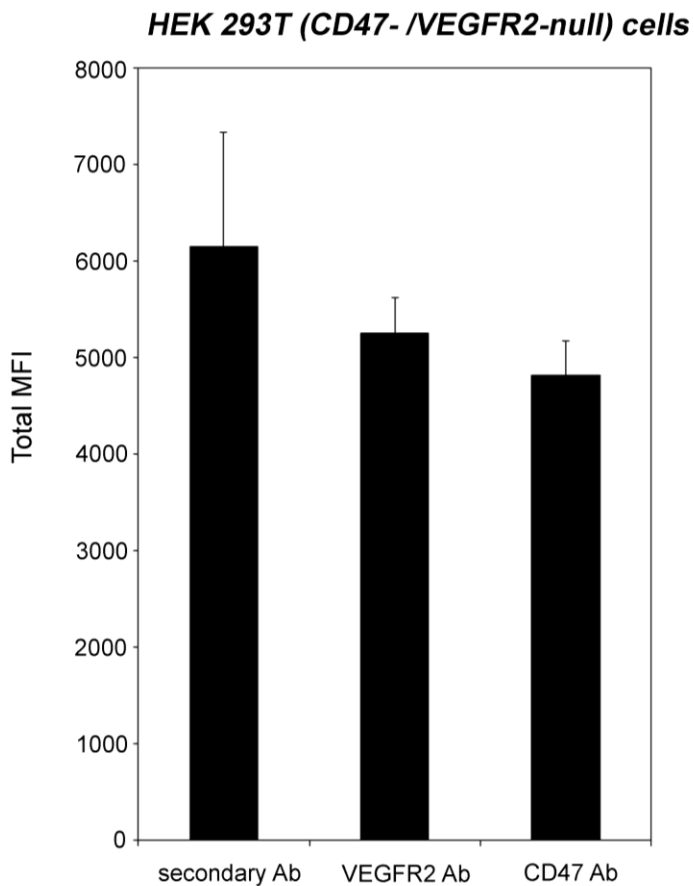


Figure 5.4. CD47 and VEGFR2 are not present on HEK 293T (CD47- /VEGFR2-null) cells. Graphical representation of Figure 5.3. Experimental setup was done as described for Figure 5.2, only done using HEK 293T (CD47- /VEGFR2-null) cells. There is no significant difference between cells incubated with only anti-mouse secondary Ab and those incubated with either anti-CD47 (B6H12) or anti-VEGFR2 (260.4) Ab followed by anti-mouse secondary Ab. $n = 3$.

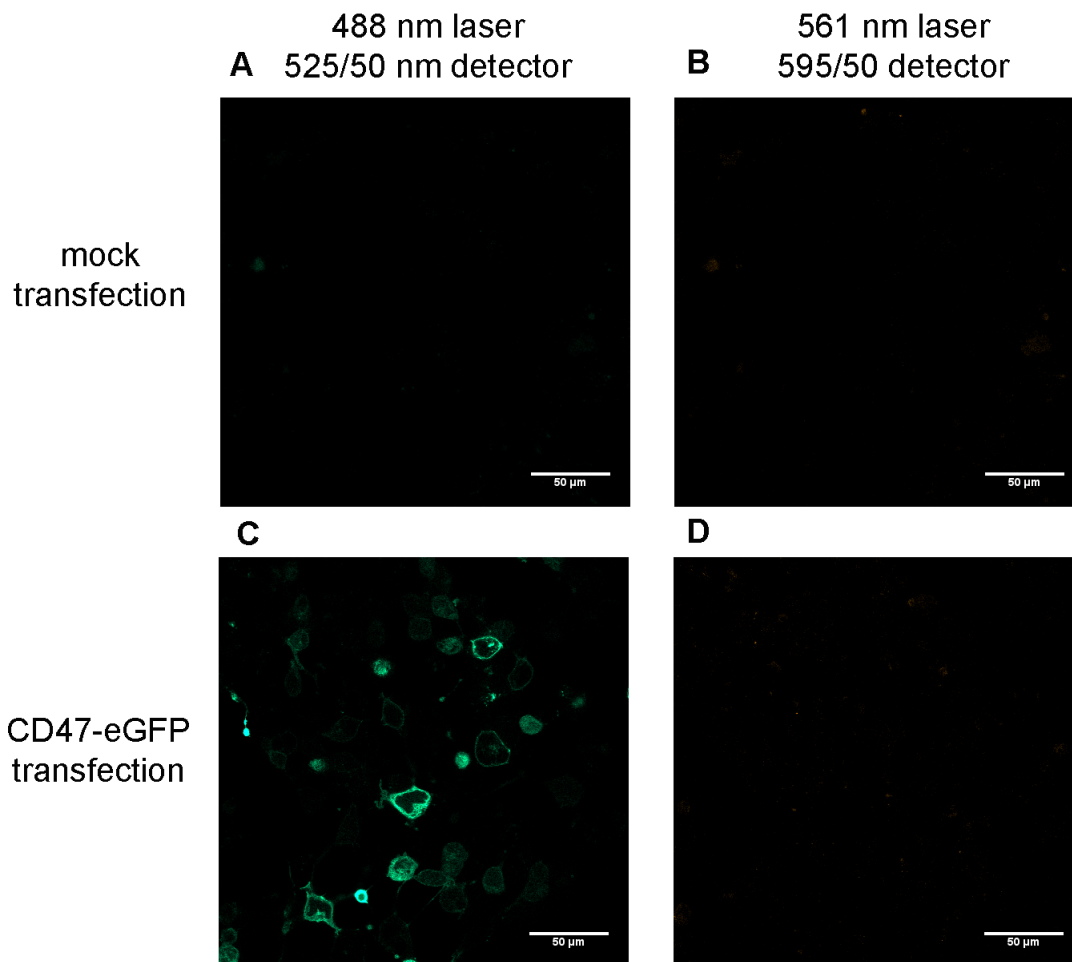


Figure 5.5. Confocal microscopy images of HEK 293T (CD47- and VEGFR2-null) cells transfected with CD47-eGFP, VEGFR2-mCherry, or both. Images were acquired using 25.6% 488 nm laser power and 24.4% 561 nm laser power, except cells transfected with CD47-eGFP and VEGFR2-mCherry, in which images were acquired using 48.7% 488 nm laser power and 43.6% 561 nm laser power. For each transfection condition, images taken using the 488 nm laser and the 561 nm laser were acquired using identical instrument settings. *A*. Fluorescence of mock transfected cells using a 488 nm laser and a 525/50 nm detector. *B*. Fluorescence of mock transfected cells using a 561 nm laser

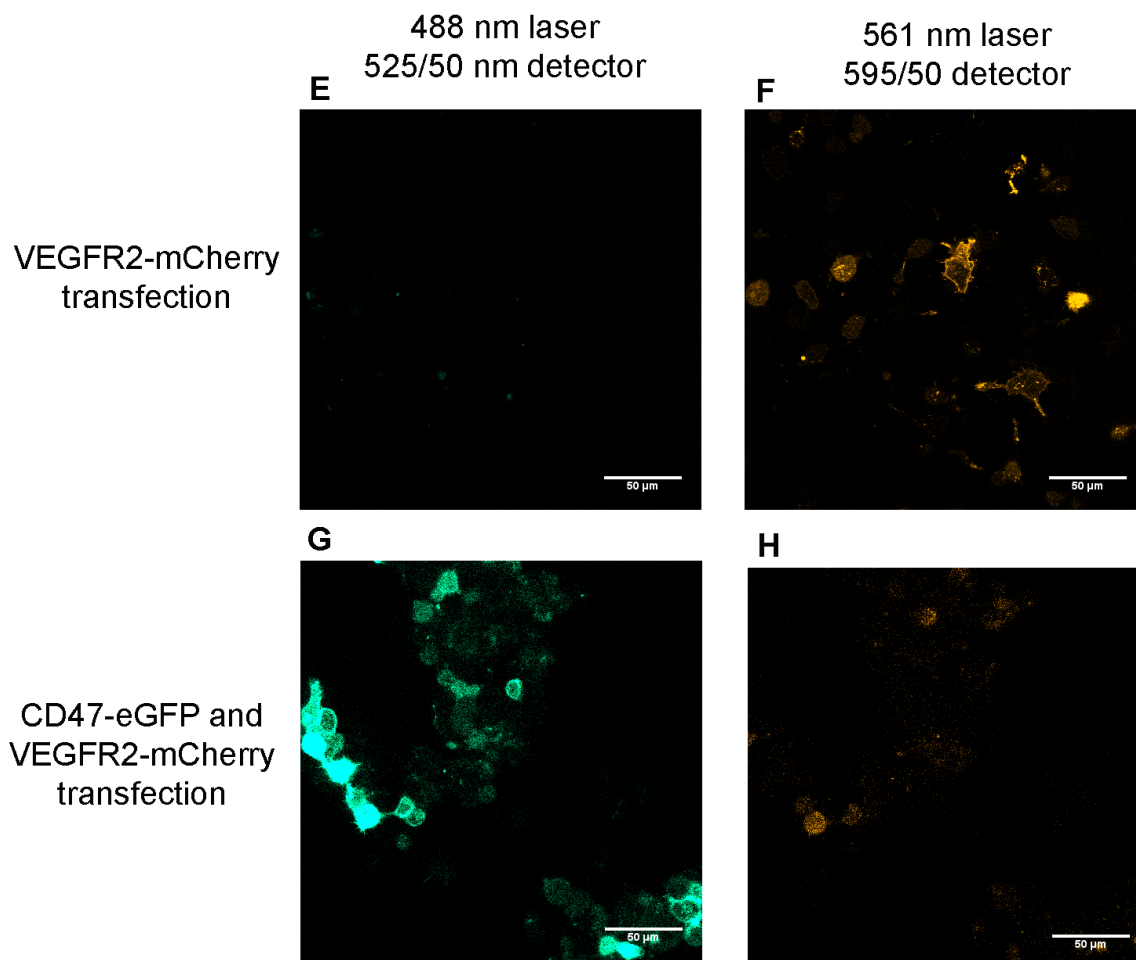


Figure 5.5 continued. *B.* continued. and a 595/50 nm detector. No fluorescence was observed using either detector. *C.* Same as *A.*, only done with cells transfected with CD47-eGFP. *D.* Same as *B.*, only done with cells transfected with CD47-eGFP. No fluorescence was observed using the 561 nm laser. *E.* Same as *A.*, only done with cells transfected with VEGFR2-mCherry. No fluorescence was observed using the 488 nm laser. *F.* Same as *B.*, only done with cells transfected with VEGFR2-mCherry. *G.* Same as *A.*, only done with cells transfected with CD47-eGFP and VEGFR2-mCherry. *H.*

Same as *B*, only done with cells transfected with CD47-eGFP and VEGFR2-mCherry.

Both CD47-eGFP and VEGFR2-mCherry fluorescence was observed in this transfection condition.

After I determined HEK 293T cells stably transduced with both CD47 and KDR shRNA could be successfully transfected with CD47-eGFP, VEGFR2-mCherry, and both, a flow cytometry calcium assay was performed to observe changes in $[Ca^{2+}]_i$ upon E3CaG1 binding. Increases in calcium due to E3CaG1 treatment (compared to mock transfection) were only observed in cells where both CD47-eGFP and VEGFR2-mCherry were transfected (Figure 5.6 and Figure 5.7). As a comparison, a calcium assay was done on native HEK293T cells, where treatment with 25 nM E3CaG1 produced a rise in intracellular calcium compared to buffer alone (Figure 5.6 and Figure 5.7). There was no significant difference between E3CaG1 treatment of native HEK 293T cells and HEK 293T (CD47- /VEGFR2-null) cells that had been transfected with both CD47-eGFP and VEGFR2-mCherry. In addition, calcium levels in response to E3CaG1 were measured in native HEK 293T cells, and there was not a significant difference between the calcium increase in these cells when compared to that observed in HEK 293T (CD47- /VEGFR2-null) cells that had been transfected with both CD47-eGFP and VEGFR2-mCherry. These data indicate cells require both VEGFR2 and CD47 for E3CaG1-induced intracellular calcium increase.

5.4 Discussion

In this chapter, I proved both CD47 and VEGFR2 are required for increases in intracellular calcium caused by E3CaG1 binding to HEK 293T cells. Therefore, the CD47/VEGFR2 complex not only exists in Jurkat T cells, but endothelial cells as well, which are more relevant to nitric oxide signaling. Cytoplasmic calcium levels are tightly regulated so that small changes in calcium concentration results in large signal

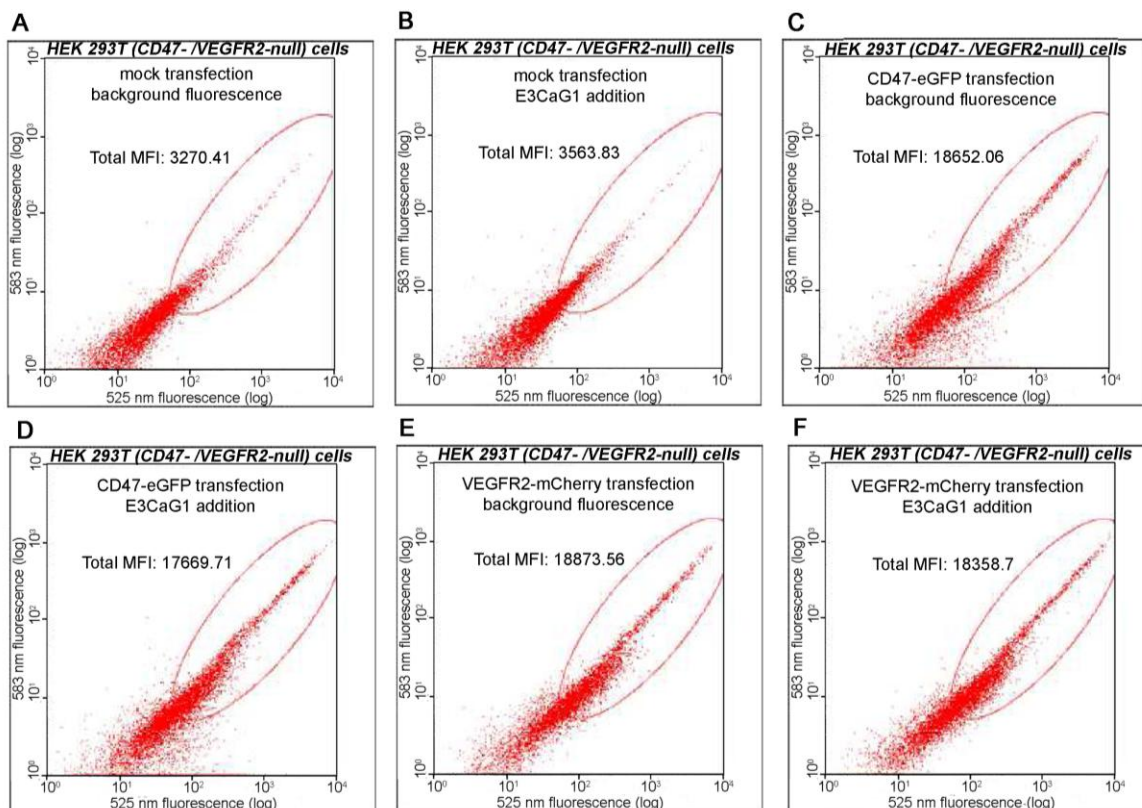


Figure 5.6. Dot plots showing $[Ca^{2+}]_i$ increases upon E3CaG1 addition in HEK 293T (CD47 and VEGFR2-null) cells transfected with CD47-eGFP, VEGFR2-mCherry, or both. Fluorescence at 525 nm is shown on the x-axis. *A.* Background calcium fluorescence in cells that were mock transfected. *B.* Calcium fluorescence in mock transfected cells treated with E3CaG1. *C.* Background calcium fluorescence in cells that were transfected with CD47-eGFP. *D.* Calcium fluorescence in CD47-eGFP transfected cells treated with E3CaG1. *E.* Background calcium fluorescence in cells that were transfected with VEGFR2-mCherry. *F.* Calcium fluorescence in VEGFR2-mCherry transfected cells treated with E3CaG1.

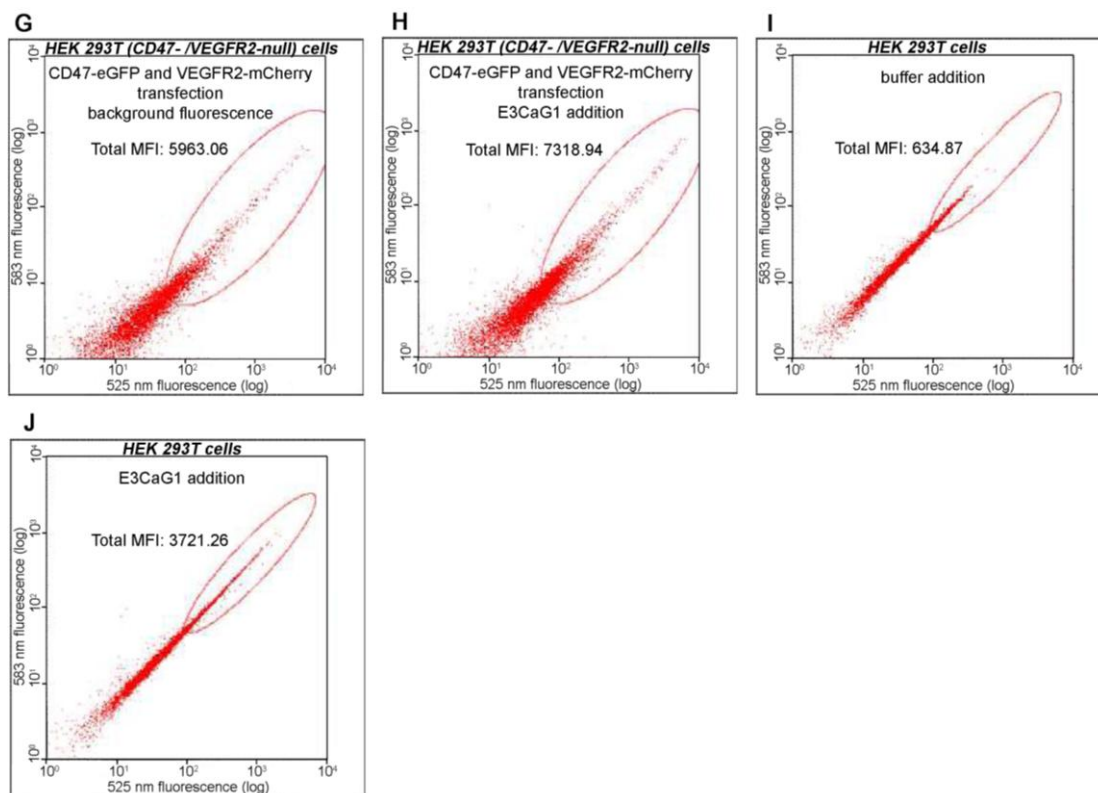


Figure 5.6 continued. *G*. Background calcium fluorescence in cells that were transfected with CD47-eGFP and VEGFR2-mCherry. *H*. Calcium fluorescence in CD47-eGFP and VEGFR2-mCherry transfected cells treated with E3CaG1. *I*. Calcium fluorescence in native HEK 293T cells treated with buffer. *J*. Calcium fluorescence in native HEK 293T cells treated with E3CaG1. Increases in calcium are observed in native HEK 293T cells and in HEK 293T (CD47- /VEGFR2-null) cells transfected with CD47-eGFP and VEGFR2-mCherry upon E3CaG1 addition.

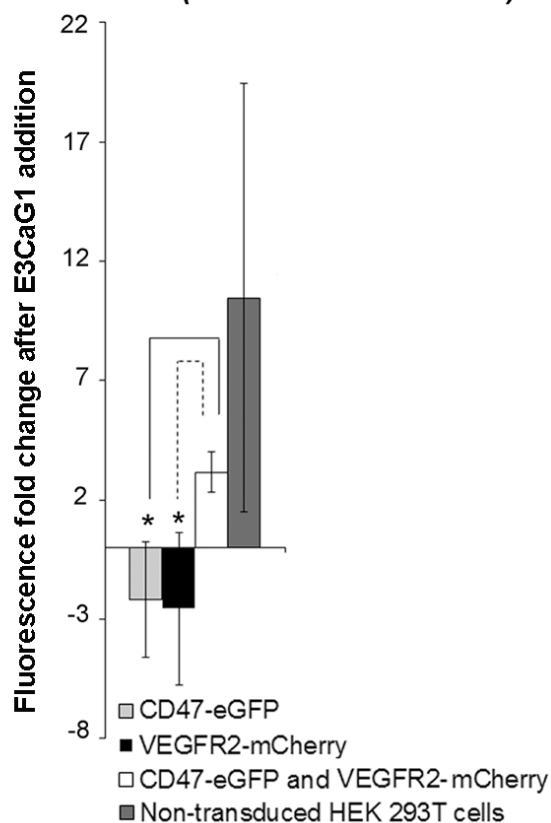
HEK 293T (CD47- /VEGFR2-null) cells

Figure 5.7. Graphical representation of Figure 5.6. CD47 and VEGFR2 are required for E3CaG1-induced $[Ca^{2+}]_i$ increase. HEK293T cells stably transduced with CD47-eGFP were mock transfected, transfected with CD47-eGFP, VEGFR2-mCherry, or both for 42 hours prior to the experiment. A calcium assay was performed as in Figure 4.2. The same calcium assay was also performed with native, non-transfected HEK293T cells. Fold changes in transfected cells were calculated by dividing the relative MFI of each condition upon E3CaG1 addition by the relative MFI upon E3CaG1 addition in mock transfected cells. For native HEK293T cells, relative MFI due to E3CaG1 treatment was compared to addition of buffer alone. An increase in intracellular calcium was only observed when both VEGFR2 and CD47 were present in HEK293T cells.

transduction effects (128). Regulation of calcium levels are closely related to angiogenesis, and cross-talk exists between many mitogen-activated angiogenic pathways (128). Fibroblast growth factor (FGF) binding to its receptor on vascular cells leads to activation of mitogen-activated protein kinase (MAPK), which in turn increases arachidonic acid (AA) levels through activation of phospholipase A2 (PLA2) (129, 130). Increases in free AA cause increases in noncapacitative calcium entry (NCCE), and it is well described that VEGF binding to VEGFR2 also leads to increases in intracellular calcium to activate eNOS (131-133). Both pathways converge to contribute to angiogenic effects such as proliferation and migration (128). Therefore, pathways involving angiogenesis are regulated by many different growth factors and receptors that involve similar second messenger systems, including calcium and nitric oxide. In addition to these known pathways, I have shown a CD47/VEGFR2 complex that binds to TSP-1 is also involved in altering intracellular calcium levels to regulate activation of sGC. TSP-1 therefore regulates angiogenesis through its multiple domains and binding receptors, including CD36 and CD47, the latter of which requires VEGFR2 for its function.

CHAPTER 6

CONCLUSIONS AND FUTURE DIRECTIONS

6.1 Conclusions

Through the identification of key receptor complexes involved in nitric oxide signaling, we can gain a more complete understanding of cardiovascular regulation. PWR is a powerful spectroscopic tool that can dissect many protein interactions that play roles in signaling pathways at the membrane level. As I have shown, even pM protein/ligand interactions can be measured using this technique, which can prove useful when developing agonists/antagonists to specific receptors. Retaining membrane proteins within their native membrane environment is also a valuable advantage of PWR, and gives a more accurate representation of receptor complexes *in vivo*.

My thesis work focused on membrane proteins that are associated with the membrane protein CD47 and are involved in the inhibition of sGC caused by the extracellular matrix protein TSP-1. CD47 is a small membrane receptor, yet is associated with is required for the activity of a variety of other membrane proteins that are known to play fundamental roles in cell migration and proliferation, including integrins and VEGFR2. Through PWR spectroscopy, I have shown there are multiple CD47 complexes that exist within the native membranes of Jurkat T cells (Figure 6.1). These include CD47/VEGFR2 and CD47/ $\alpha_v\beta_3$, which have been shown to exist on other cell lines including endothelial cells and platelets. The former binds a C-terminal fragment of TSP-1 called E3CaG1 with a pM K_d , while the latter binds E3CaG1 with a nM K_d . These same complexes were proven to exist on a CD47-null (JinB8) cell line in which CD47

was re-introduced (CD47-JinB8). However, there was also another complex not involving CD47 within JinB8 cell lines that bound E3CaG1 with a nM K_d . This complex was subsequently shown to be VEGFR2 associated with integrin $\alpha_v\beta_3$. Therefore, when CD47 is not present on a cell line, it is possible VEGFR2 instead associates with $\alpha_v\beta_3$. E3CaG1 binding to CD47 causes an increase in $[Ca^{2+}]_i$, which has been shown to inhibit sGC activity (82). The CD47/VEGFR2 complex was then proven to be the functional complex of interest in terms of sGC inhibition and the regulation of NO signaling. Incubation of live cells with E3CaG1 caused an increase in $[Ca^{2+}]_i$ through a flow cytometry based assay, and this increase was inhibited by incubation with an anti-VEGFR2 antibody on both Jurkat and CD47-JinB8 cells. VEGFR2 in complex with $\alpha_v\beta_3$ was also shown to be involved in regulating calcium levels within JinB8 cells. Incubation with E3CaG1 produced decreases in $[Ca^{2+}]_i$ within this cell line, but addition of anti-VEGFR2 and anti- α_v antibodies inhibited this decrease. This showed E3CaG1 could bind to VEGFR2/ $\alpha_v\beta_3$ to decrease calcium levels in cells that originally did not contain CD47. Finally, I showed both CD47 and VEGFR2 were required for the E3CaG1-induced $[Ca^{2+}]_i$ increase. This was done by knocking CD47 and VEGFR2 receptors down and subsequently re-introducing them into HEK 293T cells, then observing that increases in calcium upon E3CaG1 binding were only observed when both CD47 and VEGFR2 were present.

Taken together, these results show that TSP-1 can bind to CD47/VEGFR2 complexes to cause increases in intracellular calcium in order to inhibit NO signaling. In addition, my results show TSP-1 binding to $\alpha_v\beta_3$ in complex with VEGFR2 causes a

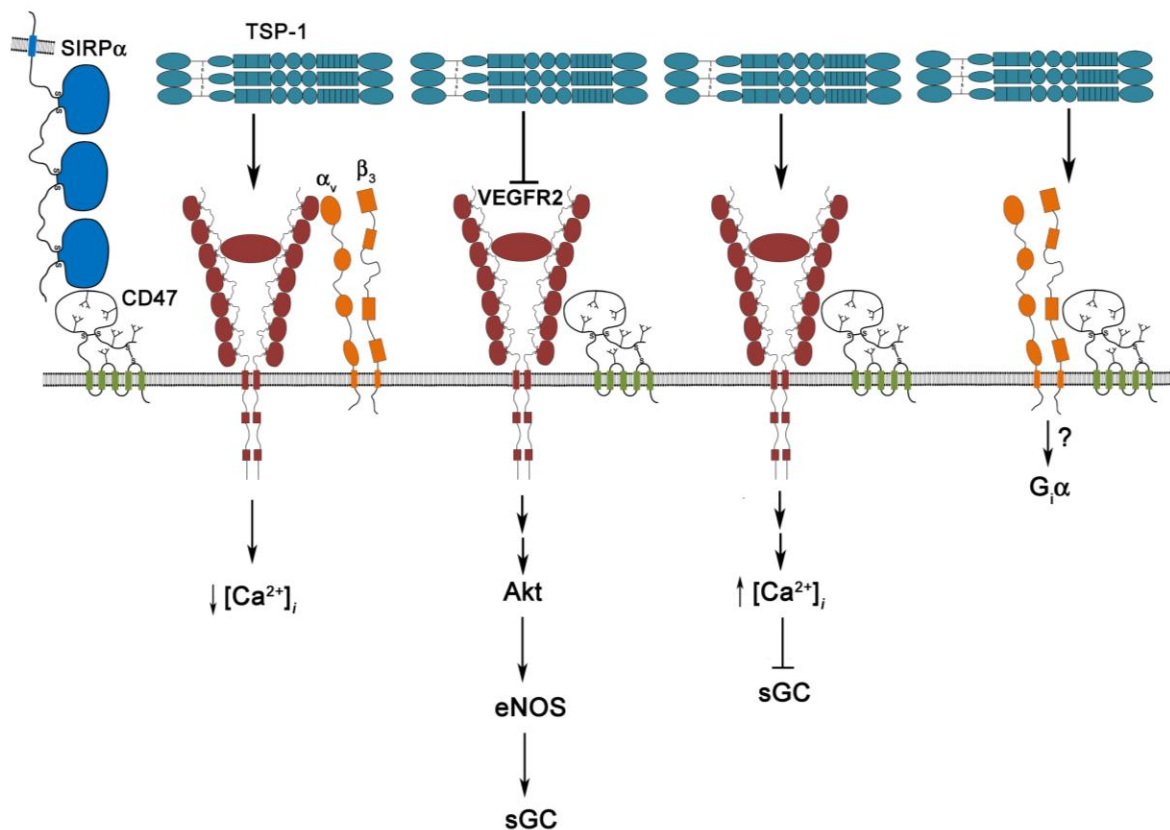


Figure 6.1. Research summary. There are multiple CD47 complexes within Jurkat plasma membranes. These include CD47/VEGFR2, with TSP-1 binding causing an inhibition of VEGFR2 signaling through an Akt pathway, which decreases sGC activity. Our laboratory has shown TSP-1 binding to CD47/VEGFR2 causes an increase in $[Ca^{2+}]_i$, which then leads to phosphorylation and inhibition of sGC. CD47 also associates with $\alpha_v\beta_3$, and has been suggested to act as a non-canonical GPCR to activate G-proteins. VEGFR2 also interacts with $\alpha_v\beta_3$, and I have shown TSP-1 binding to this complex causes a decrease in calcium. SIRP α , the other known ligand of CD47, binds to CD47 on a circulating cell to act as a marker of self, inhibiting phagocytosis. Although VEGF is

shown binding to its VEGFR2 receptor, we do not know if it is present upon TSP-1 binding to CD47 nor how VEGF affects NO signaling within Jurkat cells.

decrease in $[Ca^{2+}]_i$, which could possibly contribute to an inhibition of NOS activation to decrease cGMP levels. TSP-1 can possibly regulate its anti-angiogenic effects through multiple signaling complexes involving CD47 and VEGFR2. In addition to the inhibition of sGC by binding to CD47 in complex with VEGFR2, TSP-1 has also been shown to disrupt VEGFR2 signaling to decrease eNOS activity (76). Consequently, the CD47/VEGFR2 complex can ultimately regulate NO signaling using the same ligand through two separate approaches. Cross-talk between signaling pathways is not uncommon, and the need for multiple levels of regulation are clear in physiologic processes as important as angiogenesis and cardiovascular health.

6.2 Future Directions

6.2.1 Purification of CD47-eGFP

I have successfully developed a cell line in which functional, recombinant CD47 with a C-terminal eGFP tag is expressed in JinB8 cells. CD47 is generously expressed within this cell line, as shown through confocal microscopy and PWR spectroscopy experiments. This protein was expressed in a human cell line to ensure proper glycosylation and functionality of the protein. By attaching a C-terminal eGFP tag, the protein is easily visible through fluorescence techniques such as flow cytometry or microscopy, and can be purified using a hydrophobic interaction (HIC) column. This is a method that has been previously used to purify both soluble and membrane proteins (134, 135), so could be employed to purify CD47-eGFP as well.

6.2.1.1 Structural studies of CD47-eGFP by X-ray crystallography

Once a purification system is in place and large amounts of CD47 obtained, the

protein can be used for structural studies such as X-ray crystallography. Currently, there is no crystal structure of full-length CD47, and little is known about how its ligand TSP-1 binds and which residues are critical. It would be advantageous to have a structure in place to determine possible conformational changes that take place upon ligand binding and how this is transduced to the intracellular cytoplasmic domain.

6.2.2 Insertion of purified CD47-eGFP into synthetic lipid bilayers and determination of E3CaG1 binding by PWR spectroscopy

In addition to X-ray crystallography, purified CD47-eGFP could be used in PWR experiments to develop an assay for TSP-1 binding to recombinant protein. A synthetic lipid bilayer can be deposited on the PWR prism surface as described previously (115). After generation of the bilayer, recombinant CD47, in a detergent solution, could be introduced into the PWR sample cell, causing a decrease in the detergent concentration below its critical micelle concentration. This will cause spontaneous transfer of CD47 from the detergent micelle into the lipid bilayer, and incorporation should result in changes in the position, depth, and width of the PWR resonance curve due to the resulting mass and structural changes (104). E3CaG1 can then be added to the sample cell and the binding constant will be measured along with any conformational changes. Since I have shown VEGFR2 is required for E3CaG1 binding to CD47, it is probable that recombinant VEGFR2 would also need to be inserted into the membrane in addition to CD47 before E3CaG1 binding and conformational changes can be observed.

6.2.2.1 Identification of residues in CD47 critical for TSP-1 binding by mutagenesis

Once a PWR assay using recombinant CD47 is in place, mutagenesis experiments can

be performed on CD47 to examine what residues are important for the TSP-1/CD47 interaction. The extracellular domains of CD47 and SIRP α have been crystallized together (58), and the residues at the interface between these two proteins have been elucidated. The C-terminal domain of TSP1 has also been crystallized (136), and the structure shows a number of hydrophilic residues that could possibly participate in electrostatic interactions with CD47. For example, Q19, E104, E106, and T102 on CD47 may form hydrogen bonds or ionic interactions with E999, R1000, or T998 on TSP1. These polar residues on CD47 can be mutated to nonpolar amino acids, and E3CaG1 binding can be measured with PWR. There are also two disulfide bonds within CD47 that contribute to the overall structure and function of the protein (63, 65), so these could also be mutated to determine their significance in the overall structure of the protein and subsequent effect on E3CaG1 binding.

REFERENCES

1. Gross, S. S., and Wolin, M. S. (1995) Nitric oxide: pathophysiological mechanisms, *Annu Rev Physiol* 57, 737-769.
2. Rand, M. J., and Li, C. G. (1995) Nitric oxide as a neurotransmitter in peripheral nerves: nature of transmitter and mechanism of transmission, *Annu Rev Physiol* 57, 659-682.
3. Moncada, S., Palmer, R. M., and Higgs, E. A. (1991) Nitric oxide: physiology, pathophysiology, and pharmacology, *Pharmacol Rev* 43, 109-142.
4. Garthwaite, J., and Boulton, C. L. (1995) Nitric oxide signaling in the central nervous system, *Annu Rev Physiol* 57, 683-706.
5. Lowenstein, C. J., Dinerman, J. L., and Snyder, S. H. (1994) Nitric oxide: a physiologic messenger, *Ann Intern Med* 120, 227-237.
6. Furchgott, R. F., and Zawadzki, J. V. (1980) The obligatory role of endothelial cells in the relaxation of arterial smooth muscle by acetylcholine, *Nature* 288, 373-376.
7. Palmer, R. M., Ferrige, A. G., and Moncada, S. (1987) Nitric oxide release accounts for the biological activity of endothelium-derived relaxing factor, *Nature* 327, 524-526.
8. Vallance, P., Collier, J., and Moncada, S. (1989) Effects of endothelium-derived nitric oxide on peripheral arteriolar tone in man, *Lancet* 2, 997-1000.
9. Caulfield, J. L., Wishnok, J. S., and Tannenbaum, S. R. (1998) Nitric oxide-induced deamination of cytosine and guanine in deoxynucleosides and oligonucleotides, *J Biol Chem* 273, 12689-12695.
10. Fortier, A. H., Polsinelli, T., Green, S. J., and Nacy, C. A. (1992) Activation of macrophages for destruction of *Francisella tularensis*: identification of cytokines, effector cells, and effector molecules, *Infect Immun* 60, 817-825.
11. Varela, A. F., Runge, A., Ignarro, L. J., and Chaudhuri, G. (1992) Nitric oxide and prostacyclin inhibit fetal platelet aggregation: a response similar to that observed in adults, *Am J Obstet Gynecol* 167, 1599-1604.
12. Kwon, N. S., Nathan, C. F., Gilker, C., Griffith, O. W., Matthews, D. E., and Stuehr, D. J. (1990) L-citrulline production from L-arginine by macrophage nitric

- oxide synthase. The ureido oxygen derives from dioxygen, *J Biol Chem* 265, 13442-13445.
13. Brecht, D. S., and Snyder, S. H. (1990) Isolation of nitric oxide synthetase, a calmodulin-requiring enzyme, *Proc Natl Acad Sci U S A* 87, 682-685.
 14. Busse, R., and Mulsch, A. (1990) Calcium-dependent nitric oxide synthesis in endothelial cytosol is mediated by calmodulin, *FEBS Lett* 265, 133-136.
 15. Marsden, P. A., Schappert, K. T., Chen, H. S., Flowers, M., Sundell, C. L., Wilcox, J. N., Lamas, S., and Michel, T. (1992) Molecular cloning and characterization of human endothelial nitric oxide synthase, *FEBS Lett* 307, 287-293.
 16. Xie, Q. W., Cho, H. J., Calaycay, J., Mumford, R. A., Swiderek, K. M., Lee, T. D., Ding, A., Troso, T., and Nathan, C. (1992) Cloning and characterization of inducible nitric oxide synthase from mouse macrophages, *Science* 256, 225-228.
 17. Stuehr, D. J., Cho, H. J., Kwon, N. S., Weise, M. F., and Nathan, C. F. (1991) Purification and characterization of the cytokine-induced macrophage nitric oxide synthase: an FAD- and FMN-containing flavoprotein, *Proc Natl Acad Sci U S A* 88, 7773-7777.
 18. Alderton, W. K., Cooper, C. E., and Knowles, R. G. (2001) Nitric oxide synthases: structure, function and inhibition, *Biochem J* 357, 593-615.
 19. Friebe, A., and Koesling, D. (2003) Regulation of nitric oxide-sensitive guanylyl cyclase, *Circ Res* 93, 96-105.
 20. Russwurm, M., Wittau, N., and Koesling, D. (2001) Guanylyl cyclase/PSD-95 interaction: targeting of the nitric oxide-sensitive alpha2beta1 guanylyl cyclase to synaptic membranes, *J Biol Chem* 276, 44647-44652.
 21. Koesling, D., Schultz, G., and Bohme, E. (1991) Sequence homologies between guanylyl cyclases and structural analogies to other signal-transducing proteins, *FEBS Lett* 280, 301-306.
 22. Ohlstein, E. H., Wood, K. S., and Ignarro, L. J. (1982) Purification and properties of heme-deficient hepatic soluble guanylate cyclase: effects of heme and other factors on enzyme activation by NO, NO-heme, and protoporphyrin IX, *Arch Biochem Biophys* 218, 187-198.
 23. Kamisaki, Y., Saheki, S., Nakane, M., Palmieri, J. A., Kuno, T., Chang, B. Y., Waldman, S. A., and Murad, F. (1986) Soluble guanylate cyclase from rat lung exists as a heterodimer, *J Biol Chem* 261, 7236-7241.

24. Yuen, P. S., Potter, L. R., and Garbers, D. L. (1990) A new form of guanylyl cyclase is preferentially expressed in rat kidney, *Biochemistry* 29, 10872-10878.
25. Harteneck, C., Wedel, B., Koesling, D., Malkewitz, J., Bohme, E., and Schultz, G. (1991) Molecular cloning and expression of a new alpha-subunit of soluble guanylyl cyclase. Interchangeability of the alpha-subunits of the enzyme, *FEBS Lett* 292, 217-222.
26. Derbyshire, E. R., and Marletta, M. A. Structure and regulation of soluble guanylate cyclase, *Annu Rev Biochem* 81, 533-559.
27. Andreopoulos, S., and Papapetropoulos, A. (2000) Molecular aspects of soluble guanylyl cyclase regulation, *Gen Pharmacol* 34, 147-157.
28. Stone, J. R., and Marletta, M. A. (1994) Soluble guanylate cyclase from bovine lung: activation with nitric oxide and carbon monoxide and spectral characterization of the ferrous and ferric states, *Biochemistry* 33, 5636-5640.
29. Poulos, T. L. (2006) Soluble guanylate cyclase, *Curr Opin Struct Biol* 16, 736-743.
30. Hu, X., Murata, L. B., Weichsel, A., Brailey, J. L., Roberts, S. A., Nighorn, A., and Montfort, W. R. (2008) Allostery in recombinant soluble guanylyl cyclase from *Manduca sexta*, *J Biol Chem* 283, 20968-20977.
31. Zhao, Y., Brandish, P. E., Ballou, D. P., and Marletta, M. A. (1999) A molecular basis for nitric oxide sensing by soluble guanylate cyclase, *Proc Natl Acad Sci U S A* 96, 14753-14758.
32. Carlson, C. B., Lawler, J., and Mosher, D. F. (2008) Structures of thrombospondins, *Cell Mol Life Sci* 65, 672-686.
33. Adams, J. C., and Lawler, J. (2004) The thrombospondins, *Int J Biochem Cell Biol* 36, 961-968.
34. Bonnefoy, A., Moura, R., and Hoylaerts, M. F. (2008) The evolving role of thrombospondin-1 in hemostasis and vascular biology, *Cell Mol Life Sci* 65, 713-727.
35. Misenheimer, T. M., Huwiler, K. G., Annis, D. S., and Mosher, D. F. (2000) Physical characterization of the procollagen module of human thrombospondin 1 expressed in insect cells, *J Biol Chem* 275, 40938-40945.

36. Tolsma, S. S., Volpert, O. V., Good, D. J., Frazier, W. A., Polverini, P. J., and Bouck, N. (1993) Peptides derived from two separate domains of the matrix protein thrombospondin-1 have anti-angiogenic activity, *J Cell Biol* 122, 497-511.
37. Dawson, D. W., Pearce, S. F., Zhong, R., Silverstein, R. L., Frazier, W. A., and Bouck, N. P. (1997) CD36 mediates the In vitro inhibitory effects of thrombospondin-1 on endothelial cells, *J Cell Biol* 138, 707-717.
38. Daniel, C., Wiede, J., Krutzsch, H. C., Ribeiro, S. M., Roberts, D. D., Murphy-Ullrich, J. E., and Hugo, C. (2004) Thrombospondin-1 is a major activator of TGF-beta in fibrotic renal disease in the rat in vivo, *Kidney Int* 65, 459-468.
39. Lawler, J., and Hynes, R. O. (1986) The structure of human thrombospondin, an adhesive glycoprotein with multiple calcium-binding sites and homologies with several different proteins, *J Cell Biol* 103, 1635-1648.
40. Lawler, J., Weinstein, R., and Hynes, R. O. (1988) Cell attachment to thrombospondin: the role of ARG-GLY-ASP, calcium, and integrin receptors, *J Cell Biol* 107, 2351-2361.
41. Lawler, J., and Hynes, R. O. (1989) An integrin receptor on normal and thrombasthenic platelets that binds thrombospondin, *Blood* 74, 2022-2027.
42. Lawler, J., Derick, L. H., Connolly, J. E., Chen, J. H., and Chao, F. C. (1985) The structure of human platelet thrombospondin, *J Biol Chem* 260, 3762-3772.
43. Isenberg, J. S., Ridnour, L. A., Dimitry, J., Frazier, W. A., Wink, D. A., and Roberts, D. D. (2006) CD47 is necessary for inhibition of nitric oxide-stimulated vascular cell responses by thrombospondin-1, *J Biol Chem* 281, 26069-26080.
44. Tan, K., Duquette, M., Liu, J. H., Dong, Y., Zhang, R., Joachimiak, A., Lawler, J., and Wang, J. H. (2002) Crystal structure of the TSP-1 type 1 repeats: a novel layered fold and its biological implication, *J Cell Biol* 159, 373-382.
45. Zhang, X., Kazerounian, S., Duquette, M., Perruzzi, C., Nagy, J. A., Dvorak, H. F., Parangi, S., and Lawler, J. (2009) Thrombospondin-1 modulates vascular endothelial growth factor activity at the receptor level, *FASEB J* 23, 3368-3376.
46. Isenberg, J. S., Wink, D. A., and Roberts, D. D. (2006) Thrombospondin-1 antagonizes nitric oxide-stimulated vascular smooth muscle cell responses, *Cardiovasc Res* 71, 785-793.
47. Zhu, W., and Smart, E. J. (2005) Myristic acid stimulates endothelial nitric-oxide synthase in a CD36- and an AMP kinase-dependent manner, *J Biol Chem* 280, 29543-29550.

48. Isenberg, J. S., Jia, Y., Fukuyama, J., Switzer, C. H., Wink, D. A., and Roberts, D. D. (2007) Thrombospondin-1 inhibits nitric oxide signaling via CD36 by inhibiting myristic acid uptake, *J Biol Chem* 282, 15404-15415.
49. Iruela-Arispe, M. L., Lombardo, M., Krutzsch, H. C., Lawler, J., and Roberts, D. D. (1999) Inhibition of angiogenesis by thrombospondin-1 is mediated by 2 independent regions within the type 1 repeats, *Circulation* 100, 1423-1431.
50. Isenberg, J. S., Romeo, M. J., Yu, C., Yu, C. K., Nghiem, K., Monsale, J., Rick, M. E., Wink, D. A., Frazier, W. A., and Roberts, D. D. (2008) Thrombospondin-1 stimulates platelet aggregation by blocking the antithrombotic activity of nitric oxide/cGMP signaling, *Blood* 111, 613-623.
51. Jiang, P., Lagenaur, C. F., and Narayanan, V. (1999) Integrin-associated protein is a ligand for the P84 neural adhesion molecule, *J Biol Chem* 274, 559-562.
52. Vernon-Wilson, E. F., Kee, W. J., Willis, A. C., Barclay, A. N., Simmons, D. L., and Brown, M. H. (2000) CD47 is a ligand for rat macrophage membrane signal regulatory protein SIRP (OX41) and human SIRPalpha 1, *Eur J Immunol* 30, 2130-2137.
53. Fujioka, Y., Matozaki, T., Noguchi, T., Iwamatsu, A., Yamao, T., Takahashi, N., Tsuda, M., Takada, T., and Kasuga, M. (1996) A novel membrane glycoprotein, SHPS-1, that binds the SH2-domain-containing protein tyrosine phosphatase SHP-2 in response to mitogens and cell adhesion, *Mol Cell Biol* 16, 6887-6899.
54. Tsai, R. K., Rodriguez, P. L., and Discher, D. E. Self inhibition of phagocytosis: the affinity of 'marker of self' CD47 for SIRPalpha dictates potency of inhibition but only at low expression levels, *Blood Cells Mol Dis* 45, 67-74.
55. Oldenborg, P. A., Gresham, H. D., and Lindberg, F. P. (2001) CD47-signal regulatory protein alpha (SIRPalpha) regulates Fcgamma and complement receptor-mediated phagocytosis, *J Exp Med* 193, 855-862.
56. Motegi, S., Okazawa, H., Ohnishi, H., Sato, R., Kaneko, Y., Kobayashi, H., Tomizawa, K., Ito, T., Honma, N., Buhring, H. J., Ishikawa, O., and Matozaki, T. (2003) Role of the CD47-SHPS-1 system in regulation of cell migration, *EMBO J* 22, 2634-2644.
57. Babic, I., Schallhorn, A., Lindberg, F. P., and Jirik, F. R. (2000) SHPS-1 induces aggregation of Ba/F3 pro-B cells via an interaction with CD47, *J Immunol* 164, 3652-3658.

58. Hatherley, D., Graham, S. C., Turner, J., Harlos, K., Stuart, D. I., and Barclay, A. N. (2008) Paired receptor specificity explained by structures of signal regulatory proteins alone and complexed with CD47, *Mol Cell* 31, 266-277.
59. Brown, E., Hooper, L., Ho, T., and Gresham, H. (1990) Integrin-associated protein: a 50-kD plasma membrane antigen physically and functionally associated with integrins, *J Cell Biol* 111, 2785-2794.
60. Gao, A. G., Lindberg, F. P., Finn, M. B., Blystone, S. D., Brown, E. J., and Frazier, W. A. (1996) Integrin-associated protein is a receptor for the C-terminal domain of thrombospondin, *J Biol Chem* 271, 21-24.
61. Isenberg, J. S., Qin, Y., Maxhimer, J. B., Sipes, J. M., Despres, D., Schnermann, J., Frazier, W. A., and Roberts, D. D. (2009) Thrombospondin-1 and CD47 regulate blood pressure and cardiac responses to vasoactive stress, *Matrix Biol* 28, 110-119.
62. Lindberg, F. P., Lublin, D. M., Telen, M. J., Veile, R. A., Miller, Y. E., Donis-Keller, H., and Brown, E. J. (1994) Rh-related antigen CD47 is the signal-transducer integrin-associated protein, *J Biol Chem* 269, 1567-1570.
63. Lindberg, F. P., Gresham, H. D., Schwarz, E., and Brown, E. J. (1993) Molecular cloning of integrin-associated protein: an immunoglobulin family member with multiple membrane-spanning domains implicated in alpha v beta 3-dependent ligand binding, *J Cell Biol* 123, 485-496.
64. Reinhold, M. I., Lindberg, F. P., Plas, D., Reynolds, S., Peters, M. G., and Brown, E. J. (1995) In vivo expression of alternatively spliced forms of integrin-associated protein (CD47), *J Cell Sci* 108 (Pt 11), 3419-3425.
65. Rebres, R. A., Vaz, L. E., Green, J. M., and Brown, E. J. (2001) Normal ligand binding and signaling by CD47 (integrin-associated protein) requires a long range disulfide bond between the extracellular and membrane-spanning domains, *J Biol Chem* 276, 34607-34616.
66. Mawby, W. J., Holmes, C. H., Anstee, D. J., Spring, F. A., and Tanner, M. J. (1994) Isolation and characterization of CD47 glycoprotein: a multispanning membrane protein which is the same as integrin-associated protein (IAP) and the ovarian tumour marker OA3, *Biochem J* 304 (Pt 2), 525-530.
67. Parthasarathy, R., Subramanian, S., Boder, E. T., and Discher, D. E. (2006) Post-translational regulation of expression and conformation of an immunoglobulin domain in yeast surface display, *Biotechnol Bioeng* 93, 159-168.

68. Subramanian, S., Boder, E. T., and Discher, D. E. (2007) Phylogenetic divergence of CD47 interactions with human signal regulatory protein alpha reveals locus of species specificity. Implications for the binding site, *J Biol Chem* 282, 1805-1818.
69. Annis, D. S., Gunderson, K. A., and Mosher, D. F. (2007) Immunochemical analysis of the structure of the signature domains of thrombospondin-1 and thrombospondin-2 in low calcium concentrations, *J Biol Chem* 282, 27067-27075.
70. Isenberg, J. S., Annis, D. S., Pendrak, M. L., Ptaszynska, M., Frazier, W. A., Mosher, D. F., and Roberts, D. D. (2009) Differential interactions of thrombospondin-1, -2, and -4 with CD47 and effects on cGMP signaling and ischemic injury responses, *J Biol Chem* 284, 1116-1125.
71. Green, J. M., Zhelesnyak, A., Chung, J., Lindberg, F. P., Sarfati, M., Frazier, W. A., and Brown, E. J. (1999) Role of cholesterol in formation and function of a signaling complex involving alphavbeta3, integrin-associated protein (CD47), and heterotrimeric G proteins, *J Cell Biol* 146, 673-682.
72. Gao, A. G., Lindberg, F. P., Dimitry, J. M., Brown, E. J., and Frazier, W. A. (1996) Thrombospondin modulates alpha v beta 3 function through integrin-associated protein, *J Cell Biol* 135, 533-544.
73. Fujimoto, T. T., Katsutani, S., Shimomura, T., and Fujimura, K. (2003) Thrombospondin-bound integrin-associated protein (CD47) physically and functionally modifies integrin alphaIIb beta3 by its extracellular domain, *J Biol Chem* 278, 26655-26665.
74. Chung, J., Gao, A. G., and Frazier, W. A. (1997) Thrombospondin acts via integrin-associated protein to activate the platelet integrin alphaIIb beta3, *J Biol Chem* 272, 14740-14746.
75. Wang, X. Q., and Frazier, W. A. (1998) The thrombospondin receptor CD47 (IAP) modulates and associates with alpha2 beta1 integrin in vascular smooth muscle cells, *Mol Biol Cell* 9, 865-874.
76. Kaur, S., Martin-Manso, G., Pendrak, M. L., Garfield, S. H., Isenberg, J. S., and Roberts, D. D. (2010) Thrombospondin-1 inhibits VEGF receptor-2 signaling by disrupting its association with CD47, *J Biol Chem* 285, 38923-38932.
77. Gerber, H. P., McMurtrey, A., Kowalski, J., Yan, M., Keyt, B. A., Dixit, V., and Ferrara, N. (1998) Vascular endothelial growth factor regulates endothelial cell survival through the phosphatidylinositol 3'-kinase/Akt signal transduction pathway. Requirement for Flk-1/KDR activation, *J Biol Chem* 273, 30336-30343.

78. Ferrara, N., and Davis-Smyth, T. (1997) The biology of vascular endothelial growth factor, *Endocr Rev* 18, 4-25.
79. Zachary, I., and Gliki, G. (2001) Signaling transduction mechanisms mediating biological actions of the vascular endothelial growth factor family, *Cardiovasc Res* 49, 568-581.
80. Shen, B. Q., Lee, D. Y., and Zioncheck, T. F. (1999) Vascular endothelial growth factor governs endothelial nitric-oxide synthase expression via a KDR/Flk-1 receptor and a protein kinase C signaling pathway, *J Biol Chem* 274, 33057-33063.
81. Rosales, C., Gresham, H. D., and Brown, E. J. (1992) Expression of the 50-kDa integrin-associated protein on myeloid cells and erythrocytes, *J Immunol* 149, 2759-2764.
82. Ramanathan, S., Mazzalupo, S., Boitano, S., and Montfort, W. R. (2011) Thrombospondin-1 and Angiotensin II Inhibit Soluble Guanylyl Cyclase through an Increase in Intracellular Calcium Concentration, *Biochemistry*.
83. Gao, A. G., and Frazier, W. A. (1994) Identification of a receptor candidate for the carboxyl-terminal cell binding domain of thrombospondins, *J Biol Chem* 269, 29650-29657.
84. Miller, T. W., Isenberg, J. S., and Roberts, D. D. Thrombospondin-1 is an inhibitor of pharmacological activation of soluble guanylate cyclase, *Br J Pharmacol* 159, 1542-1547.
85. Isenberg, J. S., Martin-Manso, G., Maxhimer, J. B., and Roberts, D. D. (2009) Regulation of nitric oxide signalling by thrombospondin 1: implications for anti-angiogenic therapies, *Nat Rev Cancer* 9, 182-194.
86. Isenberg, J. S., Ridnour, L. A., Perruccio, E. M., Espey, M. G., Wink, D. A., and Roberts, D. D. (2005) Thrombospondin-1 inhibits endothelial cell responses to nitric oxide in a cGMP-dependent manner, *Proc Natl Acad Sci U S A* 102, 13141-13146.
87. Isenberg, J. S., Maxhimer, J. B., Hyodo, F., Pendrak, M. L., Ridnour, L. A., DeGraff, W. G., Tsokos, M., Wink, D. A., and Roberts, D. D. (2008) Thrombospondin-1 and CD47 limit cell and tissue survival of radiation injury, *Am J Pathol* 173, 1100-1112.
88. Isenberg, J. S., Hyodo, F., Matsumoto, K., Romeo, M. J., Abu-Asab, M., Tsokos, M., Kuppasamy, P., Wink, D. A., Krishna, M. C., and Roberts, D. D. (2007)

- Thrombospondin-1 limits ischemic tissue survival by inhibiting nitric oxide-mediated vascular smooth muscle relaxation, *Blood* 109, 1945-1952.
89. Isenberg, J. S., Romeo, M. J., Maxhimer, J. B., Smedley, J., Frazier, W. A., and Roberts, D. D. (2008) Gene silencing of CD47 and antibody ligation of thrombospondin-1 enhance ischemic tissue survival in a porcine model: implications for human disease, *Ann Surg* 247, 860-868.
 90. Haneda, M., Kikkawa, R., Maeda, S., Togawa, M., Koya, D., Horide, N., Kajiwara, N., and Shigeta, Y. (1991) Dual mechanism of angiotensin II inhibits ANP-induced mesangial cGMP accumulation, *Kidney Int* 40, 188-194.
 91. Yan, C., Kim, D., Aizawa, T., and Berk, B. C. (2003) Functional interplay between angiotensin II and nitric oxide: cyclic GMP as a key mediator, *Arterioscler Thromb Vasc Biol* 23, 26-36.
 92. Soldi, R., Mitola, S., Strasly, M., Defilippi, P., Tarone, G., and Bussolino, F. (1999) Role of alphavbeta3 integrin in the activation of vascular endothelial growth factor receptor-2, *EMBO J* 18, 882-892.
 93. Borges, E., Jan, Y., and Ruoslahti, E. (2000) Platelet-derived growth factor receptor beta and vascular endothelial growth factor receptor 2 bind to the beta 3 integrin through its extracellular domain, *J Biol Chem* 275, 39867-39873.
 94. Hodivala-Dilke, K. M., Reynolds, A. R., and Reynolds, L. E. (2003) Integrins in angiogenesis: multitasking molecules in a balancing act, *Cell Tissue Res* 314, 131-144.
 95. Mahabeleshwar, G. H., Feng, W., Phillips, D. R., and Byzova, T. V. (2006) Integrin signaling is critical for pathological angiogenesis, *J Exp Med* 203, 2495-2507.
 96. Hynes, R. O., Lively, J. C., McCarty, J. H., Taverna, D., Francis, S. E., Hodivala-Dilke, K., and Xiao, Q. (2002) The diverse roles of integrins and their ligands in angiogenesis, *Cold Spring Harb Symp Quant Biol* 67, 143-153.
 97. Tsao, P. W., and Mousa, S. A. (1995) Thrombospondin mediates calcium mobilization in fibroblasts via its Arg-Gly-Asp and carboxyl-terminal domains, *J Biol Chem* 270, 23747-23753.
 98. Schwartz, M. A., Brown, E. J., and Fazeli, B. (1993) A 50-kDa integrin-associated protein is required for integrin-regulated calcium entry in endothelial cells, *J Biol Chem* 268, 19931-19934.

99. Alves, I. D., Cowell, S. M., Salamon, Z., Devanathan, S., Tollin, G., and Hruby, V. J. (2004) Different structural states of the proteolipid membrane are produced by ligand binding to the human delta-opioid receptor as shown by plasmon-waveguide resonance spectroscopy, *Mol Pharmacol* 65, 1248-1257.
100. Salamon, Z., Hruby, V. J., Tollin, G., and Cowell, S. (2002) Binding of agonists, antagonists and inverse agonists to the human delta-opioid receptor produces distinctly different conformational states distinguishable by plasmon-waveguide resonance spectroscopy, *J Pept Res* 60, 322-328.
101. Salamon, Z., Macleod, H. A., and Tollin, G. (1997) Coupled plasmon-waveguide resonators: a new spectroscopic tool for probing proteolipid film structure and properties, *Biophys J* 73, 2791-2797.
102. Salamon, Z., and Tollin, G. (2004) Graphical analysis of mass and anisotropy changes observed by plasmon-waveguide resonance spectroscopy can provide useful insights into membrane protein function, *Biophys J* 86, 2508-2516.
103. Hruby, V. J., and Tollin, G. (2007) Plasmon-waveguide resonance (PWR) spectroscopy for directly viewing rates of GPCR/G-protein interactions and quantifying affinities, *Curr Opin Pharmacol* 7, 507-514.
104. Salamon, Z., Cowell, S., Varga, E., Yamamura, H. I., Hruby, V. J., and Tollin, G. (2000) Plasmon resonance studies of agonist/antagonist binding to the human delta-opioid receptor: new structural insights into receptor-ligand interactions, *Biophys J* 79, 2463-2474.
105. Salamon, Z., and Tollin, G. (2001) Optical anisotropy in lipid bilayer membranes: coupled plasmon-waveguide resonance measurements of molecular orientation, polarizability, and shape, *Biophys J* 80, 1557-1567.
106. McKee, K. J., Meyer, M. W., and Smith, E. A. Plasmon waveguide resonance Raman spectroscopy, *Anal Chem* 84, 9049-9055.
107. Byard, C. L., Han, X., and Mendes, S. B. Angle-multiplexed waveguide resonance of high sensitivity and its application to nanosecond dynamics of molecular assemblies, *Anal Chem* 84, 9762-9767.
108. Knoll, W. (1998) Interfaces and thin films as seen by bound electromagnetic waves, *Annu Rev Phys Chem* 49, 569-638.
109. Mosher, D. F., Huwiler, K. G., Misenheimer, T. M., and Annis, D. S. (2002) Expression of recombinant matrix components using baculoviruses, *Methods Cell Biol* 69, 69-81.

110. Alves, I. D., Bechara, C., Walrant, A., Zaltsman, Y., Jiao, C. Y., and Sagan, S. Relationships between membrane binding, affinity and cell internalization efficacy of a cell-penetrating peptide: penetratin as a case study, *PLoS One* 6, e24096.
111. Salamon, Z., Fitch, J., Cai, M., Tumati, S., Navratilova, E., and Tollin, G. (2009) Plasmon-waveguide resonance studies of ligand binding to integral proteins in membrane fragments derived from bacterial and mammalian cells, *Anal Biochem* 387, 95-101.
112. Gunther, S., Gimbrone, M. A., Jr., and Alexander, R. W. (1980) Identification and characterization of the high affinity vascular angiotensin II receptor in rat mesenteric artery, *Circ Res* 47, 278-286.
113. Nora, E. H., Tonellato, P. J., and Greene, A. S. (2000) Quantification of the contribution of type 1 and type 2 angiotensin II receptors to the net tissue specific effect of angiotensin II, *Ann Biomed Eng* 28, 653-664.
114. Bennett, J. P., Jr., and Snyder, S. H. (1976) Angiotensin II binding to mammalian brain membranes, *J Biol Chem* 251, 7423-7430.
115. Salamon, Z., Huang, D., Cramer, W. A., and Tollin, G. (1998) Coupled plasmon-waveguide resonance spectroscopy studies of the cytochrome b6f/plastocyanin system in supported lipid bilayer membranes, *Biophys J* 75, 1874-1885.
116. Bergseth, G., Lappegard, K. T., Videm, V., and Mollnes, T. E. (2000) A novel enzyme immunoassay for plasma thrombospondin. Comparison with beta-thromboglobulin as platelet activation marker in vitro and in vivo, *Thromb Res* 99, 41-50.
117. Shooshtari, P., Fortuno, E. S., 3rd, Blimkie, D., Yu, M., Gupta, A., Kollmann, T. R., and Brinkman, R. R. Correlation analysis of intracellular and secreted cytokines via the generalized integrated mean fluorescence intensity, *Cytometry A* 77, 873-880.
118. Li, Z., Calzada, M. J., Sipes, J. M., Cashel, J. A., Krutzsch, H. C., Annis, D. S., Mosher, D. F., and Roberts, D. D. (2002) Interactions of thrombospondins with alpha4beta1 integrin and CD47 differentially modulate T cell behavior, *J Cell Biol* 157, 509-519.
119. Ticchioni, M., Raimondi, V., Lamy, L., Wijdenes, J., Lindberg, F. P., Brown, E. J., and Bernard, A. (2001) Integrin-associated protein (CD47/IAP) contributes to T cell arrest on inflammatory vascular endothelium under flow, *FASEB J* 15, 341-350.

120. Brandes, M. E., Mai, U. E., Ohura, K., and Wahl, S. M. (1991) Type I transforming growth factor-beta receptors on neutrophils mediate chemotaxis to transforming growth factor-beta, *J Immunol* 147, 1600-1606.
121. Drake, A. W., Myszka, D. G., and Klakamp, S. L. (2004) Characterizing high-affinity antigen/antibody complexes by kinetic- and equilibrium-based methods, *Anal Biochem* 328, 35-43.
122. Green, N. M. (1990) Avidin and streptavidin, *Methods Enzymol* 184, 51-67.
123. Grell, M., Wajant, H., Zimmermann, G., and Scheurich, P. (1998) The type 1 receptor (CD120a) is the high-affinity receptor for soluble tumor necrosis factor, *Proc Natl Acad Sci U S A* 95, 570-575.
124. Bates, D. O., and Harper, S. J. (2002) Regulation of vascular permeability by vascular endothelial growth factors, *Vascul Pharmacol* 39, 225-237.
125. Olsson, A. K., Dimberg, A., Kreuger, J., and Claesson-Welsh, L. (2006) VEGF receptor signalling - in control of vascular function, *Nat Rev Mol Cell Biol* 7, 359-371.
126. Govers, R., and Rabelink, T. J. (2001) Cellular regulation of endothelial nitric oxide synthase, *Am J Physiol Renal Physiol* 280, F193-206.
127. Zhang, Z., Nadeau, P., Song, W., Donoviel, D., Yuan, M., Bernstein, A., and Yankner, B. A. (2000) Presenilins are required for gamma-secretase cleavage of beta-APP and transmembrane cleavage of Notch-1, *Nat Cell Biol* 2, 463-465.
128. Munaron, L. (2006) Intracellular calcium, endothelial cells and angiogenesis, *Recent Pat Anticancer Drug Discov* 1, 105-119.
129. Javerzat, S., Auguste, P., and Bikfalvi, A. (2002) The role of fibroblast growth factors in vascular development, *Trends Mol Med* 8, 483-489.
130. Gijon, M. A., and Leslie, C. C. (1999) Regulation of arachidonic acid release and cytosolic phospholipase A2 activation, *J Leukoc Biol* 65, 330-336.
131. Duda, D. G., Fukumura, D., and Jain, R. K. (2004) Role of eNOS in neovascularization: NO for endothelial progenitor cells, *Trends Mol Med* 10, 143-145.
132. Gelinas, D. S., Bernatchez, P. N., Rollin, S., Bazan, N. G., and Sirois, M. G. (2002) Immediate and delayed VEGF-mediated NO synthesis in endothelial cells: role of PI3K, PKC and PLC pathways, *Br J Pharmacol* 137, 1021-1030.

133. Mottola, A., Antoniotti, S., Lovisolo, D., and Munaron, L. (2005) Regulation of noncapacitative calcium entry by arachidonic acid and nitric oxide in endothelial cells, *FASEB J* 19, 2075-2077.
134. Peckham, G. D., Bugos, R. C., and Su, W. W. (2006) Purification of GFP fusion proteins from transgenic plant cell cultures, *Protein Expr Purif* 49, 183-189.
135. Macnair, D. C., and Kenny, A. J. (1979) Proteins of the kidney microvillar membrane. The amphipathic form of dipeptidyl peptidase IV, *Biochem J* 179, 379-395.
136. Kvensakul, M., Adams, J. C., and Hohenester, E. (2004) Structure of a thrombospondin C-terminal fragment reveals a novel calcium core in the type 3 repeats, *EMBO J* 23, 1223-1233.